1986

Analysis and testing of a switched-inertance hydraulic servo-transformer /

Stephen Clyde Tentarelli
Lehigh University

Analysis and Testing of a Switched-Inertance Hydraulic Servo-Transformer

by

Stephen Clyde Tentarelli

A Thesis

Presented to the Graduate Committee

of Lehigh University

in Candidacy for the Degree of

Master of Science

in

Mechanical Engineering

Lehigh University

1986

This thesis is accepted and approved in partial fulfillment of the requirements for the degree of Master of Science.

12/16/86
(date)

Robert T. Brown
Professor in charge

Richard W. Bucklin P.E.
Chairman of Department

Acknowledgements

Sincere gratitude is expressed to Professor Forbes T. Brown for his supervision, advice, and encouragement throughout the preparation of this thesis. I considered it a privilege to study under him and benefit greatly form his expertise.

Appreciation is also extended to Dr. S. Ramachandran for sharing his knowledge and for his overall willingness to contribute.

Finally, I wish to thank my parents, Patrick and Faye Tentarelli, for their continuous love, support, and encouragement throughout my years of study.

Financial support for this work was provided by the Office of Naval Research, the Parker Hannifin Corporation, and by Phillip Rauch and family.

Table of Contents

List of Figures

Abstract

Switched-inertance hydraulics is a novel concept that uses fluid or mechanical inertia driven by a pulse-width-modulated (PWM) fluid switch to control fluid power. Unlike the energy dissipative metering orifices used in conventional flow control, switched-inertance hydraulics uses an energy conservative principle. The form investigated herein also gives pressure control, which decouples the control device from the load dynamics. Used with feedback, then,the resulting switched-inertance servo-transformer offers the potential for a substantially wider closed-loop bandwidth than a conventional servo-valve.

In this thesis a particular system is analyzed and tested in depth with regard to its steady-state behavior. A unique motor driven four-way rotary switching valve is used in conjunction with two fluid inertance tubes and a simulated load. Theoretical models of this particular system predict significantly improved energy efficiency over conventional methods (up to double the efficiency at middle range flows and pressures). They also predict that cavitation is negligible near the null condition, but becomes increasingly more important away from null.

Experimentally, blocked-load pressure-gain characteristics generated by the hydraulic transformer are very linear over 90% of the control range. Pressure-vs-flow characteristics are also quite linear and consistent for small flows. At larger flows, however, dynamic head losses and other possible non-linear phenomena dominate the behavior. Overall, the experimental results are promising.

Chapter 1
INTRODUCTION

Hydraulic control valves control fluid power in a hydraulic circuit. The fluid power in a channel is the product of flow and total pressure. Therefore fluid power may be controlled in essentially three ways. In pure flow control the valve regulates only flow, and output pressure depends only on the characteristics of the load. In pure pressure control, pressure alone is regulated and flow depends only on the load characteristics. Finally, there is a combination of the first two. Methods one and two represent ideal behavior and are in practice impossible. However, it is possible to have combinations of them, as suggested in method three. Behaviorally this last method can come close to either flow control or pressure control.

Conventional means of controlling hydraulic fluid driven by a nearly constant supply pressure use metering orifices to control velocity. These metering orifices are analogous to electrical resistors. They can be thought of as fluid resistors that perform control simply by dissipating energy. This technique is closer to flow control than to pressure control, especially when the valves are designed not to leak much near null conditions. In many applications, however, pressure control would be preferred, as is suggested briefly below.

In a fundamentally different approach, a fluid switch alternately accelerates and decelerates flow in an inertive channel to achieve a desired time average pressure at the output end. The signal, then, is in the form of pulse-width-modulation. Fluid compliance can be used to smooth the output variations. The novelty here is that rather than using the resistive or dissipative property of the fluid to acheive control, the inertive and compliant (or reactive)

properties of the fluid are used. This gives rise to the concept of switched-reactance or switched-inertance hydraulics [1]. Inherent to this approach are the twin advantages of operating with an energy-conservative principle and the tendency to behave more like pressure control.

1.1 Concepts of Switched Inertance Hydraulics

To understand the concepts of switched-inertance hydraulics it is perhaps easiest to first look at an analogy to modern electrical switched power converters [2], and then look at the equivalent fluid power circuit. Fig. 1.1 shows a DC step-down transformer. The double-throw switch is considered ideal, meaning instantaneous switching. A control signal drives the switch in a pulse-width-modulated mode with period T and ratio of "on" time α. With the switch "on", current through the inductor increases nearly linearly with time at a rate proportional to the voltage difference $(v_l - v_s)$. When the switch is "off", current decreases nearly linearly at a rate proportional to v_l. So, at equilibrium conditions the increase in current equals the decrease in current over one period, giving

$$\alpha(v_s - v_l) = (1-\alpha)v_l \tag{1.1}$$

so that

$$v_l = \alpha v_s, \tag{1.2}$$

and since power is conserved,

$$v_s i_{s(avg)} = v_s i_{l(avg)}. \tag{1.3}$$

Thus i_l averages

$$i_{l(avg)} = \frac{i_{s(avg)}}{\alpha}. \tag{1.4}$$

The capacitor largely absorbs the fluctuations in the current i, therefore acting as a filter. The break frequency $(IC)^{-1/2}$ is less than the switching frequency, but not too much less since it defines the bandwidth of control.

By placing two of the step-down transformers in Fig. 1.1 together and using a double-throw two-way switch, push-pull action results. This is shown in Fig. 1.2. If we define T and α the same as in Fig. 1.1, the equations analogous to (1.1) are

$$\alpha(v_s - v_{la}) = (1-\alpha)v_{la} \tag{1.5}$$

$$\alpha v_{lb} = (1-\alpha)(v_s - v_{lb}). \tag{1.6}$$

Solving for $(v_{la}$ and $(v_{lb}$, and defining $\Delta v_l = v_{la} - v_{lb}$ we get

$$\Delta v_l = (2\alpha - 1)v_s. \tag{1.7}$$

The hydraulic analogies of the circuits in Figs. 1.1 and 1.2 become three-way and four-way transformers respectively, and are described below.

The electrical D/A conversion which occurs because of the IC filter can be implemented into hydraulic circuits. To do this consider the analogies of voltage and current to pressure and flow, inductance L to fluid inertance I, and capacitance C to fluid compliance.

If pressure and flow are chosen as the power variables, the fluid inertance of a channel is defined as $I = \rho l/A$, where, ρ is the fluid density, l is the channel length, and A is the channel cross-sectional area. Along with the inertance there is always an associated undesirable fluid resistance. One design task requires keeping this at an acceptable minimum while simultaneously maximizing the inertance. Since both inertance and resistance are inversely proportional to the cross-sectional area A, a compromise is needed. The equation defining inertance also indicates that increasing the channel length l will increase

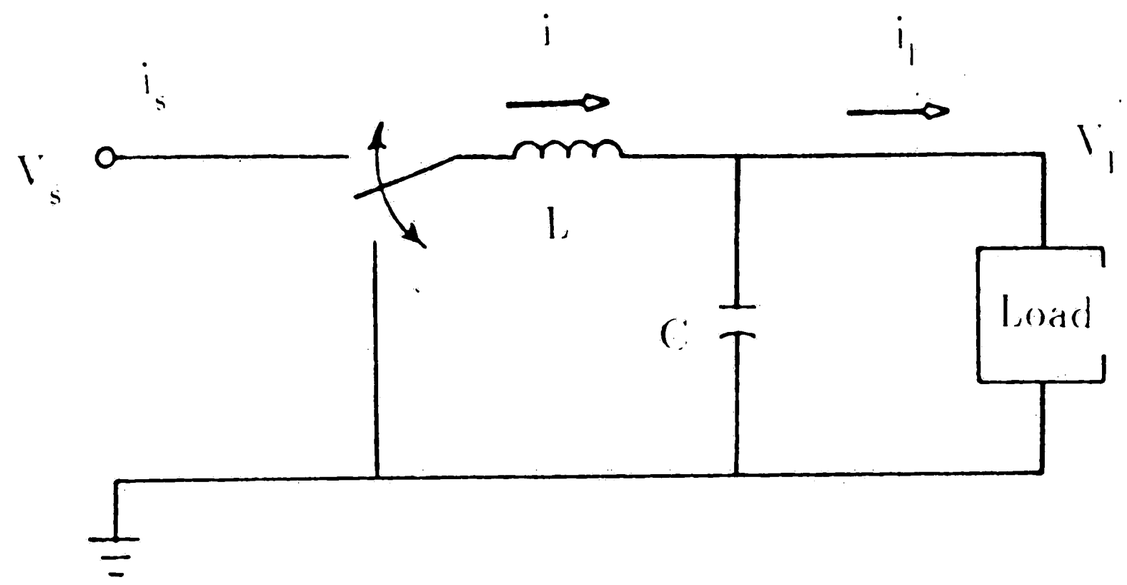

Figure 1-1: Step-Down Transformer

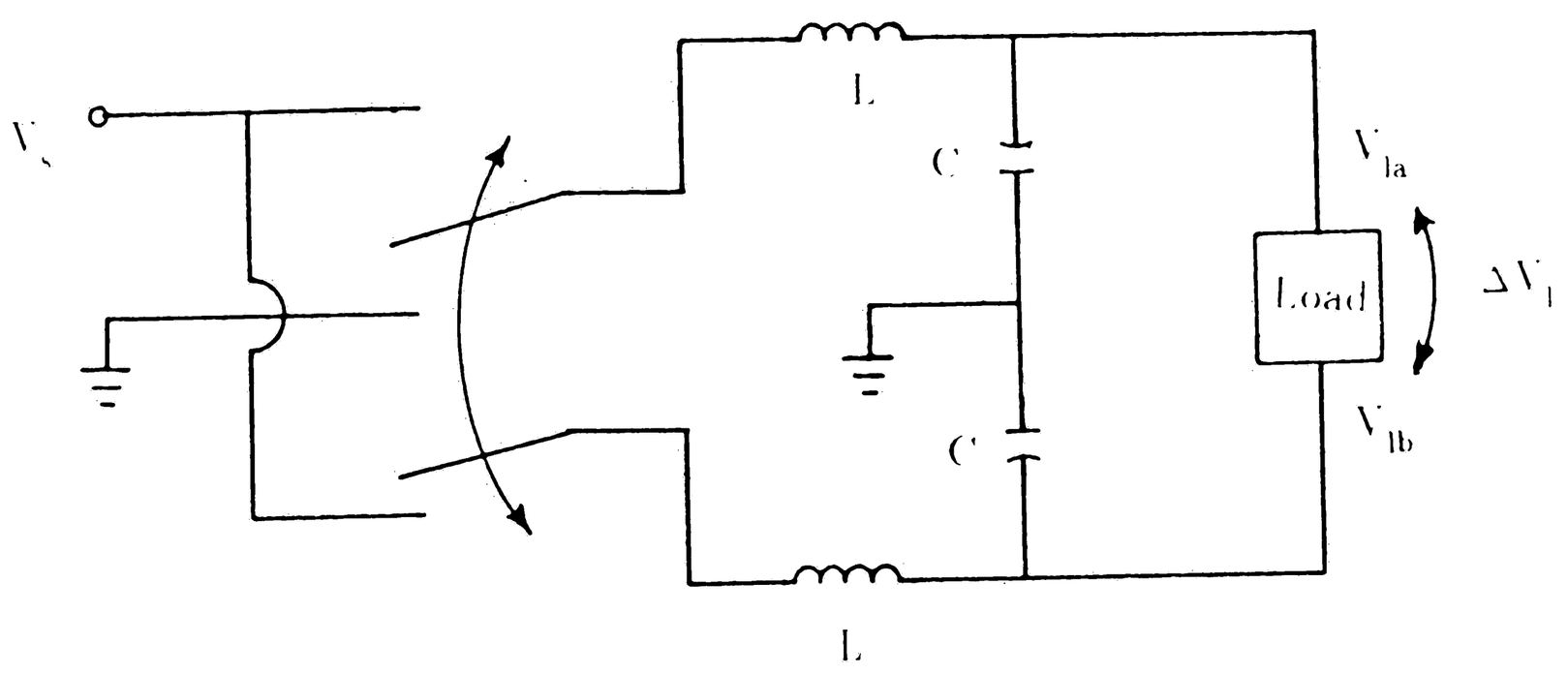

Figure 1-2: Push-Pull Transformer

l. However, wave propogation effects may become severe at longer channel lengths. To keep these effects at a tolerable level F.T. Brown developed a rule of thumb that channel length should not exceed about 1/20 of a wave length, defined for the switching frequency. In addition, a single round tube is preferred since multiple or non-round channels generally increase the resistance.

There are two other components left in the electrical analogy that need to be implemented into hydraulics. First, a moderate sized capacitance or fluid compliance is needed. Normally it is acheived with a bladder accumulator, and in this case is defined as $C=\partial V/\partial P$, where V and P are pressure and volume of the accumulator respectively. Since the compliance needed varies with the inverse of the switching frequency it is possible that a rather small value of compliance will be optimal. For higher frequencies the natural fluid compliance of the load chambers, which is V/β, where V is volume and β is bulk modulus of the fluid, may be adequate. There is even the possibility at very high frequencies for the desired compliance to be smaller than that which is naturally present. The second component needed is the two-way double-throw switch. Hydraulically, this device alternately switches from high pressure (supply) to low pressure (tank). In addition, the operating frequency of this switch limits the bandwidth of control for the system. Therefore it is important to make the switching frequency as high as possible. Doing so is a major design objective.

A basic look at the desired or ideal characteristics of the hydraulic circuit analogous to the electrical circuit in Fig. 1.2 may be helpful at this time. Fig. 1.3 schematically shows such a circuit with the inertance tubes and accumulators indicated. The PWM switching (or driving) signal is shown in Fig. 1.4 with α set at 0.75. The flow through the inertance tube is assumed to in-

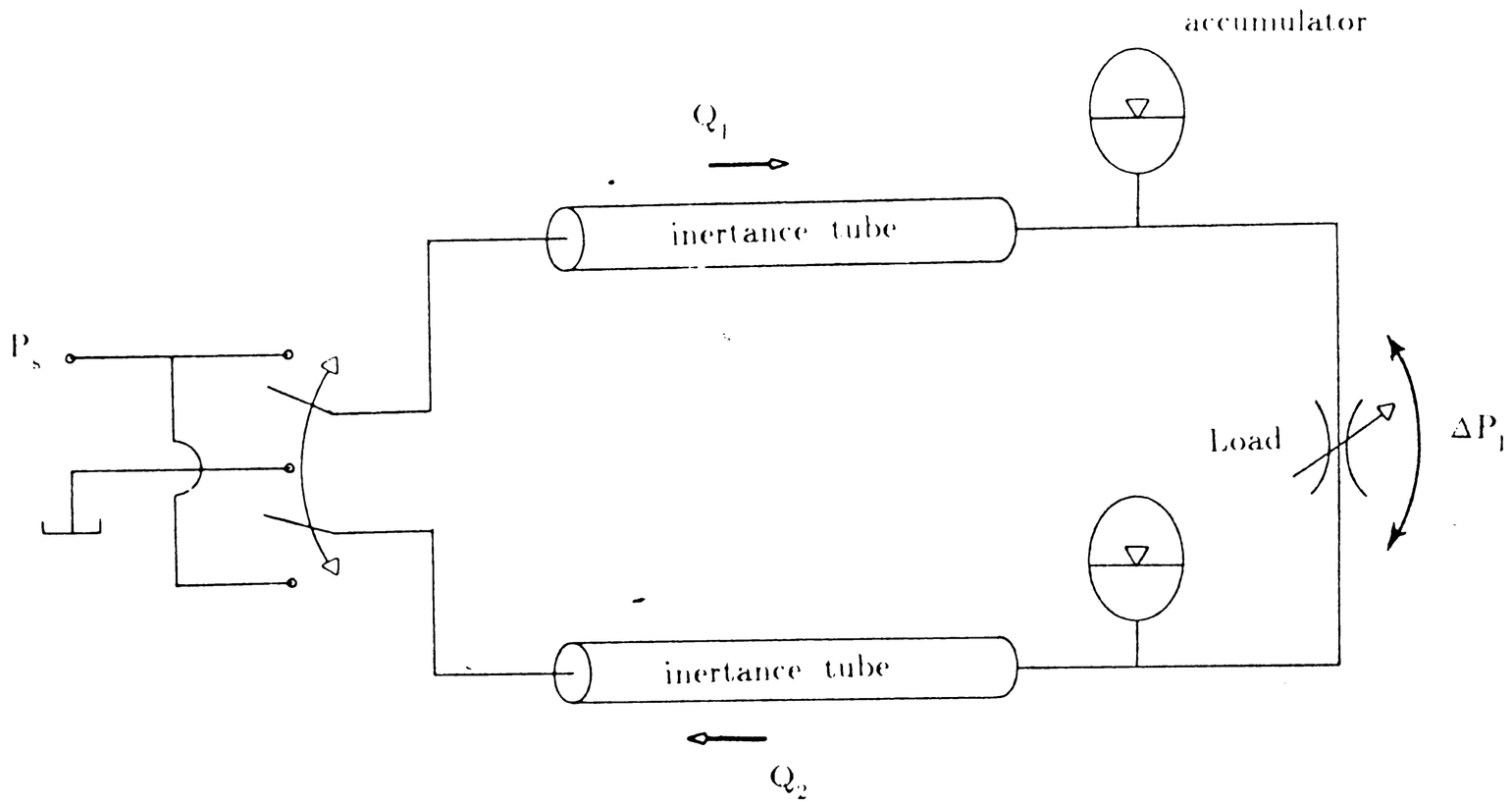

Figure 1-3: Hydraulic Push-Pull Transformer

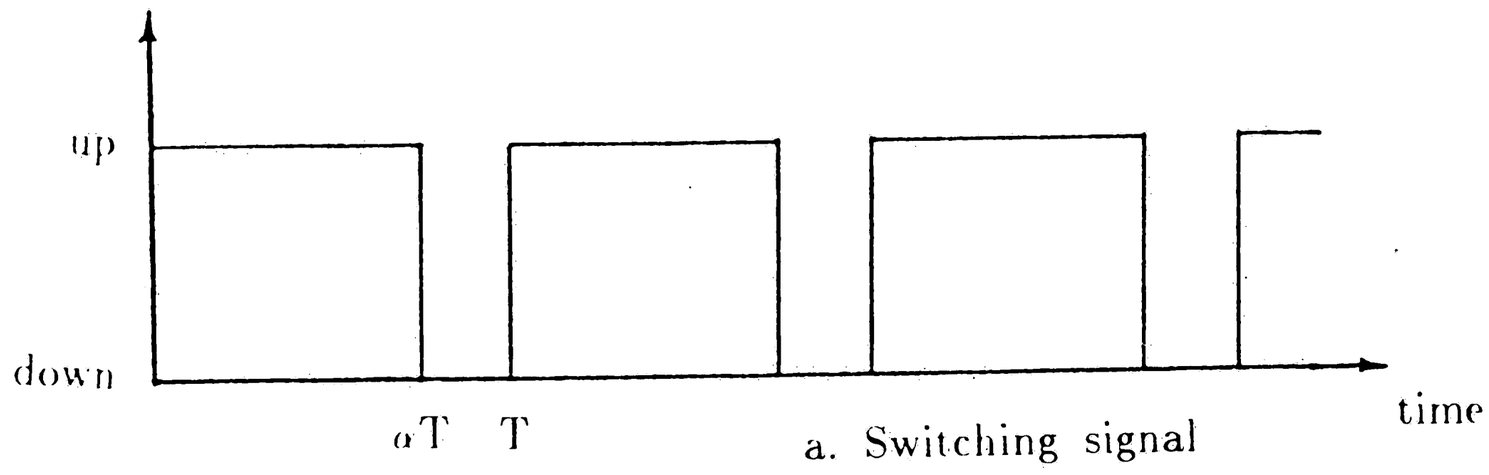

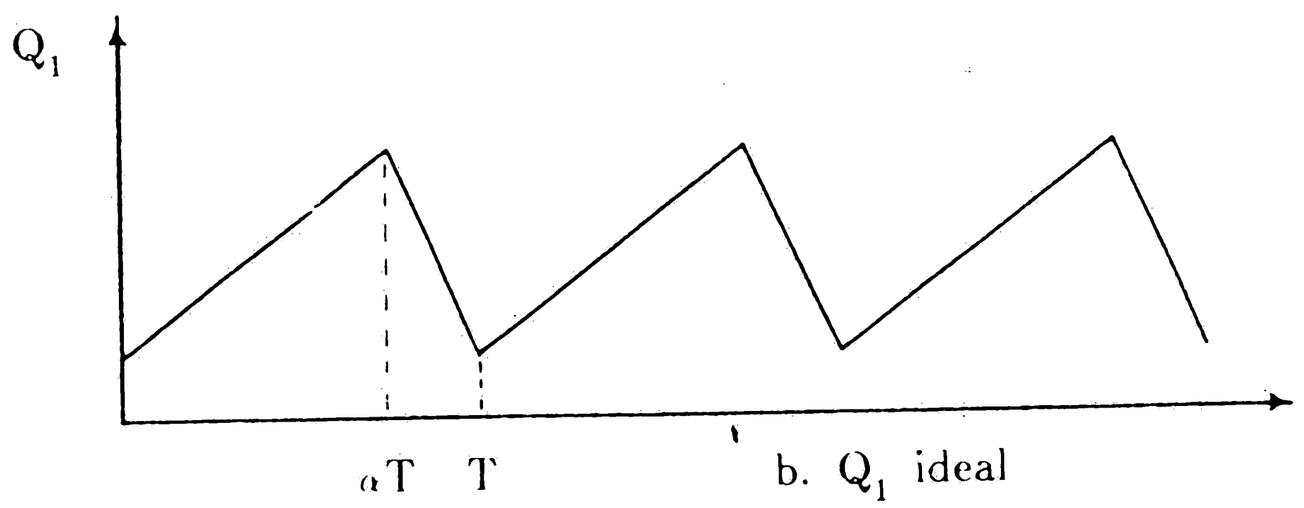

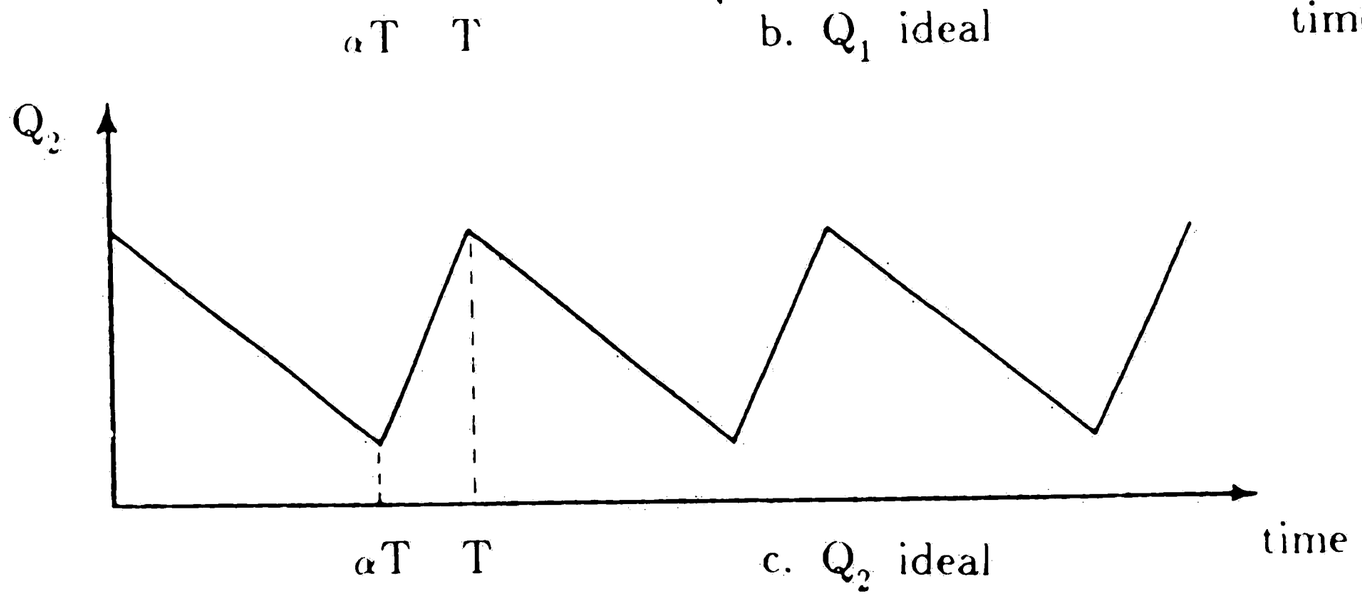

Figure 1-4: Ideal Switching Signal and Flow Responses

crease or decrease at a rate linearly proportional to the pressure drop across it, thus giving the idealized flows Q_1 and Q_2 seen in Fig. 1.4(b,c). Finally, the hydraulic equivalent of equation (1.6) is

$$\Delta P_l=(2\alpha-1)P_s. \tag{1.8}$$

This is the desired ideal characteristic for P_l, and it is pure pressure control since it is independent of flow.

1.2 Evaluation of Concept

The following section investigates some major advantages and disadvantages of a switched-inertance hydraulic transformer versus a conventional orifice metered valve. This section is condensed from Brown [1].

BANDWIDTH: A fundamental difference between conventional flow control valves and switched-inertance hydraulics is the potential for the latter to give a substantially wider bandwidth when the switching frequency is high. To understand this, consider a properly designed conventional system with position feedback. For simplicity, assume that break frequencies of the valve are significantly higher than the hydraulic natural frequency, so

$$\omega_h=\frac{2A\beta^{1/2}}{(VM)^{1/2}} \tag{1.9}$$

where, β is effective fluid bulk modulus, A is area of load piston, V is total fluid volume in cylinder, and M is the effective load mass. The damping ratio, assuming no load damping, is

$$\varsigma_h=(K_c/A)(\beta M/V)^{1/2} \tag{1.10}$$

which is generally very small, particularly around the null position.

A stability requirement from a bode plot in Brown [1] then limits the bandwidth at

$$\omega < 2\zeta_h \omega_h - 2\beta K_c / V_c \tag{1.11}$$

which is strongly dependent on the load volume. It turns out that even with various compensation techniques it is very difficult to increase this limit.

In contrast, Fig. 1.5 shows the block diagram for a properly designed switched-inertance system. I and R represent the inertance and associated resistance of the two inertance tubes, and C is one-half the compliance of one side. This gives

$$\omega_r^2 = \frac{1 + IA^2/m}{IC} \tag{1.12}$$

Then, stability conditions give

$$\omega < \zeta_r \omega_r \tag{1.13}$$

Therefore if ζ_r is assumed approximately equal to ζ_h, the ratio of (1.13) to (1.11) is

$$\frac{\zeta_r \omega_r}{2\zeta_h \omega_h} = \frac{\omega_r}{2\omega_h} \tag{1.14}$$

Since ω_h is essentially fixed, this ratio is only limited by ω_r, which in turn is limited by the switching frequency through the relation $\omega_r = k\omega_s$. Here, k is a constant chosen sufficiently small to allow D/A conversion of the switching signal through the IC filter, and the subscript indicates switching frequency.

STATIC ERROR COEFFICIENT: For a steady velocity input, the steady-state position error is inversely proportional to the static velocity error coefficient, K_e. For a conventional system

$$K_{ec} = 2\zeta_h \omega_h \tag{1.15}$$

and for the switched-inertance system

$$K_{es} = \frac{\zeta_r \omega_r M}{2IA^2}. \tag{1.16}$$

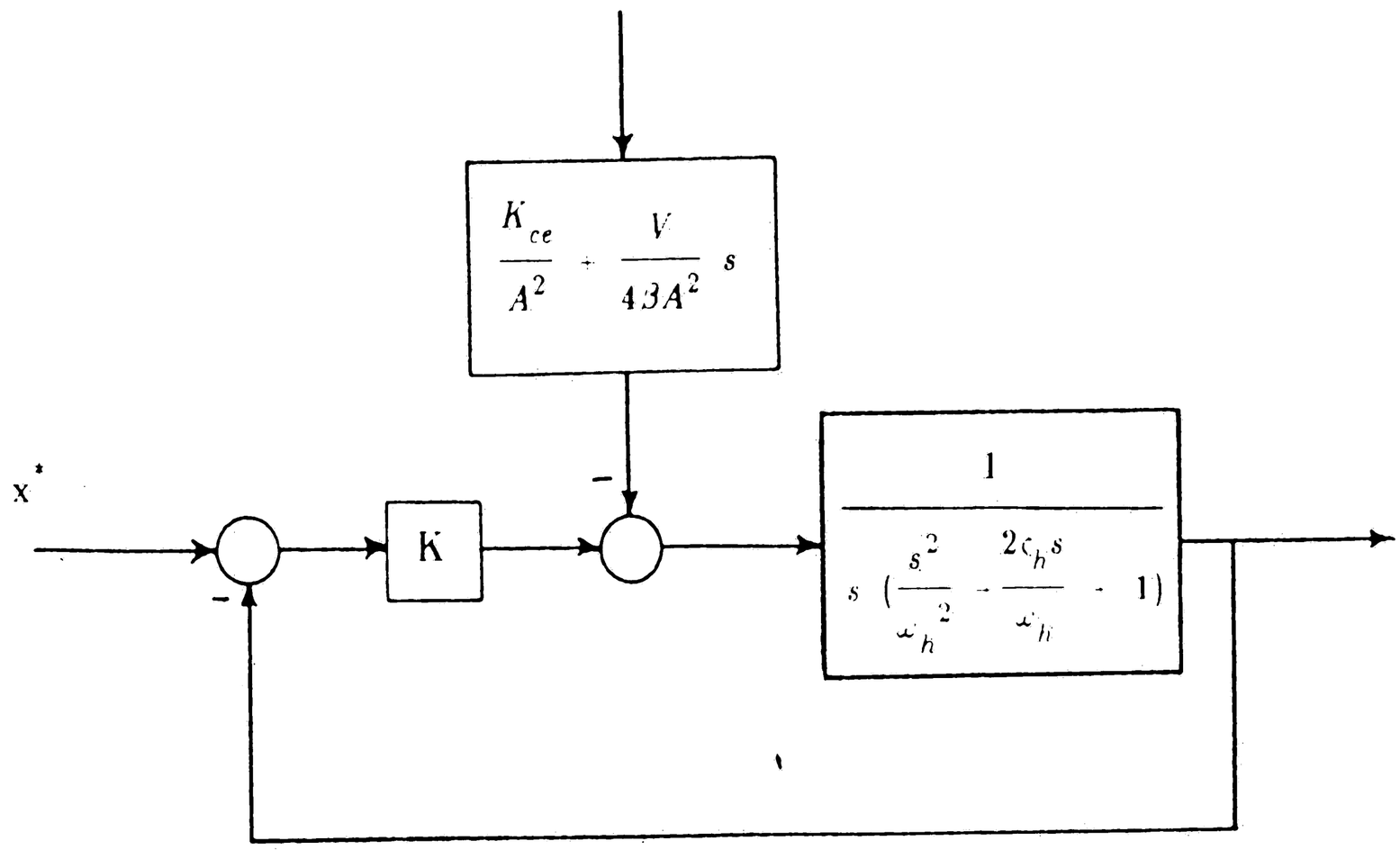

Figure 1-5: Block Diagram for Switched Inertance System

Here the subscripts c and s indicate conventional and switched, respectively. The ratio of (1.16) to (1.15) gives

$$\frac{K_{es}}{K_{ec}} = \frac{\zeta_r \omega_r M}{\zeta_h \omega_h I A^2} \tag{1.17}$$

which potentially favors the switched-inertance system when ω_s is high.

EFFICIENCY: Another fundamental difference between the two systems deals with energy efficiency. The conventional technique of flow control uses a purely dissipative means to achieve control. For such a system, the source supplies flow to the control valve at nearly constant pressure. Then the flow passes through resistive metering orifices that reduce the pressure as desired. This gives an efficiency independent of flow:

$$\eta = P_l / P_s. \tag{1.18}$$

Thus efficiency is low for low load pressures. In addition, for large flows operating at low load pressures, the energy dissipation can be quite large.

To contrast, the switched-inertance transformer is ideally non-dissipative, which is why it is called a "transformer" rather than a "valve". If we assume that the system in Fig. 1.3 has ideal components, meaning no resistance in the tubes and an isentropic accumulator, then it should act as an ideal transformer, with 100 percent efficiency. Of course there are actual parasitic resistances and other inherent losses. These will be discussed in chapter 3 for a particular switched-inertance system design.

An initial implementation of switched-inertance hydraulics was made by C.J. Liaw in a Ph.D. dissertation [3]. His particular switching valve used a modified Moog flapper valve as the first stage and a specially designed spool valve as the second stage. This translating type switch seemed to operate best

at about 50 Hz. Analytical work on optimizing switching parameters for this valve was done by Brown [4,5] and Koseoglu [5] prior to the work by Liaw.

The concept of a rotating switch, introduced subsequently by Brown [1], greatly reduces the complication of Liaw's valve, eliminates mechanical impact, and permits a higher switching frequency. Detailed analysis and testing of the first implementation of this concept is the primary subject of this thesis.

Chapter 2
Concept of Rotary Switching Valve

In designing a switching valve there are three basic goals. To begin, the device needs to give a switching signal that is as close as possible to ideal. In this case, it means we want to produce a PWM square-wave signal. Attaining high frequency switching is another very desirable goal since bandwidth is directly related to it. Compared to Liaw's device which operates at 50 Hz, a device which could operate at a frequency of 500 Hz is considerably better. Finally, economics becomes quite important. Keeping cost in mind is always essential especially if switched-inertance hydraulics is to be competitive with conventional control systems. To accomplish these goals a rotating switching valve was designed by F.T. Brown, with help from S. Ramachandran, and is analyzed in this thesis.

To understand the operation of this rotary valve, first consider a very simplified three-way switching mechanism as shown in Fig. 2.1. The device is shown in two dimensions and is assumed to have a unit depth. The lower porting plate connects the supply pressure P_s and tank pressure P_T to the valve through ports of width d and distance d apart. The upper porting plate connects pressure P_a to the valve through a port also of width d. Between the upper and lower porting plates is the switching plate. This plate is an infinitely long series of slots and "fingers" that can close-off or open-up flow paths. Now let the switching plate move to the right with a constant velocity U_o. By doing this the pressure port P_a is alternately connected to P_s and P_T. In addition, if the lower porting plate is allowed to move side to side, while the upper porting plate remains fixed, the ratio of time that P_a is connected to P_s

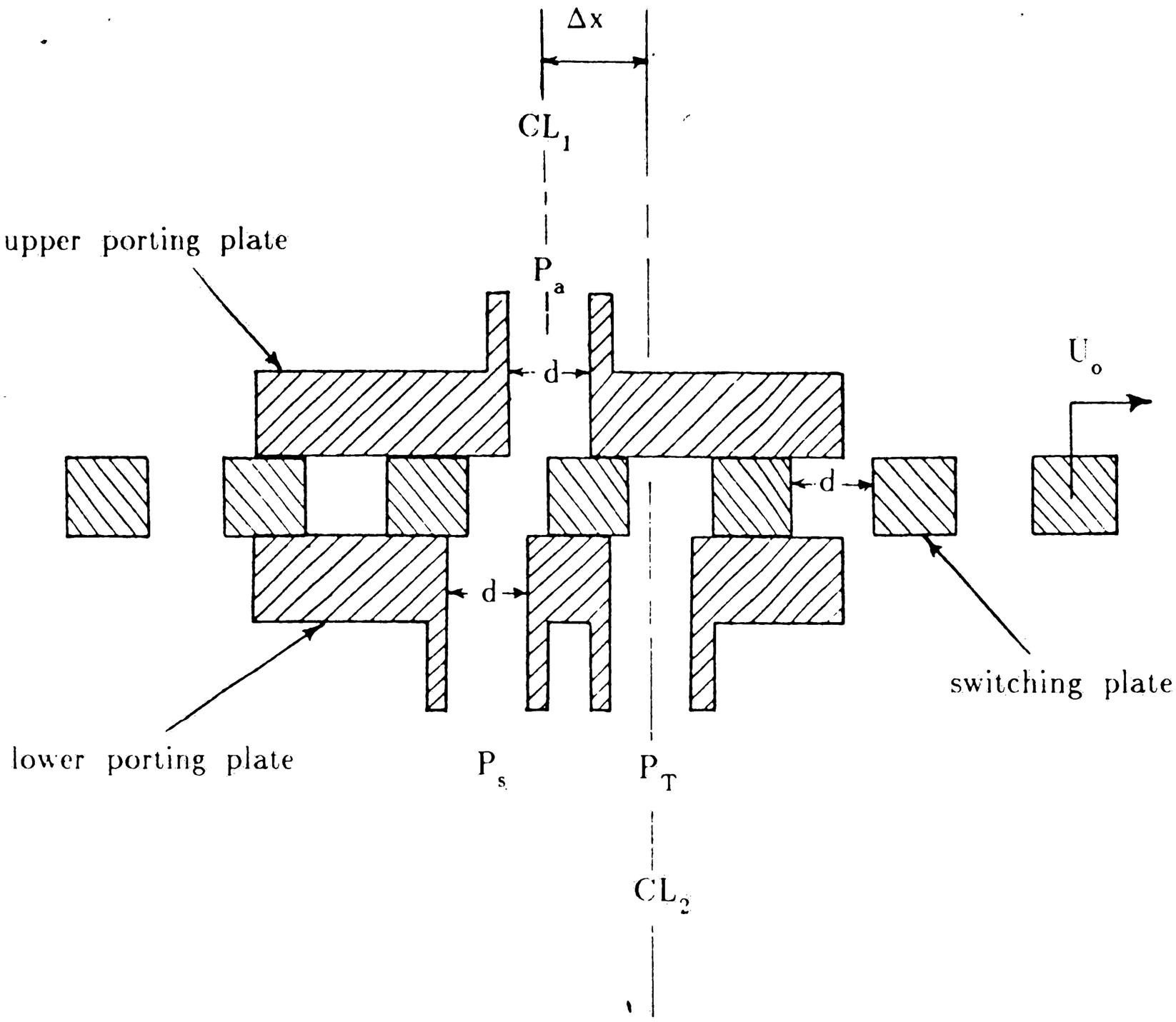

Figure 2-1: Three-Way Switching Mechanism

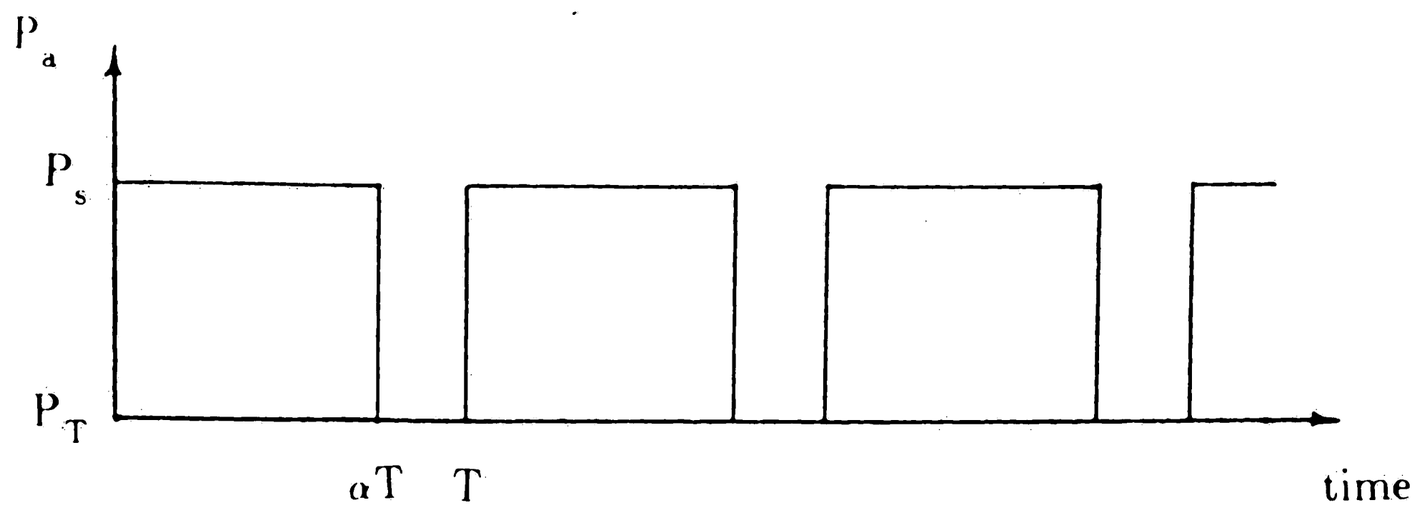

Figure 2-2: Pressure P_a for Zero Flow

relative to P_T can be modulated. Therefore, for zero flow through the valve, P_a should be the PWM signal in Fig. 2.2, where Δx measures the distance between the centerlines of ports P_a and P_T. This ratio,

$$\alpha = \Delta x / d, \tag{2.1}$$

which has the useful range $0 < \alpha < 1$, will be considered the control variable.

This three-way switching valve can be modified to give a four-way switching valve by adding another port P_b to the upper plate and a second tank port to the lower plate. Fig. 2.3 shows this four-way mechanism which works the same as before. The switching plate moves rightward at velocity U_o and the lower porting plate can move a small distance side to side. The modulation variable α is still defined as $\Delta x/d$. Now both P_a and P_b are PWM signals as shown in Fig. 2.4. These signals can then be connected to a hydraulic IC filter for smoothing.

The need for an infinite rack may seem to make these two designs impossible. Imagine however that the mechanism is wrapped around in a circular fashion so that the infinite rack becomes a hollow cylinder with slots cut in it. We will call this piece the rotor. The lower porting plate also gets wrapped around and becomes a solid cylinder with grooves, and it fits inside the rotor. We will call this piece the control shaft. Finally, the upper porting plate becomes the valve housing or stator, containing the fixed ports for P_a and P_b. A schematic representation for this four-way rotating switching valve is shown in Fig. 2.5.

The operation of this device is essentially the same as for the linear valve of Fig. 2.3. Additional ports for P_a and P_b are added in the stator to take advantage of the rotor's full periphery. Likewise there are additional ports for P_s

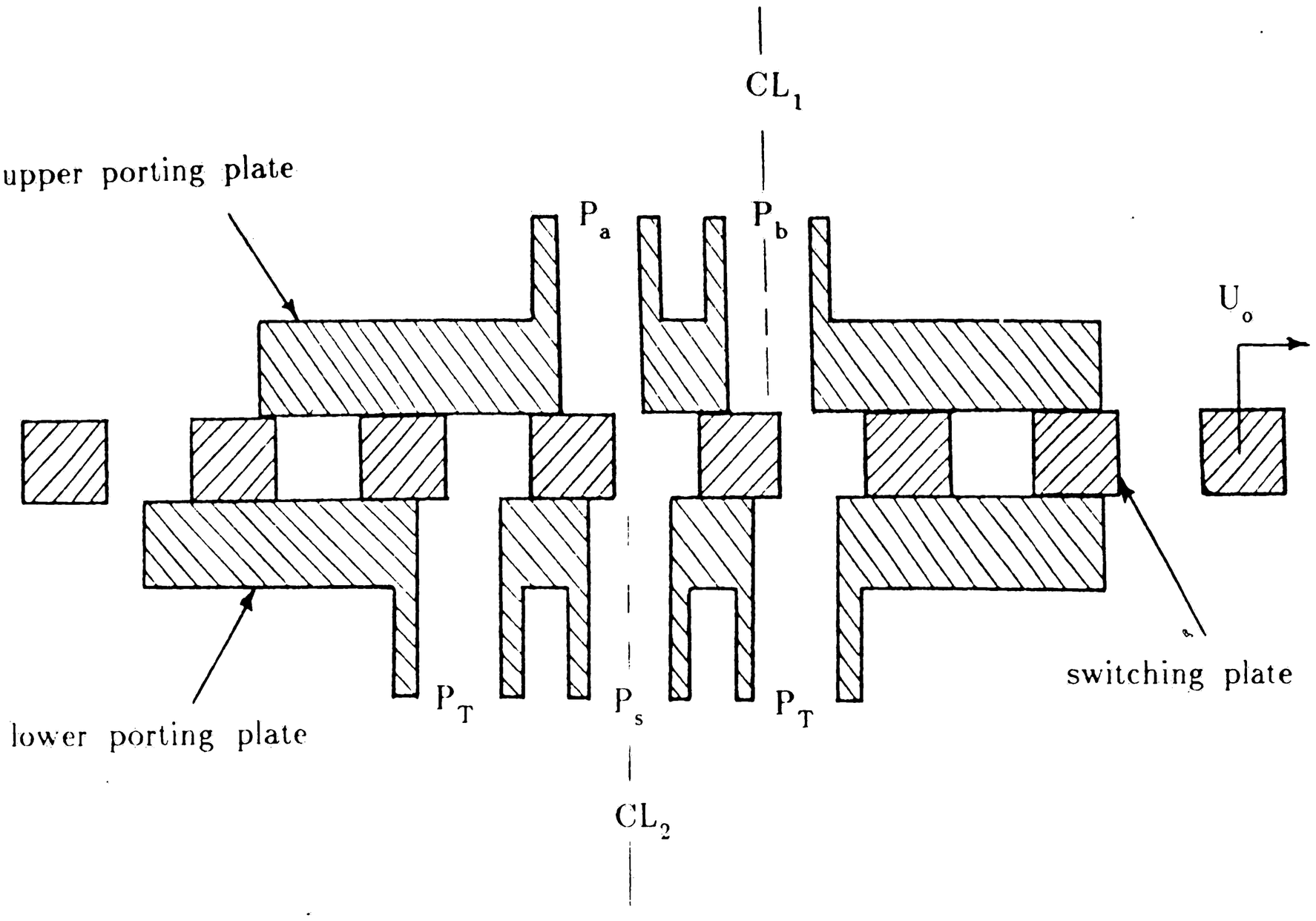

Figure 2-3: Four-Way Switching Mechanism

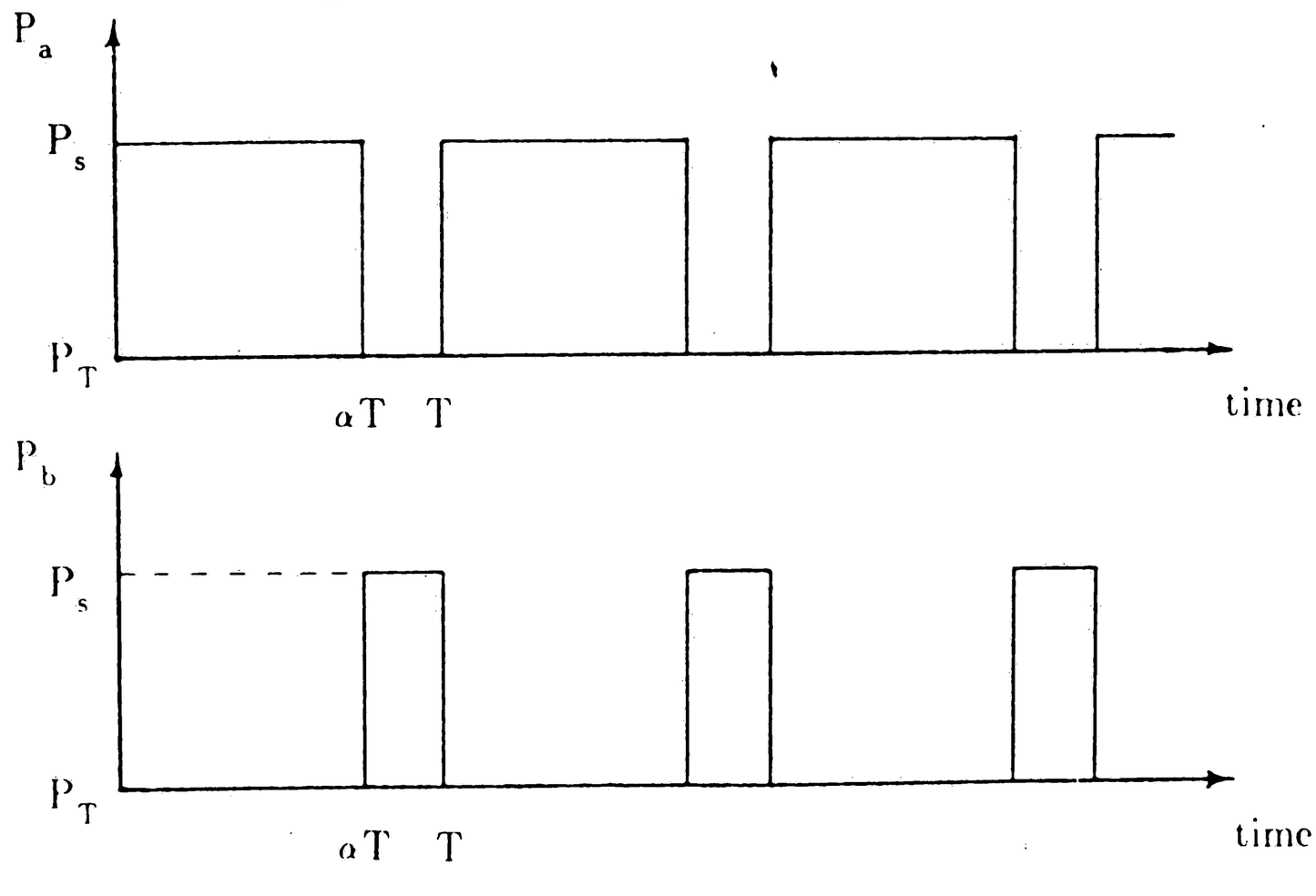

Figure 2-4: PWM Signals, P_a and P_b

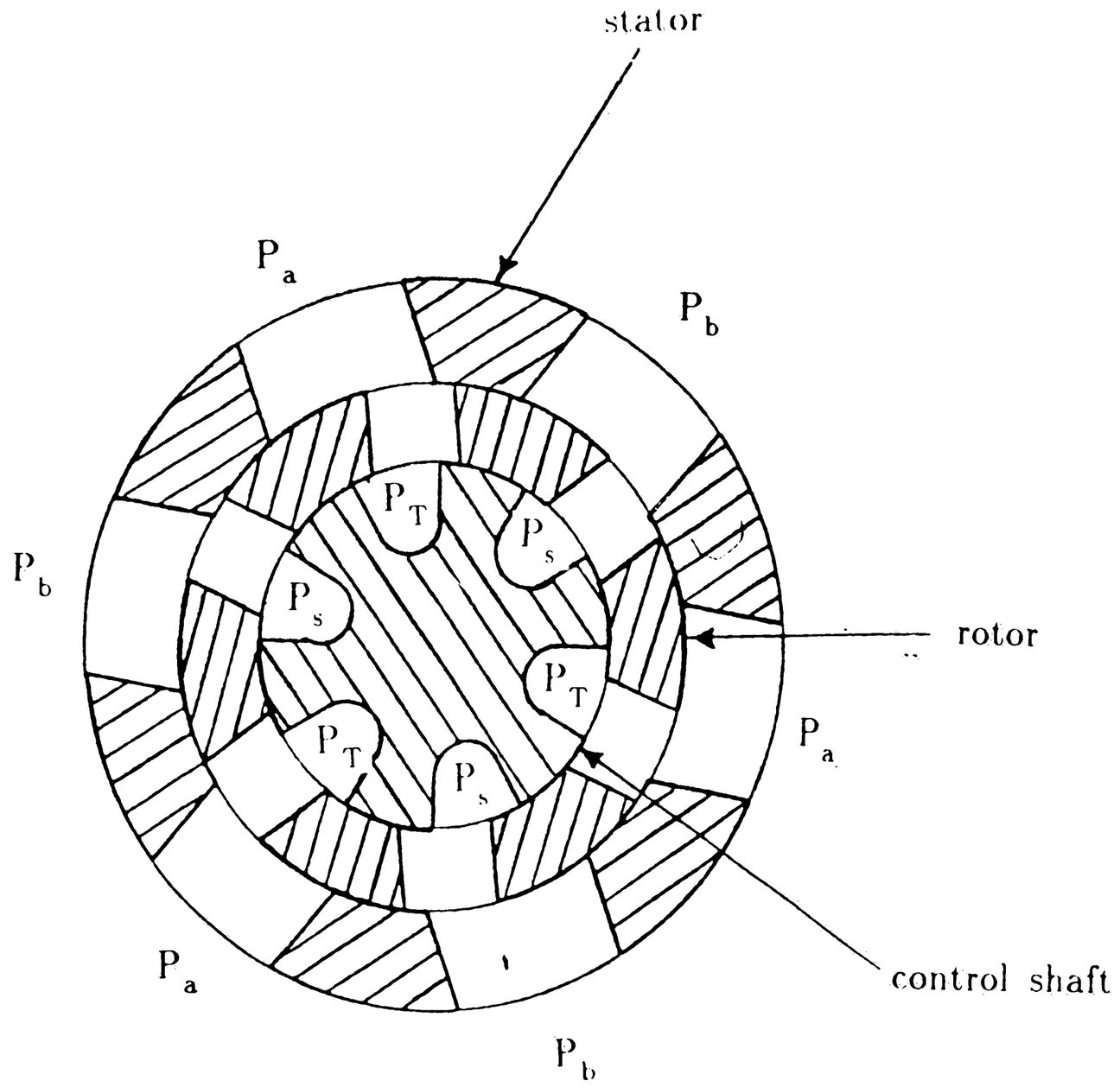

P_a and P_B pressure ports connected externally.

Figure 2-5: Rotary Switching Mechanism

and P_T in the control shaft. The various P_a ports are interconnected externally, and similarly for P_b, P_s, and P_T. The rotor spins at a constant speed ω, so that the ports P_a and P_b are alternately connected to the P_s and P_T ports. This gives the same PWM signal for P_a and P_b in the rotary switching valve as it did for the linear valve. The control variable α can be interpreted as an angle θ. The useful range of θ is

$$0 < \theta < 180^o/n$$

where n is the number of P_a or P_b ports. In the case of Fig. 2.5, n is 3. As with α, θ equal to zero gives P_a equal to zero for all time.

The concept of rotation permits much higher frequencies than the translating spool switch. An external motor turns the rotor rapidly at a constant speed producing a fixed pulse-width-modulation frequency equal to the motor shaft speed times the number of slots in the rotor. Since, the design in Fig. 2.5 has six rotor slots, an external motor driving the rotor at 5000 rpm gives a switching frequency of f_s=500 Hz. This in fact has been acheived in practice. Another advantage of the rotary valve is the elimination of mechanical impact with its noise and potential metal fatigue which occur in the translating switch. Also note that unlike electrohydraulic servo-valves, the rotary switching valve is essentially a single stage device, made possible by the fact that effective flow forces on control members are orders of magnitude smaller than in conventional valves. Verification of this feature is given by a simulation developed in chapter 4.

In the design of the four-way rotary switching valve considerable attention was placed on properly a.) interconnecting the various pressure ports, b.) balancing internal pressure forces, c.) locating drain ports, and d.) specifying

tolerances and clearances to assure an acceptable compromise between internal leakages and viscous shear forces seen by the external motor. The following briefly explains the various members of the rotating valve and how they work together.

Fig. 2.6, 2.7 and 2.8 comprise an assembly drawing of the prototype four-way switching valve. The housing contains all the external porting connections to the inertance tubes, supply pressure, tank pressure, and two Greer bladder accumulators. These accumulators are at the supply pressure and tank pressure ports to help stabilize pressures. To acheive the complicated internal connectons two separate pieces were made and then press-fitted together. These in turn were pressed into the housing so that all three pieces become the stationary portion of the valve called the stator. The next piece inside the stator is called the rotor. The rotor shaft protrudes out through the housing where it can be connected to an external motor. The control shaft sits in the center of the valve. Its shaft also protrudes through the valve housing where it can easily interface with some type of control driver (ie: stepper motor). Finally, seals and end caps are placed over the two shafts to complete the valve.

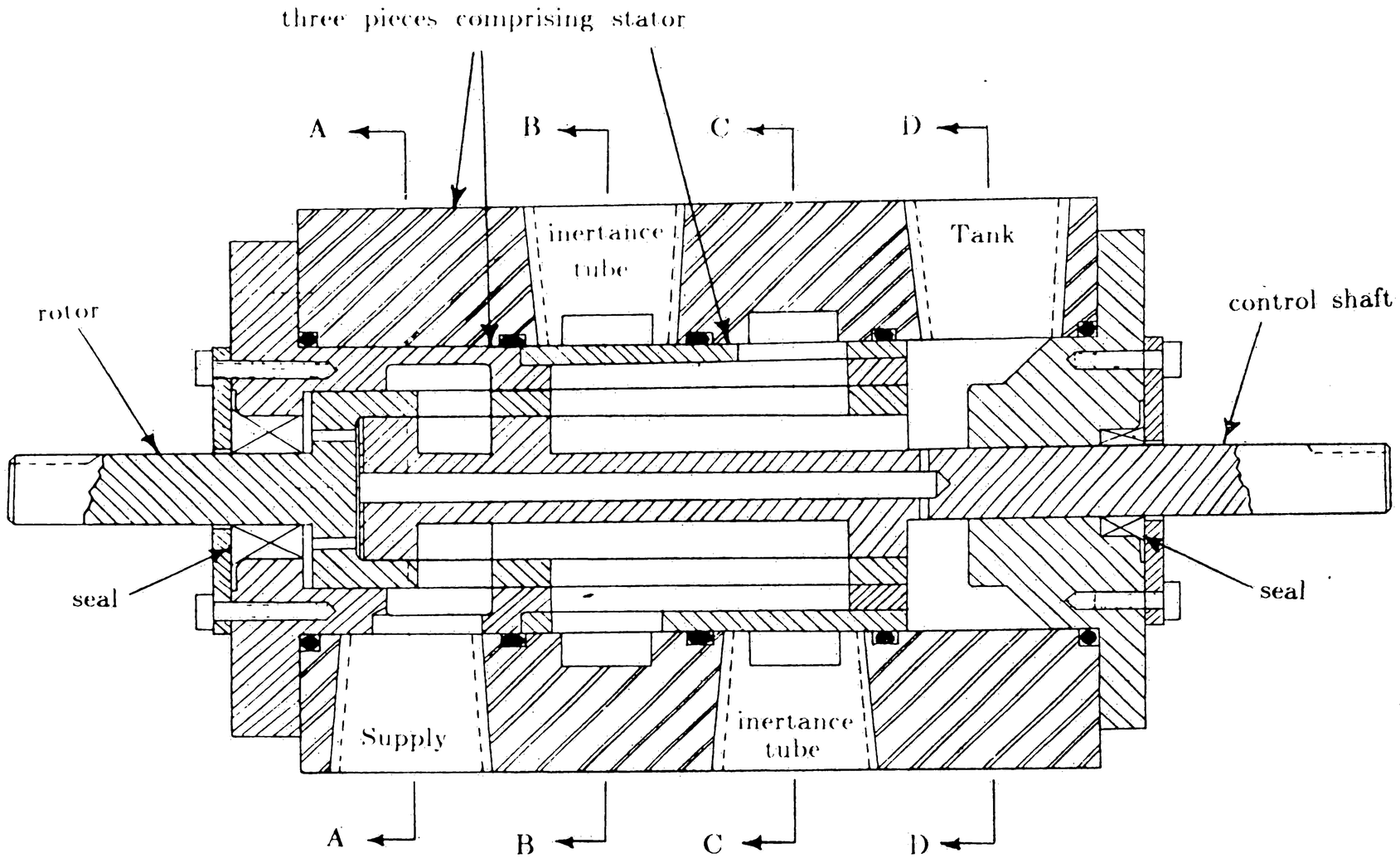

Figure 2-6: Four-Way Rotary Switching Valve Prototype

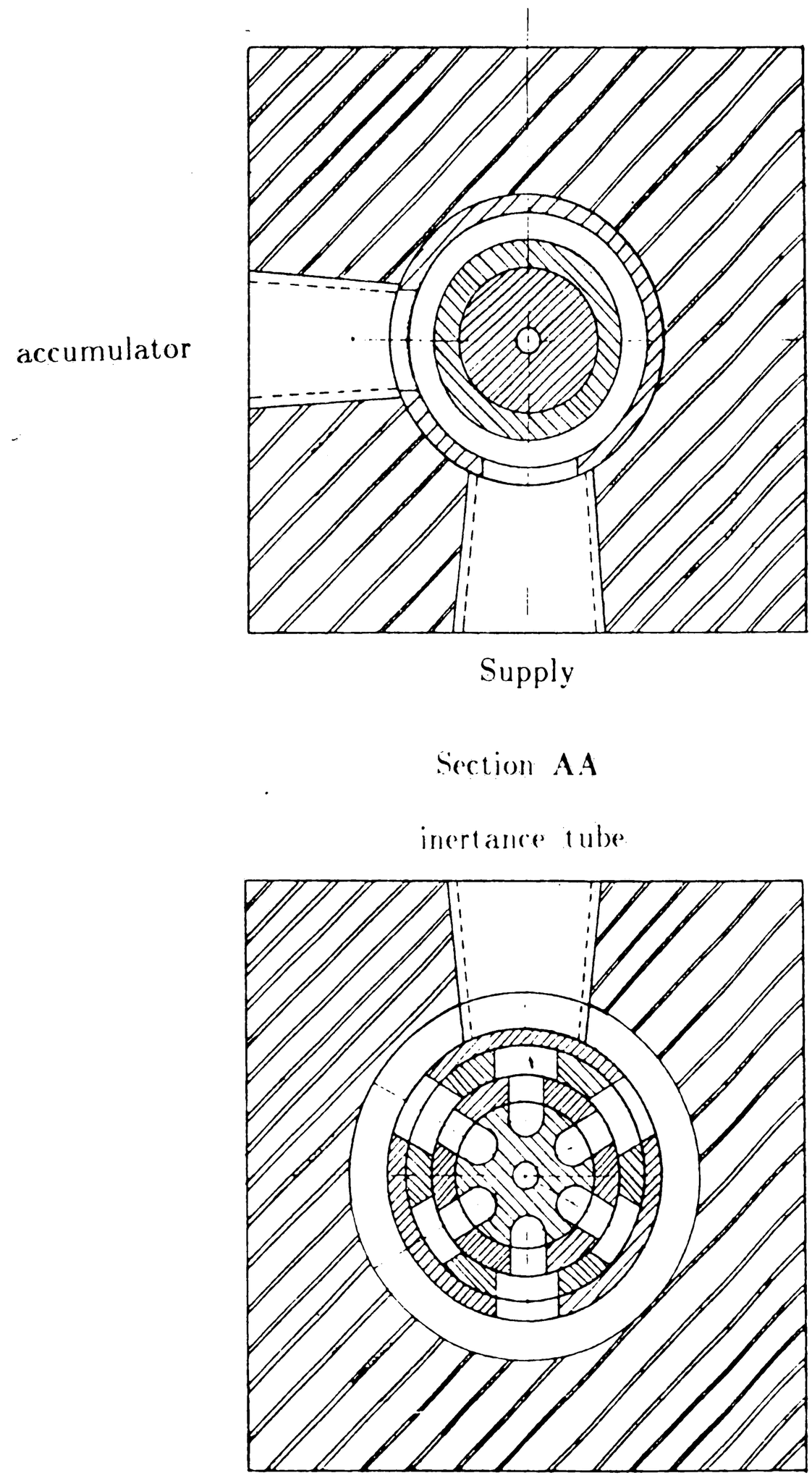

Figure 2-7: Section Views

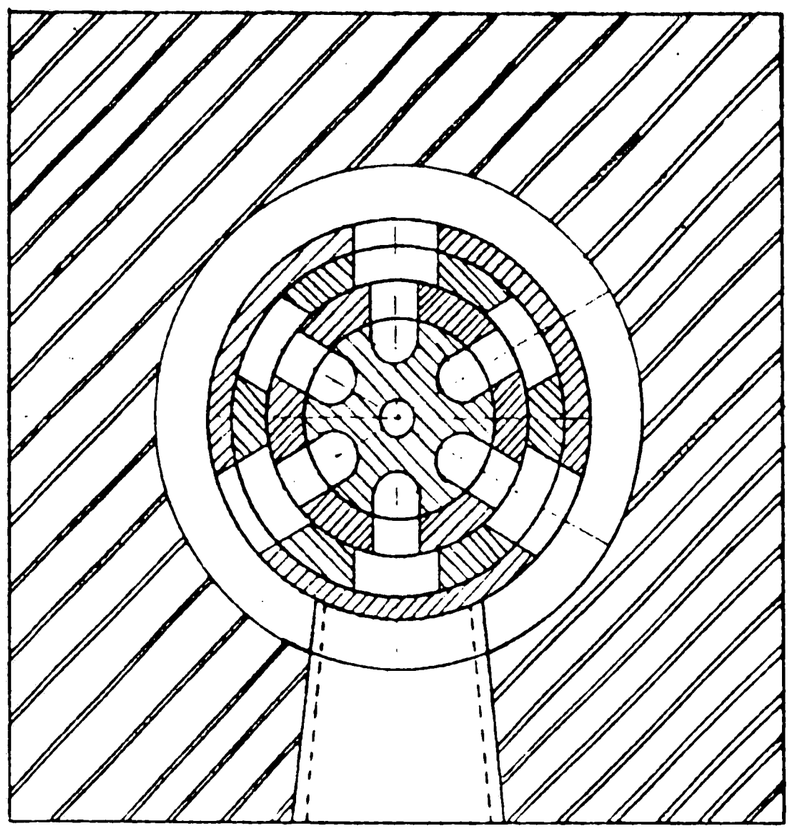

inertance tube

Section CC

Tank

accumulator

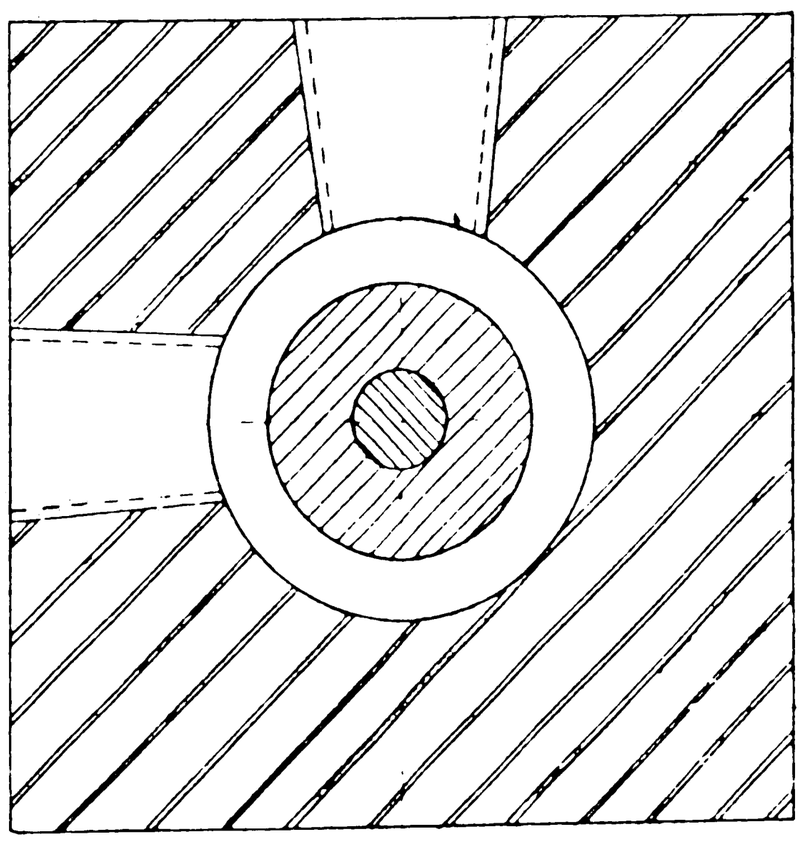

Section DD

Figure 2-8: Section Views

Chapter 3
Efficiency Analysis

Increased efficiency over conventional servo-valves is considered to be one of the major advantages of switched-inertance servo-transformers. As mentioned earlier, using the inertive and compliant properties of the fluid for control makes switched-inertance hydraulics ideally 100% efficient. This of course is not possible in practice. Non-ideal phenomena in the system causing less than 100% efficiency include, primarily, tube flow resistance and dynamic head loss, and secondarily, cavitation, internal leakage, and non-isentropic accumulator operation. Because of their complex behavior, losses due to the secondary dissipative phenomena are not included in the two models developed in this chapter. The effects of cavitation, however, will be addressed in a more elaborate model presented in chapter 4.

The simple models in Fig. 3.1 show both the electrical and hydraulic analogies of a three-way step-down transformer. The assumption here is that I, C, and R are lumped parameters. I represents the fluid inertance of the tube, and C represents the fluid compliance of the accumulator. The resistance R, represents several different fluid flow resistances through the system. The first model will make simplifying assumptions on R so that the system equations can be solved analytically. The second model allows for a more complicated resistance R, so the efficiency analysis must be done numerically.

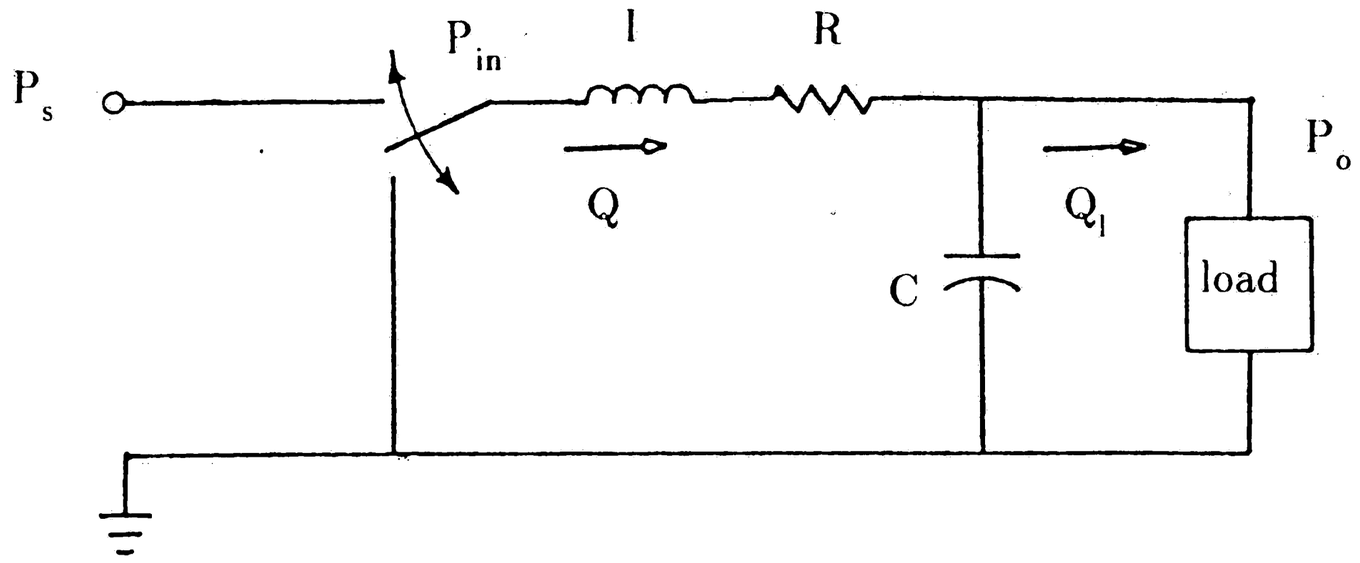

a. electrical

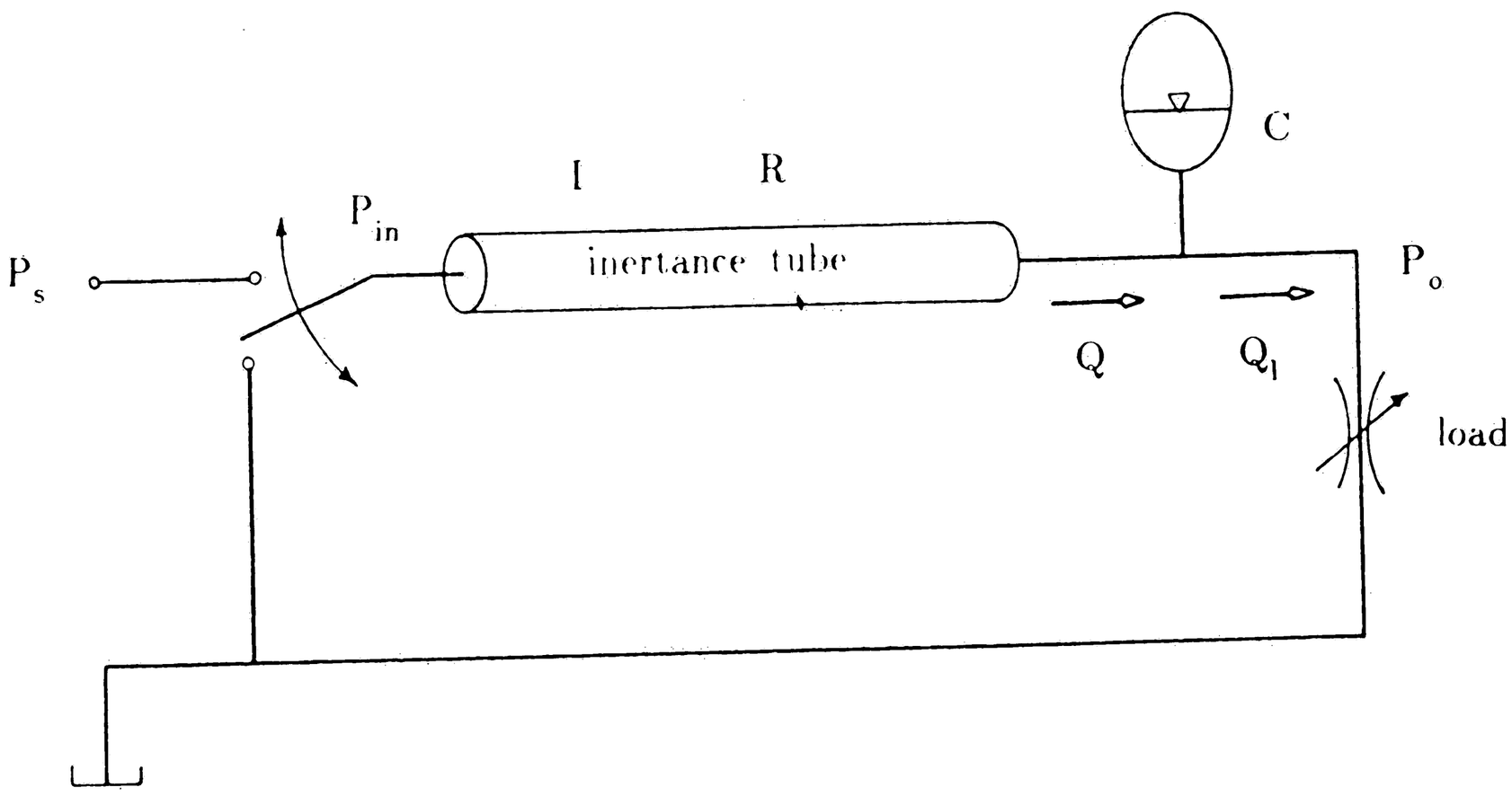

b. hydraulic

Figure 3-1: Three-way Step-down Transformers. (electrical and hydraulic)

3.1 Efficiency Analysis Using a Linear Model

The first model developed to analyze efficiency of the three-way step-down transformer assumes only linear behavior so that the system equations can be simplified enough to solve analytically. The lumped parameter C represents the compliance of the bladder accumulator. Any fluid compliance in the inertance tube is considered negligible and therefore ignored. Doing this immediatedly excludes wave propogation effects. The lumped parameter I represents the total inertance of the tube. Both I and C are considered to be constants. The resistance R, is a little more complicated than I or C, and is described below.

If we assume that the input signal is an ideal PWM pressure signal, flow through the inertance tube will be highly unsteady. This unsteadiness can cause the velocity profile to be slug-like, thus increasing shear forces near the wall. As a result we will express dissipative losses in the fluid channel due to resistance as a sum of two separate linear terms. First, there is the classical laminar steady flow resistance for fully developed pipe flow,

$$R_s = \frac{128\mu l}{\pi D^4}, \tag{3.1}$$

where μ is viscosity, and l and D are the inertance tube length and diameter respectively. The second term accounts for unsteadiness in the flow and is a frequency dependent resistance. The technique used to model this resistance was taken from Trikha [6]. The equations were modified to get them in a form compatible with state variable formulation. After doing this, the expression for total pressure drop in the inertance tube due to flow resistance becomes

$$\Delta P_r = R_s Q + R_s(y_1 + y_2 + y_3)/2 \tag{3.2}$$

with

$$y'_i = -n_i \frac{\nu}{A^2} y_i(t) + m_i Q'(t) \tag{3.3}$$

$i=1,2,3,$

where, $n_1=800$, $m_1=40$, $n_2=200$, $m_2=8.1$, $n_3=26.4$, $m_3=1.0$, and ν is the kinematic viscosity , A is the tube area, and Q is the flow through the tube (the primes indicate differentiation with respect to time).

Writing the state equations for the system of Fig. 3.1 in terms of pressure P and flow Q gives

$$IQ' = (P_{in} - P_o) - R_s Q - R_s(y_1+y_2+y_3)/2 \tag{3.4}$$

$$CP'_o = Q - Q_l, \tag{3.5}$$

where y_1, y_2, y_3 are defined in Eq. 3.3. Combining these linear equations gives a fourth order transfer function between Q and P_{in} of the form

$$\frac{Q(s)}{P_{in}(s)} = \frac{2(s^3+b_2s^2+b_1s+b_o)}{a_4s^4+a_3s^3+a_2s^2+a_1s+a_o}. \tag{3.6}$$

Converting this back to the differential equation form gives

$$a_4Q'''' + a_3Q''' + a_2Q'' + a_1Q' + a_oQ = 2(P_{in}''' + b_2P_{in}'' + b_1P_{in}' + b_oP_{in}). \tag{3.7}$$

Taking the Laplace transform of this differential equation and noting that P_{in} is a step input, so that

$$P_{in}(s) = (P_s - P_t)/s \quad or \quad (F_t - P_s)/s, \tag{3.8}$$

we get a new fifth order Laplace transform equation,

$$\frac{Q(s)}{Q_o} = \frac{s^4+A_3s^3+A_2s^2+A_1s+A_o}{s(a_4s^4+a_3s^3+a_2s^2+a_1s+a_o)/a_4}, \tag{3.9}$$

where Q_o is Q(0) and the constants A_3, A_2, A_1, and A_o become functions of b_2, b_1, b_o, $(P_{in}-P_o)$, and the initial conditions of $P_{in}(t)$ and Q(t). The problem is that the initial conditions of Q(t) and its derivatives are unknown. Once the

roots of the denominator in Eq. 3.9 are known, the inverse Laplace transform can be taken from McCollum and Brown [7] as,

$$Q(t) = \frac{2b_o \Delta P}{b_4 \lambda_1 \lambda_2 \lambda_3 \lambda_4} + C_1 e^{-\lambda_1 t} + C_2 e^{-\lambda_2 t} + C_3 e^{-\lambda_3 t} + C_4 e^{-\lambda_4 t}, \tag{3.10}$$

where λ_1, λ_2, λ_3, λ_4 are the roots of the denominator in Eq. 3.9, and C_1, C_2, C_3, C_4 are functions of A_1, A_2, A_3, A_4 in Eq. 3.9 and λ_1, λ_2, λ_3, λ_4 (see appendix). Therefore, for a given value of ΔP the flow $Q(t)$ is known as a function of its initial conditions.

The objective now is to find an analytical expression for $Q(t)$ over one complete period of the input signal with the flow at an equilibrium condition. To do this it is necessary to divide the period T into two parts. We then write Eq. 3.10 for each part to give expressions for $Q_1(t)$ and $Q_2(t)$, where the subscripts indicate part one and two. $Q_1(t)$ is written in terms of its initial conditions, and $P_{in}(s)$ is $(P_s-P_t)/s$ and $P_{in}(t=0)$ is P_t-P_s. Similary, $Q_2(t)$ is written in terms of its initial conditions, but with $P_{in}(s)=(P_t-P_s)/s$ and $P_{in}(t=0)$ $=P_s-P_t$. If the period T is divided so that the first piece has a duration of αT and the second $(1-\alpha T)$, then by continuity $Q_1(t)$ and $Q_2(t)$ can be related as follows (primes indicate differention with respect to time):

$$Q_1(t=0) = Q_2(t=(1-\alpha)T) \tag{3.11}$$

$$Q_1'(0) = Q_2'((1-\alpha)T)$$

$$Q_1''(0) = Q_2''((1-\alpha)T)$$

$$Q_1'''(0) = Q_2'''((1-\alpha)T)$$

$$Q_2(t=0) = Q_1(t=\alpha T)$$

$$Q_2'(0) = Q_1'(\alpha T)$$

$$Q_2''(0) = Q_1''(\alpha T)$$

$$Q_2'''(0) = Q_1'''(\alpha T).$$

These relations can be substituted back into the expressions for the constants C_1, C_2, C_3, and C_4, in Eq. 3.10. The result is a system of eight linear algebraic equations that must be solved to give the constants C_1, C_2, C_3, and C_4 for both $Q_1(t)$ and $Q_2(t)$. Going through this exercise requires a substantial amount of algebra. The appendix gives a brief outline of the procedure. The result however is a solution for Q(t) of the form,

$$Q(t)=\begin{cases} Q_1(t) & 0<t<\alpha T \\ Q_2(t) & \alpha T<t<T \end{cases} \tag{3.12}$$

It is now possible to define energy efficiency for a three-way transformer with this analytical expression for Q(t). Fig. 3.2 shows a typical plot of Q(t) for α equal to about 0.75. Between t=0 and t=αT, P_{in} equals P_s so that energy into the system is

$$E_1 = P_s\int_0^{\alpha T} Q(t)dt. \tag{3.13}$$

Then for the rest of the period, P_{in} equals P_t so that

$$E_2 = P_t\int_{\alpha T}^{T} Q(t)dt. \tag{3.14}$$

In the case when $P_t$is zero, E_2 equals zero. The energy out of the system is simply

$$E_{out} = P_o\int_0^{T} Q(t)dt \tag{3.15}$$

where $P_o$is the filtered time average output pressure. The system efficiency for a three-way set up becomes

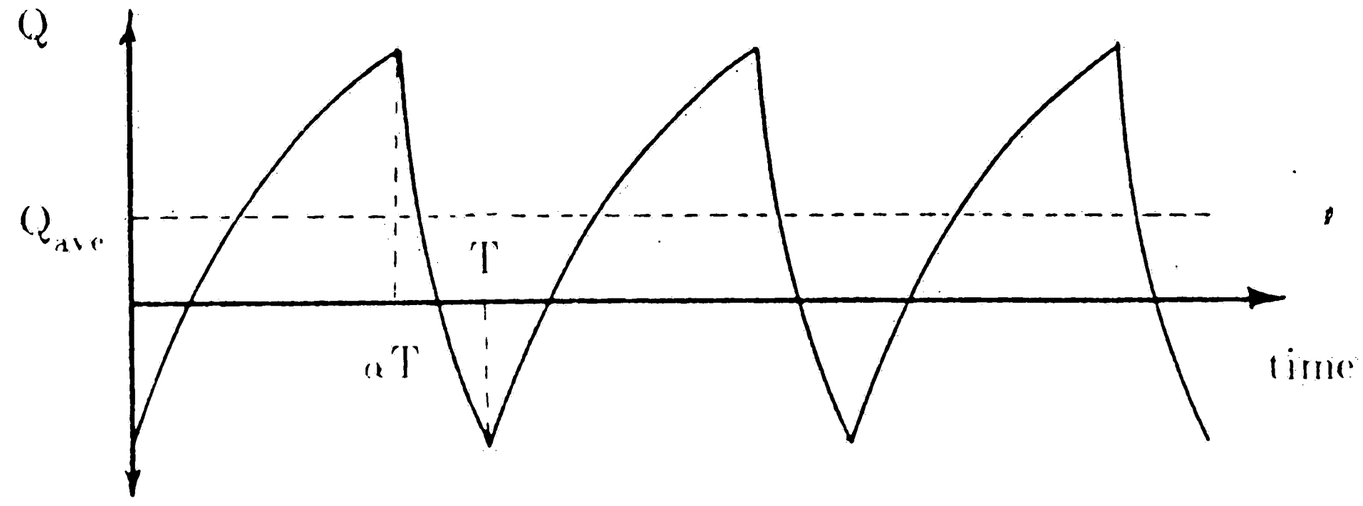

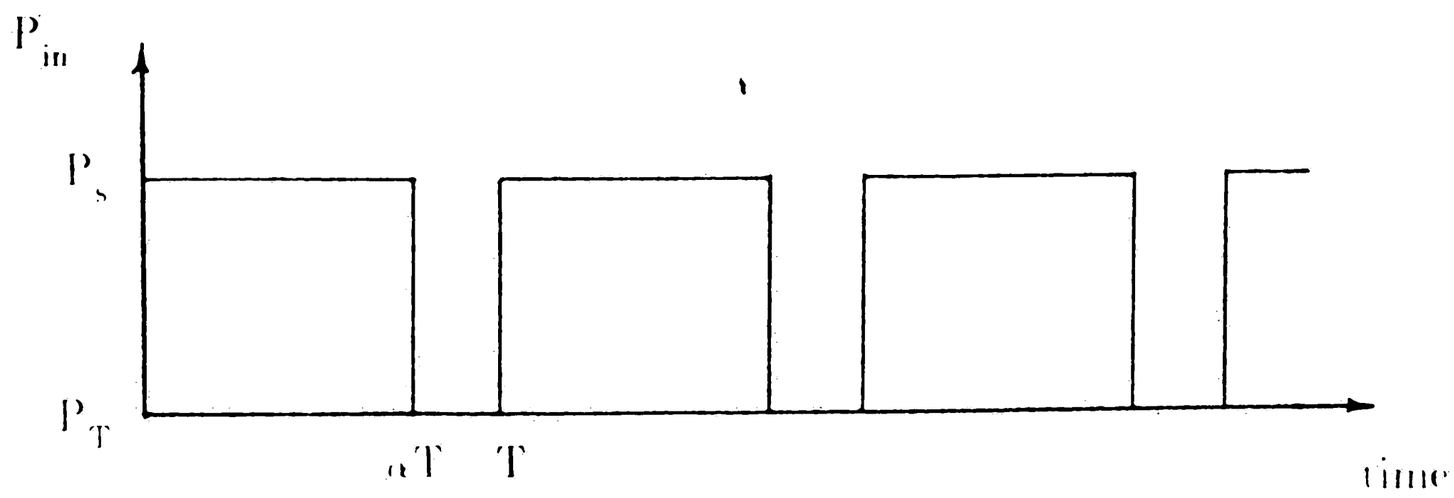

Figure 3-2: Typical Q(t) vs time for α = 0.75

$$\eta = \frac{E_{out}}{E_{in}} = \frac{E_{out}}{E_1 + E_2} = \frac{P_o Q_{ave} T}{E_1 + E_2}, \tag{3.16}$$

This is easily expanded to the four-way set-up suggested in Fig. 1.3. Because the system is symmetric, the energy lost on one side equals that lost on the other side. Taking this into account, the energy efficiency for a four-way set-up is

$$\eta = \frac{(2P_o - P_s)Q_{ave}T}{2(E_1 + E_2)} - 1 \tag{3.17}$$

This analysis was performed and the results are given in Fig. 3.3 for a four-way valve set-up. The plot shows constant efficiency lines for two different values of the parameter $\omega I/R_s$. The P_l and Q_l curves for different control positions are simply straight lines of slope $1/R_s$ because the system equations are linear. The interesting point here is that for flows above about 3% of Q_{max}, the switched-inertance transformer is considerably more efficient than conventional flow control valves which have an efficiency equal to P_l/P_s.

3.2 Non-linear Model Efficiency Analysis

A second efficiency analysis was performed using a slightly more complicated model than that in section 3.1. The same lumped model configuration of Fig. 3.1 can be applied in this case. I and C are defined exactly the same as they were in the first model. The difference this time is that additional terms were added to the flow resistance expression.

The first model accounted for laminar steady flow resistance and frequency dependent resistance only. Minor losses, or entrance and exit losses were ignored in an effort to keep the system equations linear. These losses are proportional to the square of the flow and are quite important even at small average

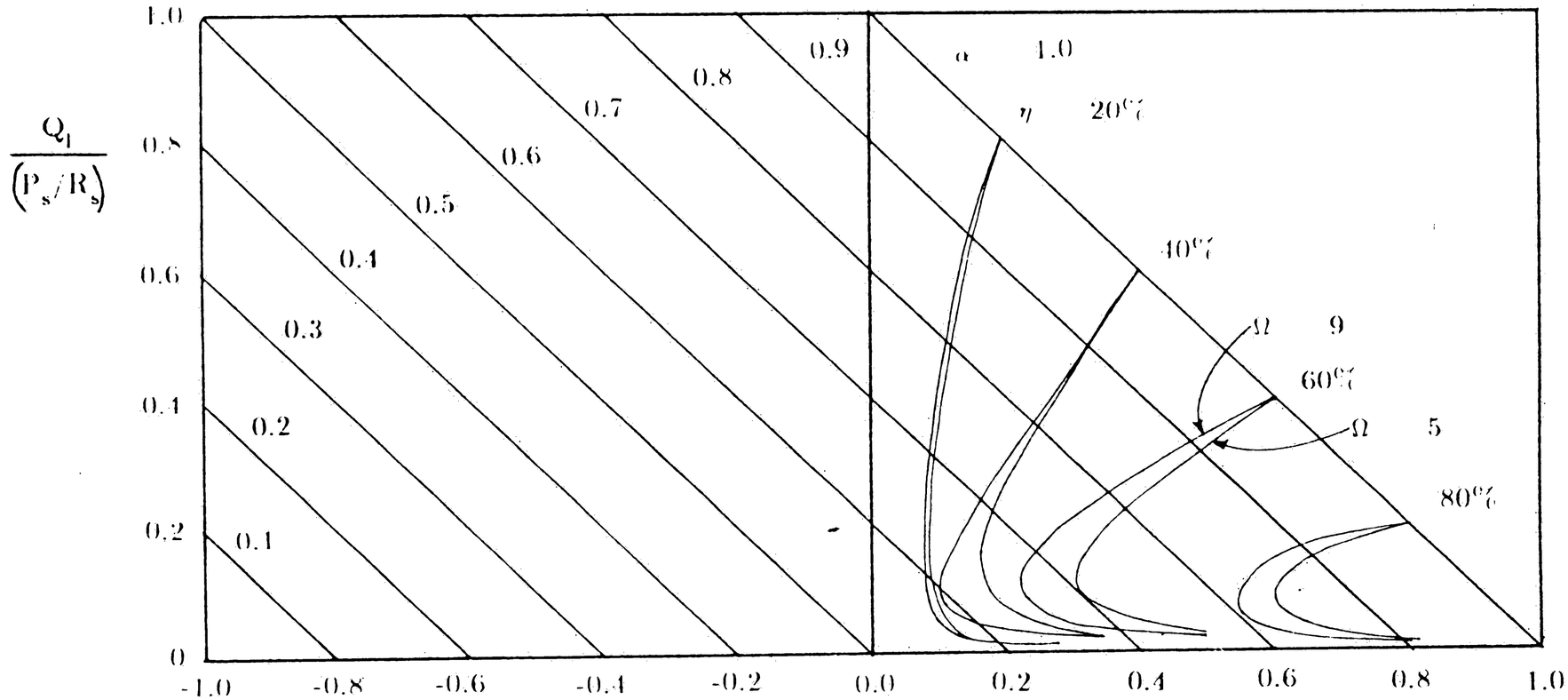

Figure 3-3: Flow vs Pressure characteristics and constant efficiency lines for four-way set-up using linear model

output flows, since instaneous flow can be quite high. The pressure drop due to these entrance and exit losses is approximately 2.53 dynamic head losses assuming that inlets are slightly rounded [8], or

$$\Delta P_m = 2.53 \frac{\rho Q^2}{2A^2} \tag{3.18}$$

where A is the cross-sectional area of the tube.

Another resistance to fluid flow is present because the input switching signal is not ideal. The rotary switching valve presented in chapter 2 suggests that flow goes through orifices that are opening and closing with time. These orifices were designed to be relatively large over most of the cycle so losses due to them would be very small. However, during brief periods of each cycle, when the openings are just closing and then opening again, these orifice areas get very small. When this happens the fluid inertia tries to keep the flow moving and thus it is possible to have high pressure drops, but only for a brief portion of the cycle. To account for this loss, the following procedure was performed.

Fig. 3.4 shows how typical flows through the valve are expected to behave. The key point here is that the flow does not drop to zero at the point of switching. In fact it is at a maximum or minimum. The opening and closing of orifices in the valve are modeled directly as functions of time in chapter 4. During the early stages of developing the chapter 4 model it was shown that flow through the switching valve does looks something like Fig. 3.4, thus indicating that substantial energy losses may occur during the brief switching period. Of course fluid compliances are present in the real system to absorb some of this effect, but presently we will ignore them for simplification. To quantify these effects, Q_{max} and Q_{min} were assumed to be constant for a period

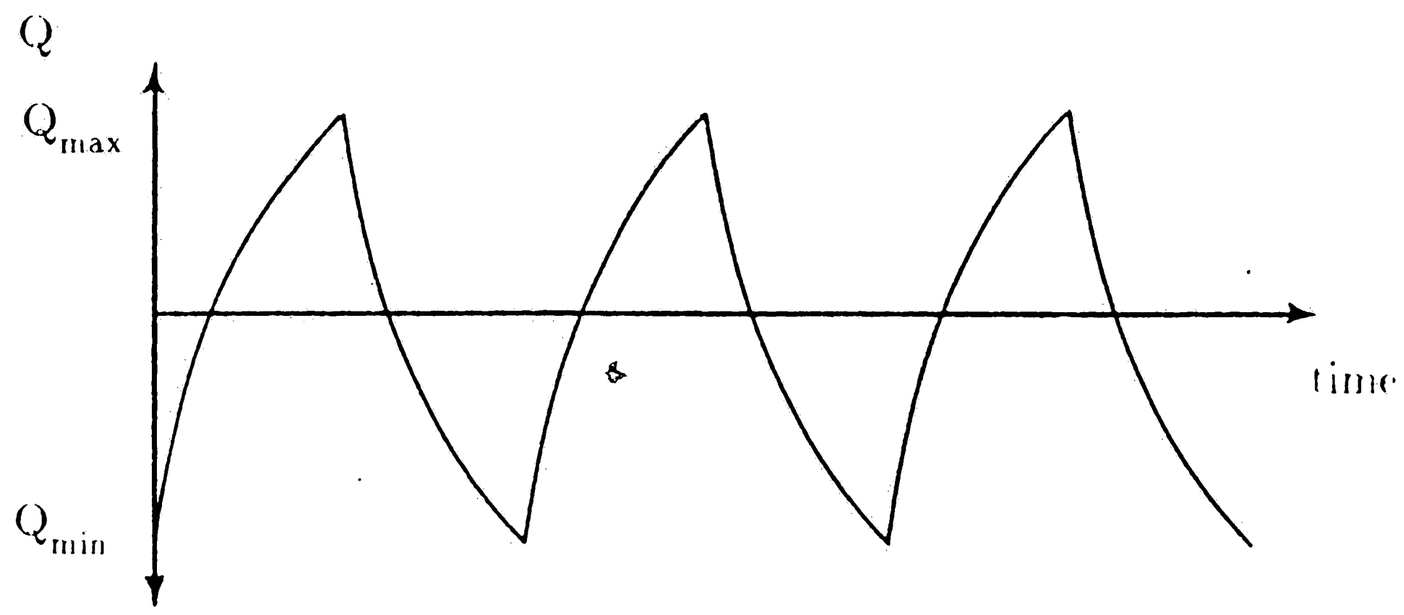

a 0.5 Q_{ave} 0

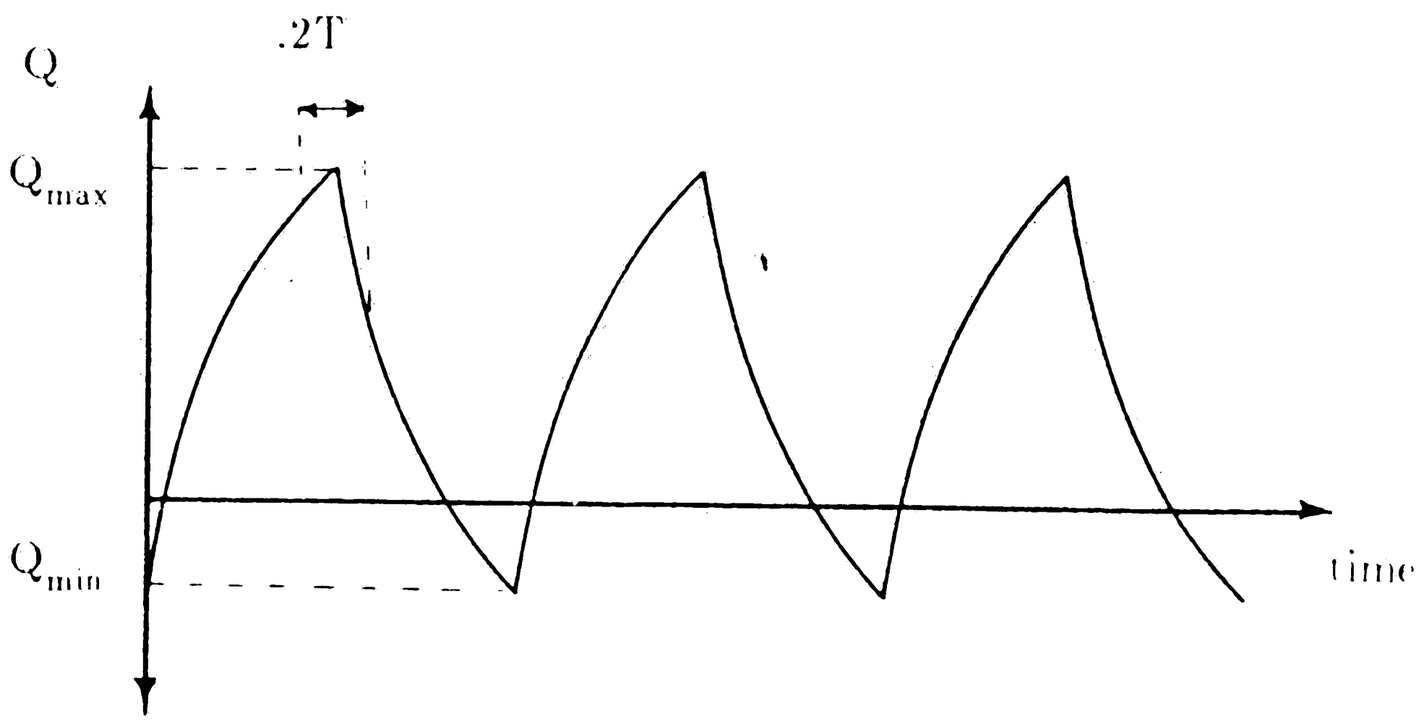

a 0.5, Q_{ave} 0

Figure 3-4: Expected flows through valve

of approximately 0.1T on each side of the switch. With this assumption, and an expression for the orifice area as a function of time, the pressure drop could be written as

$$\Delta P = \frac{Q^2 \rho}{2A^2(t)c_d}. \tag{3.19}$$

Then the power dissipated due to this effect is,

$$Power = \Delta PQ, \tag{3.20}$$

where Q is either Q_{max} or Q_{min}. Integrating this power over each switch in a cyle gives the energy dissipated for one cycle as

$$E = \int_{-0.1T}^{+0.1T} \Delta PQ_{max} dt - \int_{-0.1T}^{+0.1T} \Delta PQ_{min} dt, \tag{3.21}$$

with the appropriate time dependent areas used. Therefore this energy E represents the energy dissipated over one period T, due to the fact that flows can be quite high when the valve orifices are switching from P_s to P_t or vice-versa.

E can now be evaluated for different conditions of α and various average flows Q_{ave}. This was done numerically using a fourth order Runge-Kutta integrator to give a set of E's. Again, to simplify the calculations it was assumed that Q_{max}-Q_{min} equaled a constant, ΔQ, and that Q_{ave} equaled $(Q_{max}+Q_{min})/2$. The results showed the approximate relationship

$$\Delta E = E - E_o = K_o \, Q_{ave}^{\,2}, \tag{3.22}$$

where, E_o stands for E, when Q_{ave} equals zero. The constant K_o depends on the rate at which orifices within the valve open and close, and on the chosen value for ΔQ. Note that this expression is independent of α, probably due to some of the simplifying assumptions that were made. Next by letting average

power dissipated equal $\Delta P_{ave} Q_{ave}$ we can say

$$\Delta P_{ave} Q_{ave} = (E-E_o)/T = K_o Q_{ave}^2/T, \tag{3.23}$$

or,

$$\Delta P_{ave} = \frac{K_o}{T} Q_{ave}. \tag{3.24}$$

K_o was found to be 1.07 (kPa-sec)/liter, for the specific case of ΔQ equal to .328 liters/sec, a pressure drop across the valve of P_s-P_T = 4.14 MPa, and the orifice areas defined by the valve design in Figs. 2.6 and 2.7 operating at 500 Hz.

The development of Eq. 3.23 may seem inexact and somewhat questionable over a wide range of flows. It does however serve in helping to quantify orifice flow losses due to switching in the valve and is included in the second model. Therefore, Eq. 3.18 and Eq. 3.23 are added to Eq. 3.2 to give a new expression for pressure drop in the second model,

$$\Delta P_r = R_s Q + R_s(y_1+y_2+y_3)/2 + 1.265 \frac{\rho Q^2}{A^2} + \frac{K_o}{T} Q. \tag{3.25}$$

This expression is substituted into Eq. 3.4 to complete the second model.

Because of the Q^2 term, the system equations are non-linear. Therefore they were evaluated numerically, again using a fourth order Runge-Kutta integrator. The efficiency η was defined the same as it was for the first model. P_s and P_T were set equal to 4.14 MPa and 0 MPa respectively to correspond with experimental data presented in chapter 5. Fig. 3.5 shows a plot of Q_{ave} or Q_l versus P_l for different control positions of α, along with lines of constant efficiency. Comparing these results with those given in Fig. 3.3, we see that efficiency has decreased, especially at large flows. Still, the efficiency is better than that of a conventional flow control valve. A final point to notice is the

slope of the characteristic lines for zero load flow. If we graphically linearize P_l versus Q_l in Fig. 3.5 near the P_l axis, the ratio P_l/Q_l equals about 5.5 (MPa-sec)/liter.

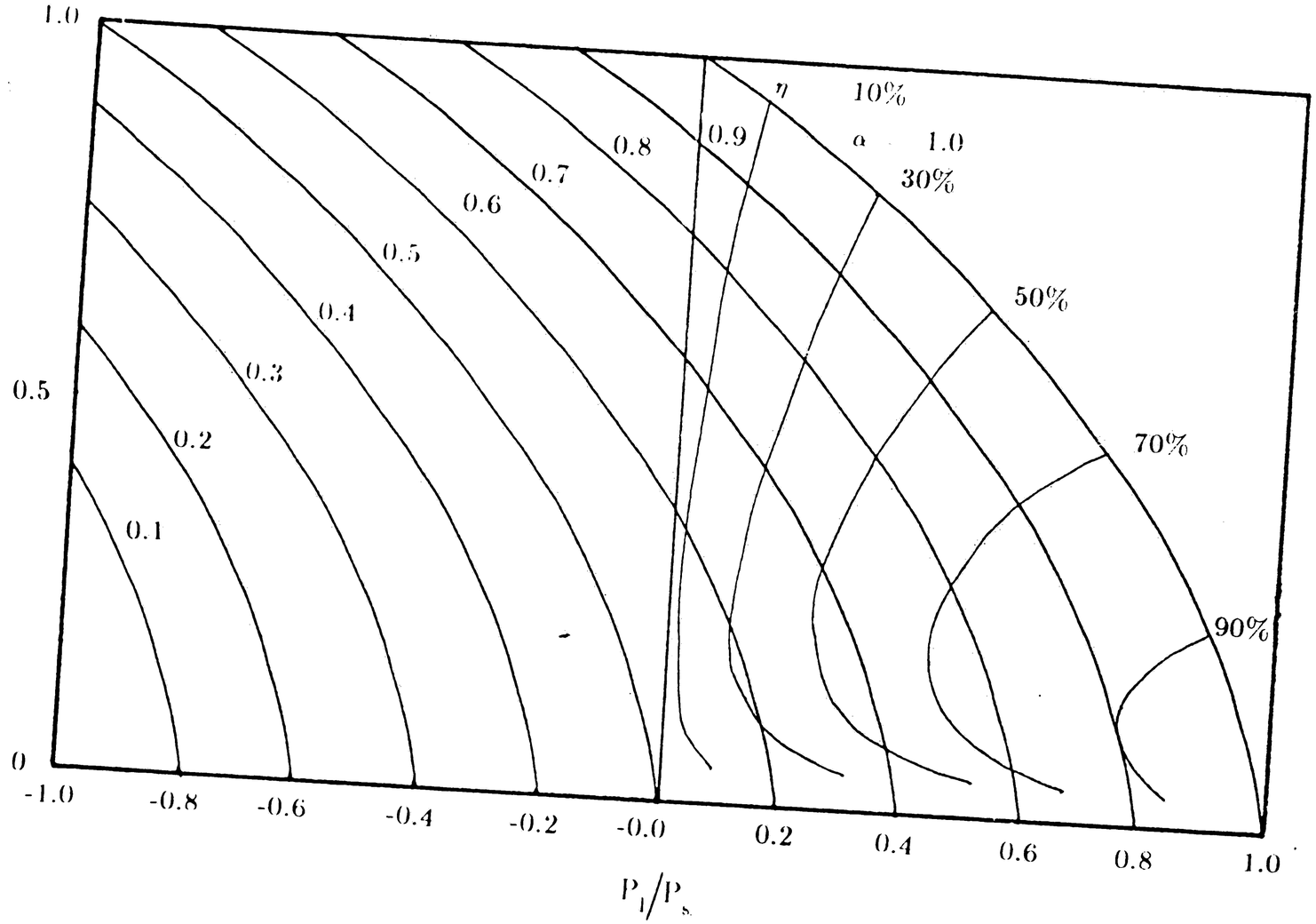

Q_{max} .315 liters/sec. f = 500 hz.

P_s 4.14 MPa tube length = 10.16 cm.

Figure 3-5: Flow vs Pressure characteristics and constant efficiency lines for four-way set-up using non-linear model

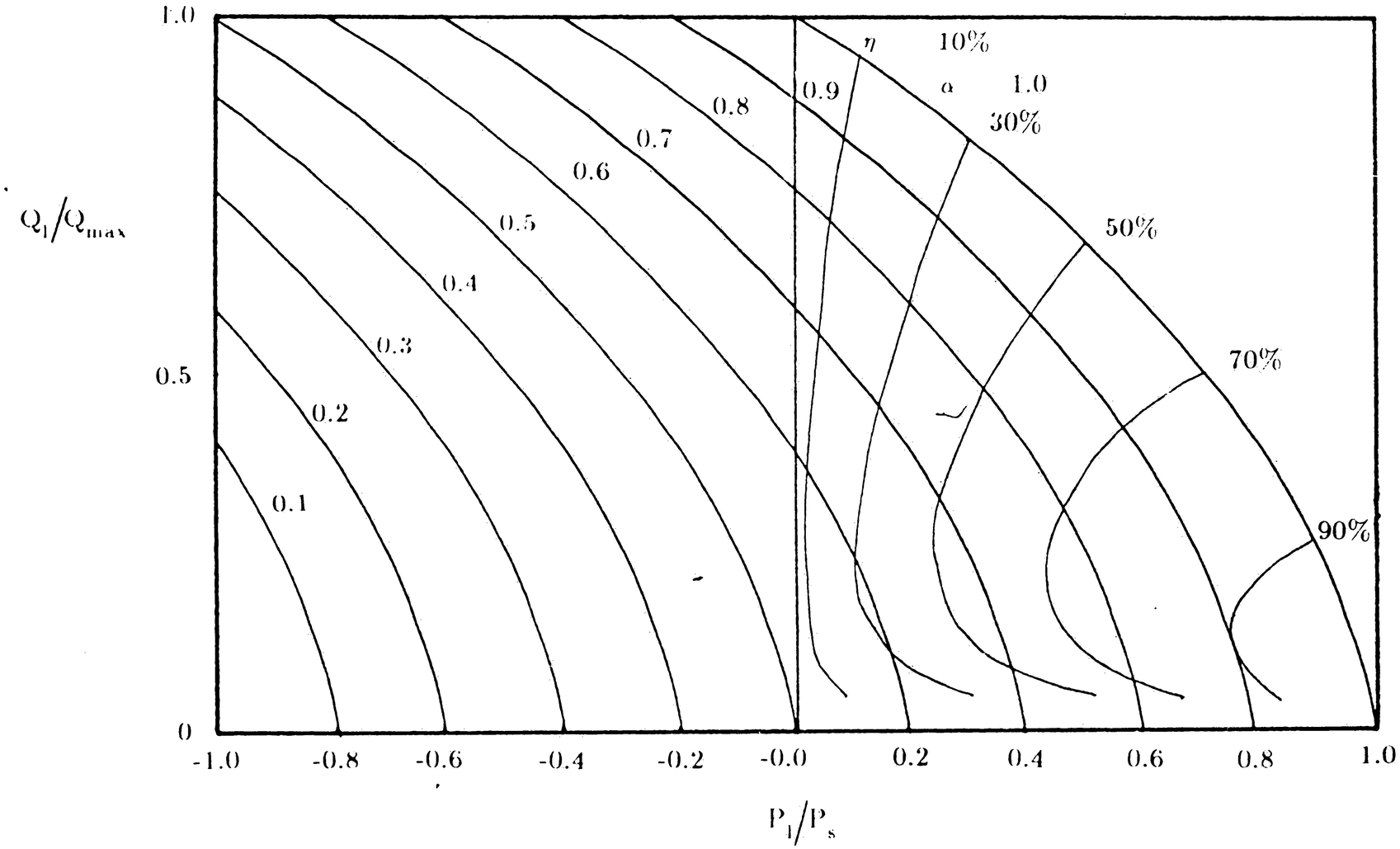

Q_{max} .315 liters/sec. f = 500 hz.

P_s 4.14 MPa tube length = 10.16 cm.

Figure 3-5: Flow vs Pressure characteristics and constant efficiency lines for four-way set-up using non-linear model

Chapter 4
Simulation Model

The design and analysis of hydraulic systems is often complicated by the effects of inherent non-linear phenomena. In general, these effects may become increasingly more important as dynamic response times get faster and faster. Since switched-inertance hydraulics uses high speed fluid switching (in our case 500 Hz), these non-linear phenomena may be very important. Understanding their behavior is then useful in designing and evaluating a switched-inertance system.

There are basically three separate phenomena which we would like to model. First, is the presence of non-linear resistances. They may result from either orifice flow or entrance and exit losses in channel flow. Secondly, there is cavitation. Because flows in a switched-inertance system are expected to surge back and forth in response to a PWM signal, it is likely that pressures may dip down to zero, developing a cavitation bubble. Lastly, there will undoubtedly be wave propogation effects since the hydraulic fluid in the line has compliance.

Minimizing certain undesirable effects may be possible with careful component design. For example, proper inertance tube design is crucial to the system's performance. As stated in chapter 1, we want the inertance I as large as possible, yet at the same time fluid resistance needs to be kept at a tolerable level. Since $I = \rho l/A$, we can increase the inertance by either making the tube longer or the area A smaller. The resistance is decreased by making the tube shorter or the area bigger. To minimize wave propagation effects inside the tube, its length needs to be small relative to the wave length. The rule of

thumb we are using is that tube length should not exceed 1/20 of a wave length in order for propagation effects to be kept at a tolerable level [1]. Therefore, as stated earlier some compromise between inertance I, and fluid resistance needs to be chosen. Once chosen, this compromise and the rule of thumb need to be evaluated. Cavitation is another effect that may be lessened by properly designing fluid compliances into the system. The linear differential equation relating pressure to flow is

$$\frac{dP}{dt} = \frac{1}{C}\Delta Q. \tag{4.1}$$

During a period of time, if ΔQ is negative, it is possible for the pressure to dip below zero. However, increasing C will slow down the rate at which the pressure drops, thereby reducing the chance of cavitation. For these reasons we need to develop a model of the rotary switching valve and the inertance tube that can be simulated on a computer.

4.1 Dynamic Model

This section develops a lumped model for the rotary switching valve and inertance tube, switched-inertance system. The variables used in this model are the same as defined earlier (ie: V=volume of fluid, β=bulk modulus, P=pressure, etc). It also uses the relations,

$$\frac{dP}{dt} = P' = \frac{\Delta Q}{C}$$

$$\frac{dQ}{dt} = \frac{\Delta P}{I}$$

and the orifice flow equation

$$Q = Ac_d(\frac{2}{\rho}\Delta P)^{1/2}.$$

To begin we will start by modeling an inertance tube alone. Fig 4.1

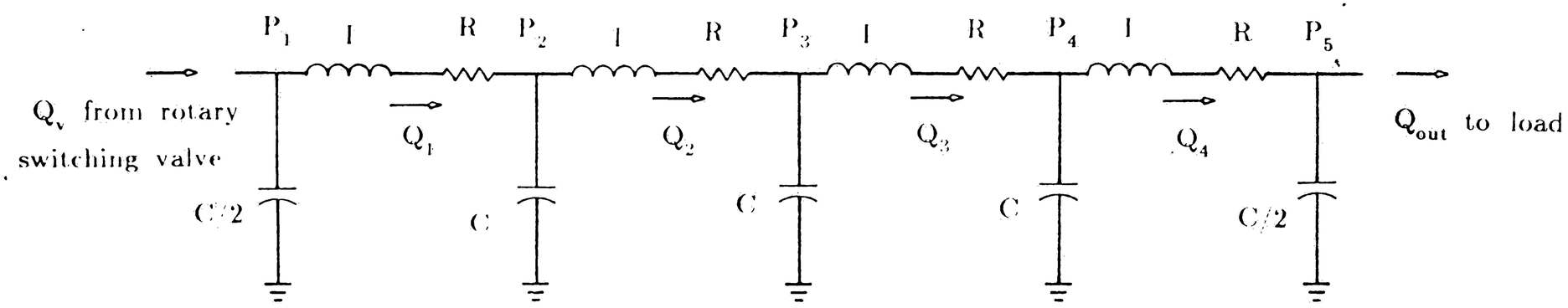

Figure 4-1: Lumped model of inertance tube

shows this model. The tube is divided into four equal sections or lumps so that wave propogation effects may be observed. The inertances I, each represent one fourth of the total tube inertance, ie $4I=I_t$. Similarly, each compliance C equals one fourth the total compliance in the tube so $4C=C_t$. Tube flow resistances are essentially the same for this model as those developed in section 3.2, however, dividing them up between four sections is slightly more complicated than dividing up I_t and C_t. Because the tube is split into four sections, the steady laminar tube flow resistance R_s given by Eq 3.1 and the frequency dependent resistance given by Eqs 3.2 and 3.3 are split evenly between the four section. Dynamic head losses are not distributed along the length of the tube. Instead they occur only at the tube inlet defined by the flow direction. With this model, differential equations can be written for the pressures and flows within the inertance as

$$\frac{C}{2} P_1' = Q_v - Q_1 \tag{4.2}$$

$$IQ_1' = (P_1 - P_2) - RQ_1 - R(y_{11}+y_{12}+y_{13})/2 - .664\ Q^2$$

$$CP_2' = Q_1 - Q_2$$

$$IQ_2' = (P_2 - P_3) - RQ_2 - R(y_{21}+y_{22}+y_{23})/2, \quad etc.,$$

where $R = R_s/4$, and subscript i of y_{ij} indicates the section of tube being described. All together this gives five pressure equation, four flow equations and twelve y_{ij} equations, just to describe the inertance tube, as yet without cavitation.

The next step is to model the pressures and flows within the rotary switching valve of Fig. 2.6. This model is shown in Fig. 4.2. The resistances R_1 and R_2 represent orifice type losses that occur due to the rotor opening and

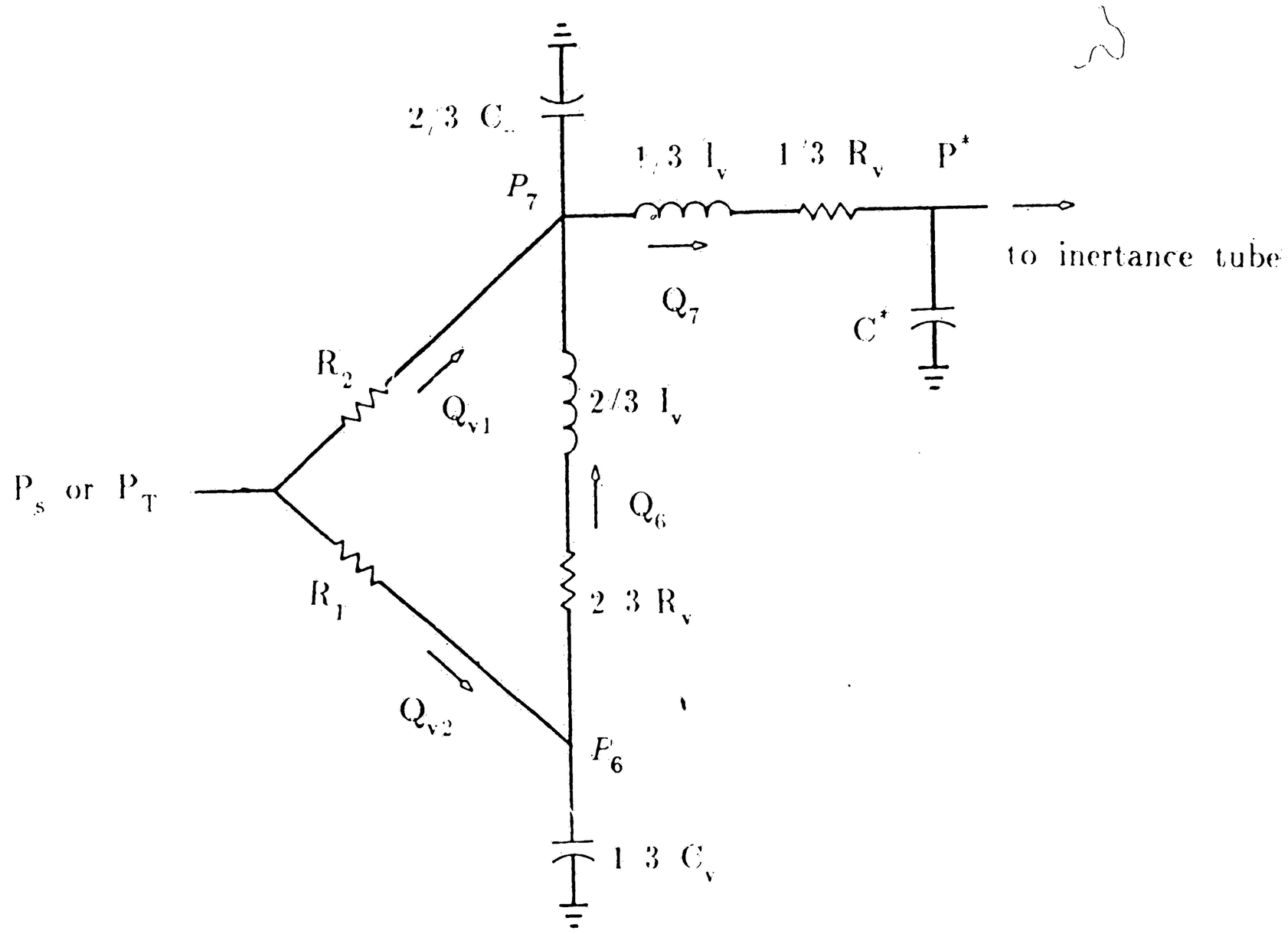

Figure 4-2: Lumped model of rotary switching valve

closing orifices in the valve as it spins. By studying Fig. 2.5 it is apparent that flow from either P_s or P_T must pass through two time dependent orifices before reaching the inertance tube. Writing square law equations for each orifice and then combining them gives,

$$Q_{v1} = A_1(t)A_2(t)\left(\frac{2(P_{in}-P_7)}{\rho(A_1^2(t)+A_2^2(t))}\right)^{1/2} \tag{4.3}$$

$$Q_{v2} = A_3A_4\left(\frac{2(P_{in}-P_6)}{\rho(A_3^2+A_4^2)}\right)^{1/2}$$

where P_{in} is the input pressure P_s or P_T. The areas A_1,A_2, A_3, and A_4 are all known functions of time as the rotor spins. C_v, l_v, and R_v represent the compliance, inertance and resistance respectively of a porting annulus in the stator. In this case, R_v is a steady laminar flow resistance only. Frequency dependent resistance could have been added, but was not because of the added complexity. The compliance C^* accounts for a volume of fluid present at the connection between the valve and inertance tube.

The differential equations for the switching valve are therefore:

$$\frac{1}{3}C_vP_6' = Q_{v2}-Q_6 \tag{4.4}$$

$$\frac{2}{3}C_vP_7' = Q_{v2}+Q_6-Q_7$$

$$\frac{2}{3}I_vQ_6' = P_6-P_7-2R_vQ_6/3$$

$$\frac{1}{3}I_vQ_7' = P_7-P^*-R_vQ_7/3.$$

Now if we attach these to the inertance tube, $P^* = P_1$, $Q_7 = Q_v$, and the compliances C^* and C combine to give the first equation in Eq. 4.2 as,

$$(C_t/8+C^*)P_1' = Q_7-Q_1.$$

The model in Fig. 4.2 assumes that P_s and P_T are supplied directly to the

valve. Actually, this is not so because flow from the pump must travel through long fluid lines which have both inertance and compliance. In addition, in practice an accumulator was added where P_s and P_T connect to the valve to help stabilize these pressures. Fig. 4.3 shows a model of the fluid lines and accumulator between the pump and valve. I_l, C_l, and R_l stand for the fluid line inertance, compliance, and resistance. C_A represents the compliance of the added external accumulator, and I_A the inertance leading into that accumulator. The differential equations are

$$\begin{aligned} C_A P_A' &= Q_A \\ C_l P_s^{*\prime} &= Q_s - Q_A - (Q_{v1} + Q_{v2}) \\ I_l Q_s' &= P_s - P_s^* - R_l Q_s \\ I_A Q_A' &= P_s^* - P_A - R_A Q_A. \end{aligned} \tag{4.5}$$

A similar model is then used for the line between the tank and the valve. This part of the model can be connected into the valve model simply be letting P_s and P_T in Fig. 4.2 become P_s^* and P_T^* respectively, so that P_{in} in Eq. 4.3 is either P_s^* or P_T^*.

If an accumulator is added to the load end of the inertance tube, the IC filter discussed in chapter 1 is complete so that,

$$(C_t/8 + C_A) P_5' = Q_4 - Q_{load}, \tag{4.6}$$

with Q_{load} dependent on the load characteristics.

All three pieces can be joined together to give a lumped model for three-way operation of the system. Expanding to four-way operation only requires putting two three-way models together. Fig. 4.4 shows the lumped model for four-way operation.

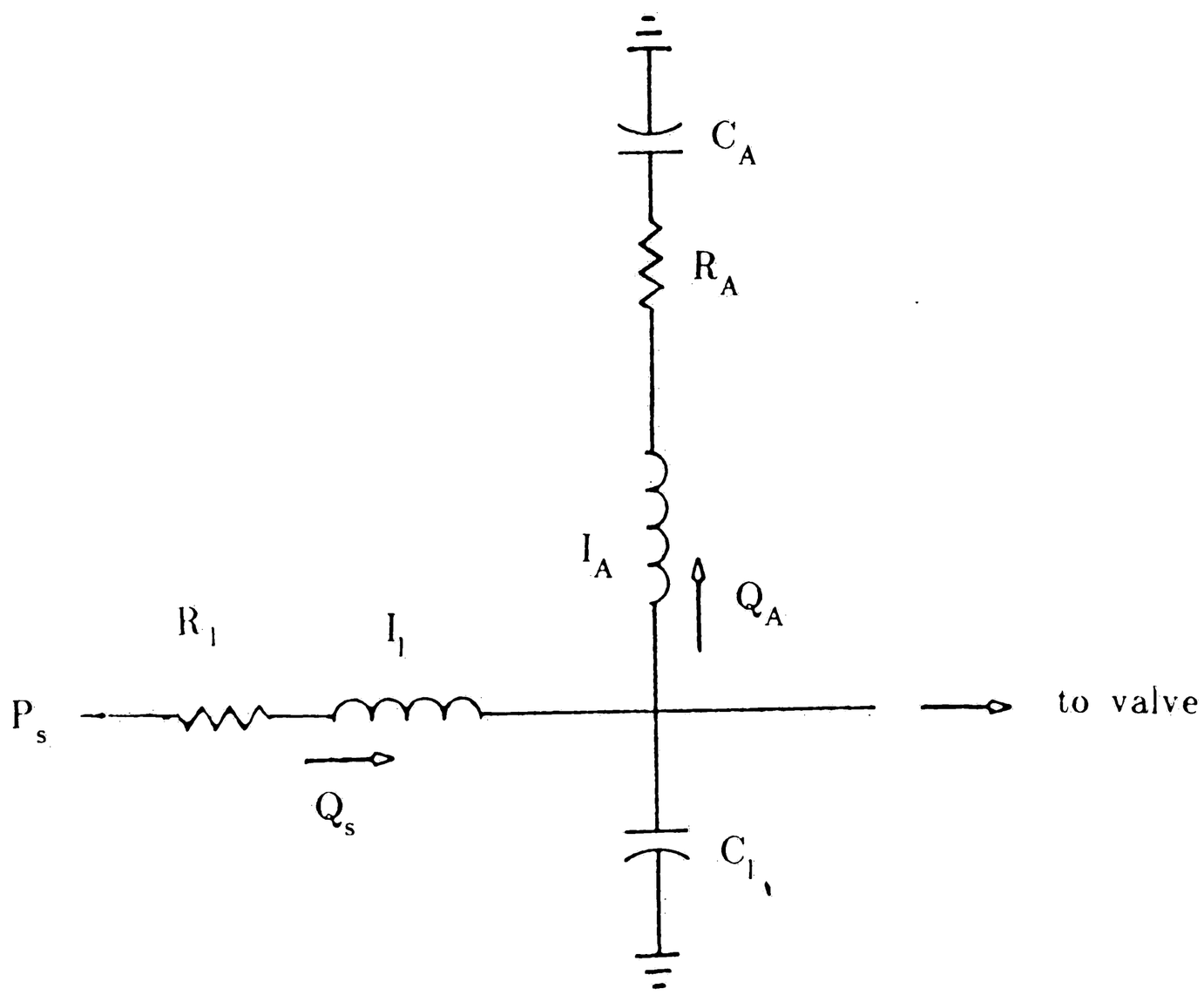

Figure 4-3: Lumped model of fluid lines and accumulator before the valve

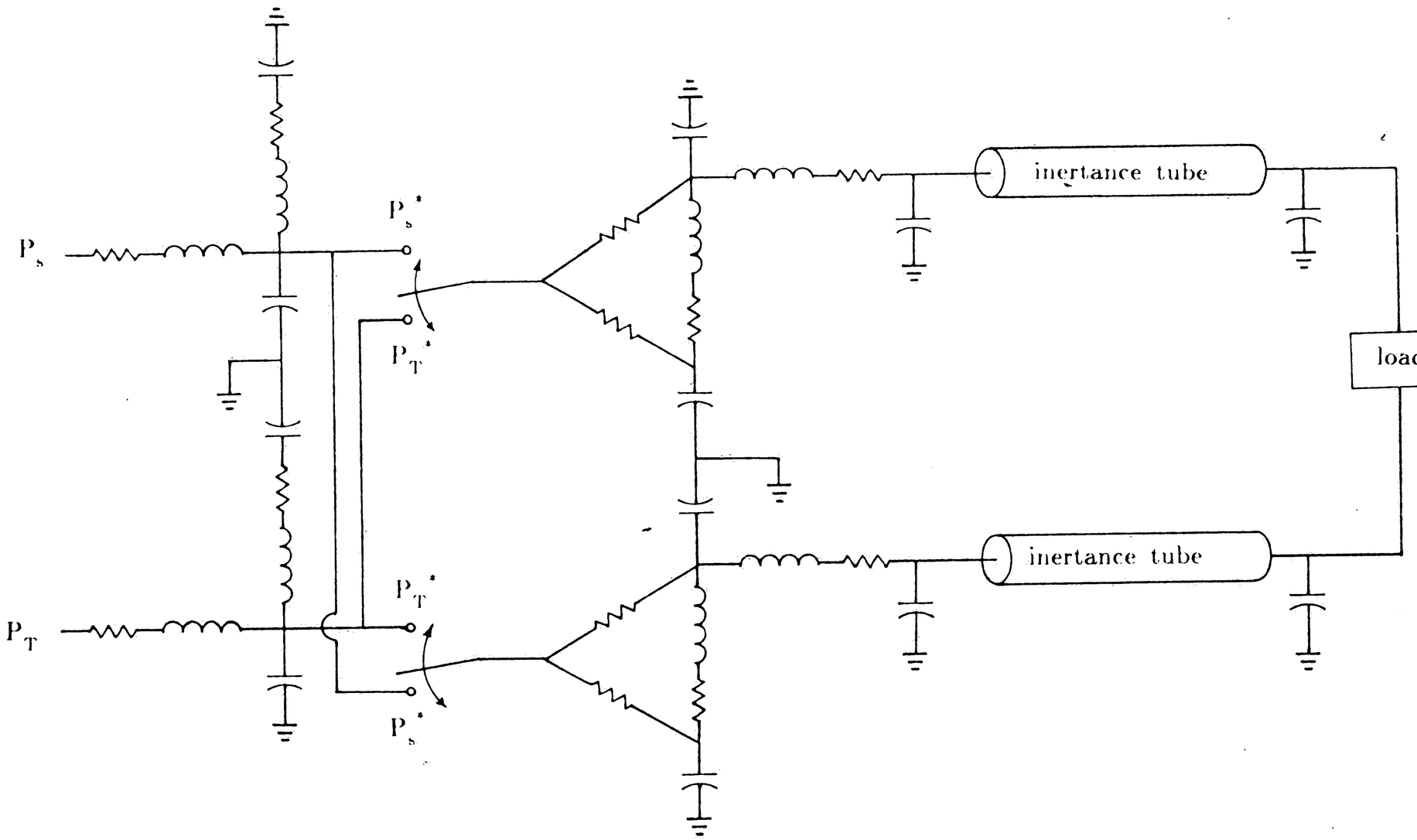

Figure 4-4: Lumped model of four-way operation

Up to this point, the model cannot account for cavitation. To do so, we have to introduce a new state variable at any place where pressures are suspected to drop below zero. For example, to include cavitation at P_2 in Fig. 4.1, define a new variable V. When P_2 is greater than zero, there is no cavitation so V=0 and V′=0. However, when a simulation of the model detects that P_2 is trying to go below zero, it simply does not allow it to do so by setting P_2=0 and P_2′=0. At the same time a cavitation bubble starts to develop so V′=Q_2-Q_1. This bubble V, is integrated in time until it falls back to zero. Once this occurs V′ is reset to zero and P_2 continues on according to Eq. 4.2. The model simulated by the author included cavitaion at P_1, P_2,P_3, for both intertance tubes and at P_T*.

One final feature was added into the model to predict flow forces acting on the control shaft. According to Merritt [8] the flow forces in a valve are

$$F = \frac{\rho Q^2}{A} cos\theta \quad with\ \theta=69^o. \tag{4.7}$$

In terms of the rotating switching valve, Q is Q_{v1} and Q_{v2}, and A is the respective orifice area. This force can be related to a torque by

$$torque = 2Fr, \tag{4.8}$$

where r is the length of the torque arm. Integrating this torque over time and then dividing by time will give an average torque felt by the control shaft,

$$average\ torque = \frac{2}{T}\int_0^T \frac{2\rho Q^2}{A} cos\theta\ r\ dt. \tag{4.9}$$

At this stage the model is rather lengthy. There is a total of 64 state variable differential equations, and many of them are extremely non-linear. To simulate this model the entire set of equations defining the system were com-

piled together in FORTRAN. A fourth-order Runge-Kutta variable step integrator then numerically integrated the system. Because of its size, extremely non-linear behavior, and high frequencies present, the simulation required a very small time step to keep everything stable. As a result the computing time was very long so the model was only simulated for about ten switches at three different conditions.

4.2 Simulation Results

The following values defining the resistances, compliances, inertances, etc., were evaluated for the rotary valve, inertance tube, and test set-up equipment and then used in the computer simulation:

A_{max} = maximum orifice area within valve = 2.58 cm^2

C_A = compliance of load and accumulator = 7.6 * 10^{-13} m^5/N

C_V = accumulator compliance at P_s and P_T inlet ports to the valve = 7.6 * 10^{-13} m^5/N

C_l = compliance of fluid lines between the pump/tank and the rotary switching valve = 2.139 * 10^{-15} m^5/N

C_t = inertance tube compliance = 1.29 * 10^{-15} m^5/N

C_v = compliance in rotary valve = 2.567 * 10^{-15}

C^* = compliance at valve and inertance tube connection = 0.0 (omitted)

I_A = inertance leading into accumulator = 1.051 * 10^5 kg/m^4

I_l = inertance of fluid lines between the pump/tank and the rotary valve = 3.366 * 10^6 kg/m^4

I_t = inertance of inertance tube = 1.051 * 10^7 kg/m^4

I_v = inertance in rotary valve = 7.70 * 10^5 kg/m^4

L = length of ineratnce tube = .102 m

P_{Supp} supply pressure = 4.24 MPa

P_{Tank} return or tank pressure = .23 MPa

R_A = linear resistance leading into accumulator = 9.25 (MPa-s)/m^3

R_l = linear resistance of fluid lines between the pump/tank and the valve = 16.6 (MPa-s)/m^3

R_s = linear laminar resistance of inertance tube = 580 (MPa-s)/m^3

R_v = linear resistance in valve = 67 (MPa-s)/m^3

ρ = fluid density = 833.5 kg/m^3

ω = switching frequency = 3143 rad./s

The valve was simulated at three different contitions. They are:

1. α=0.5, P_s=4.24 MPa, P_T=.23 MPa, Q_{load}=0.
2. α=0.75, P_s=4.24 MPa, P_T=.23 MPa, Q_{load}=0.
3. α=0.75, P_s=4.24 MPa, P_T=.23 MPa, Q_{load} about .1 liters/sec.

all with switching frequency of 500 Hz. The next several pages give these results. (Refer to Figs. 4.1, 4.2, 4.3, and 4.4 for corresponding variables.)

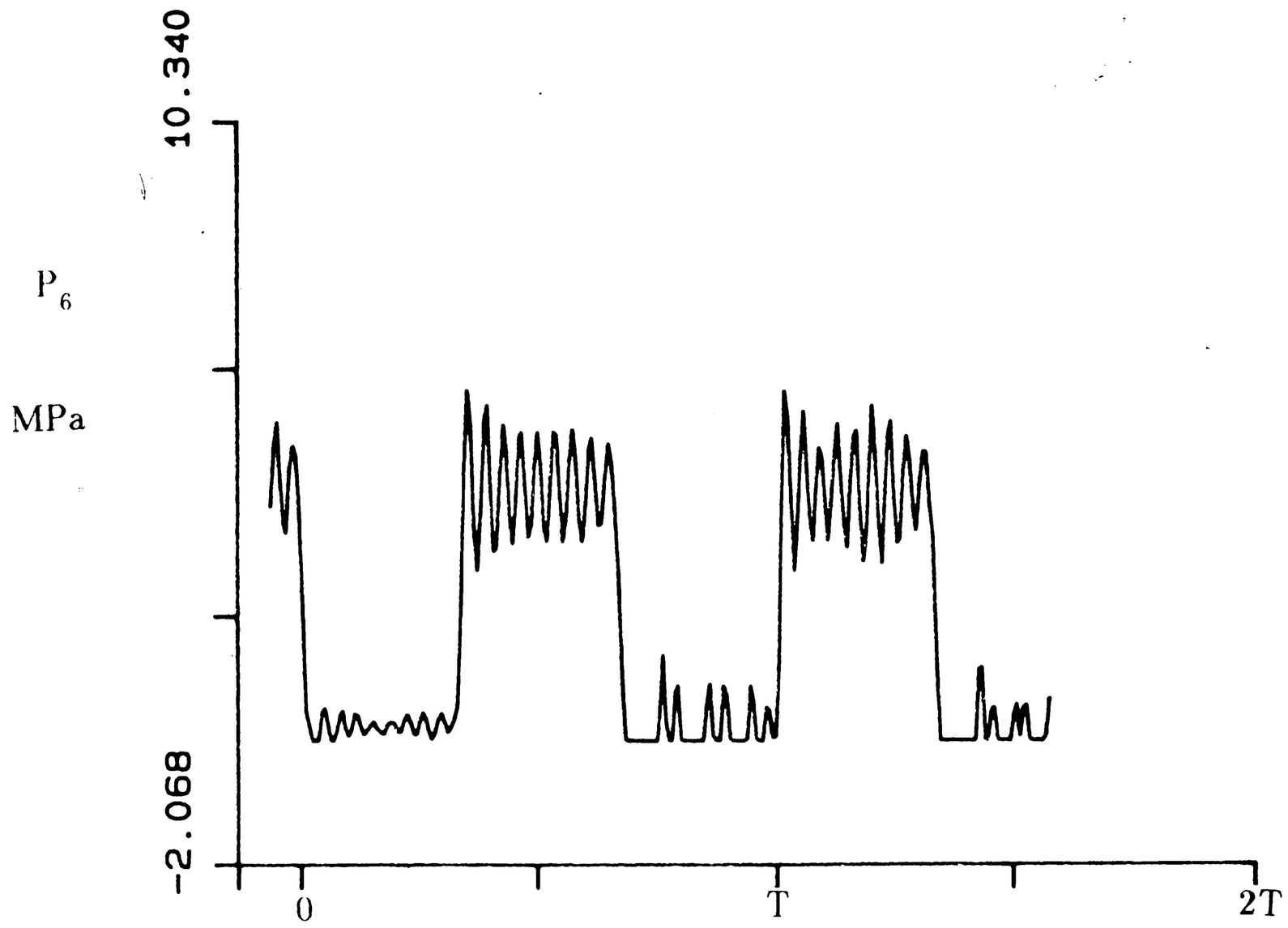

Figure 4-5: Case 1 - Pressure P_6 inside the valve (see Fig. 4.2)

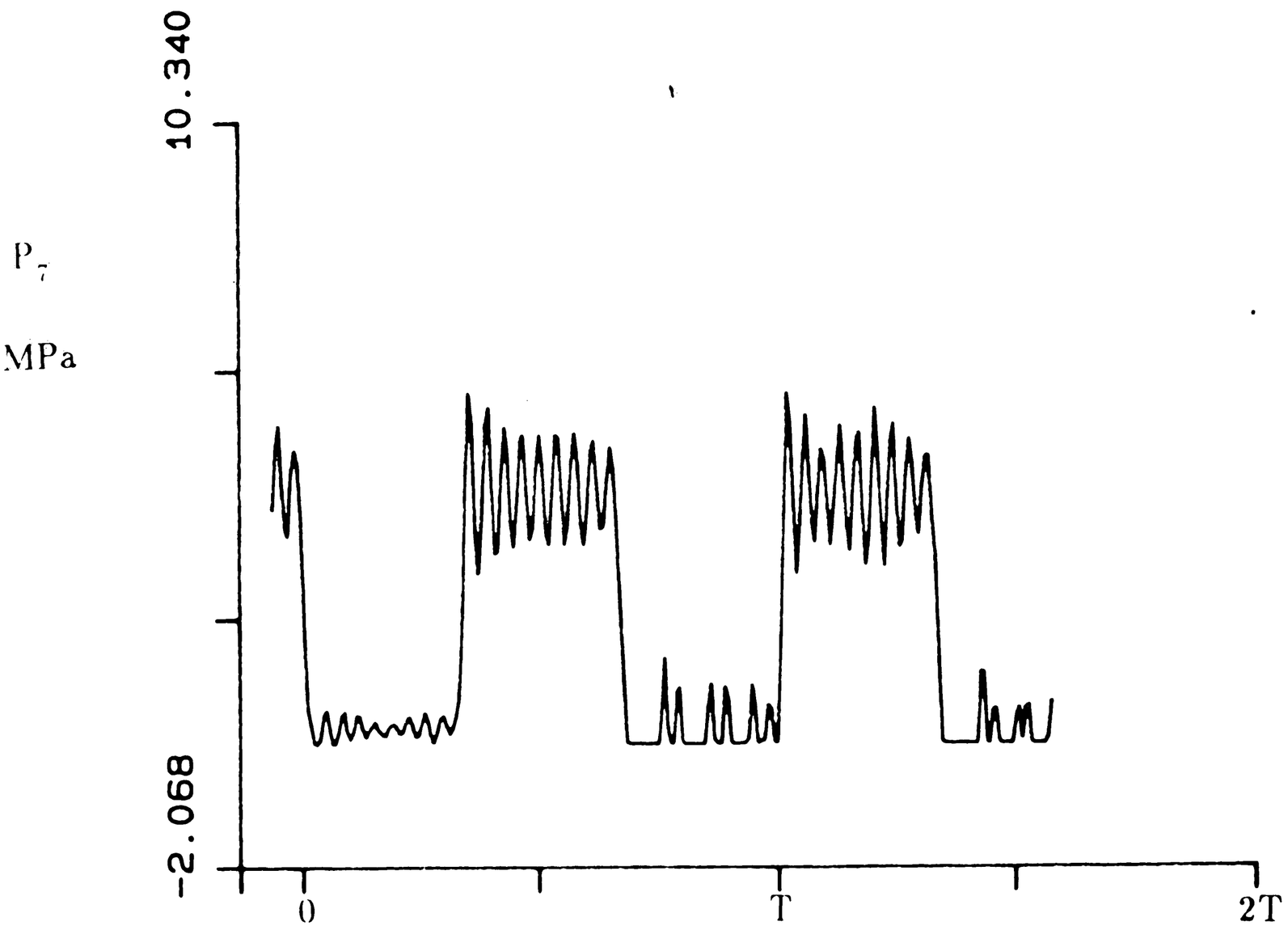

Figure 4-6: Case 1. Pressure P_7 inside the valve (see Fig. 4.2)

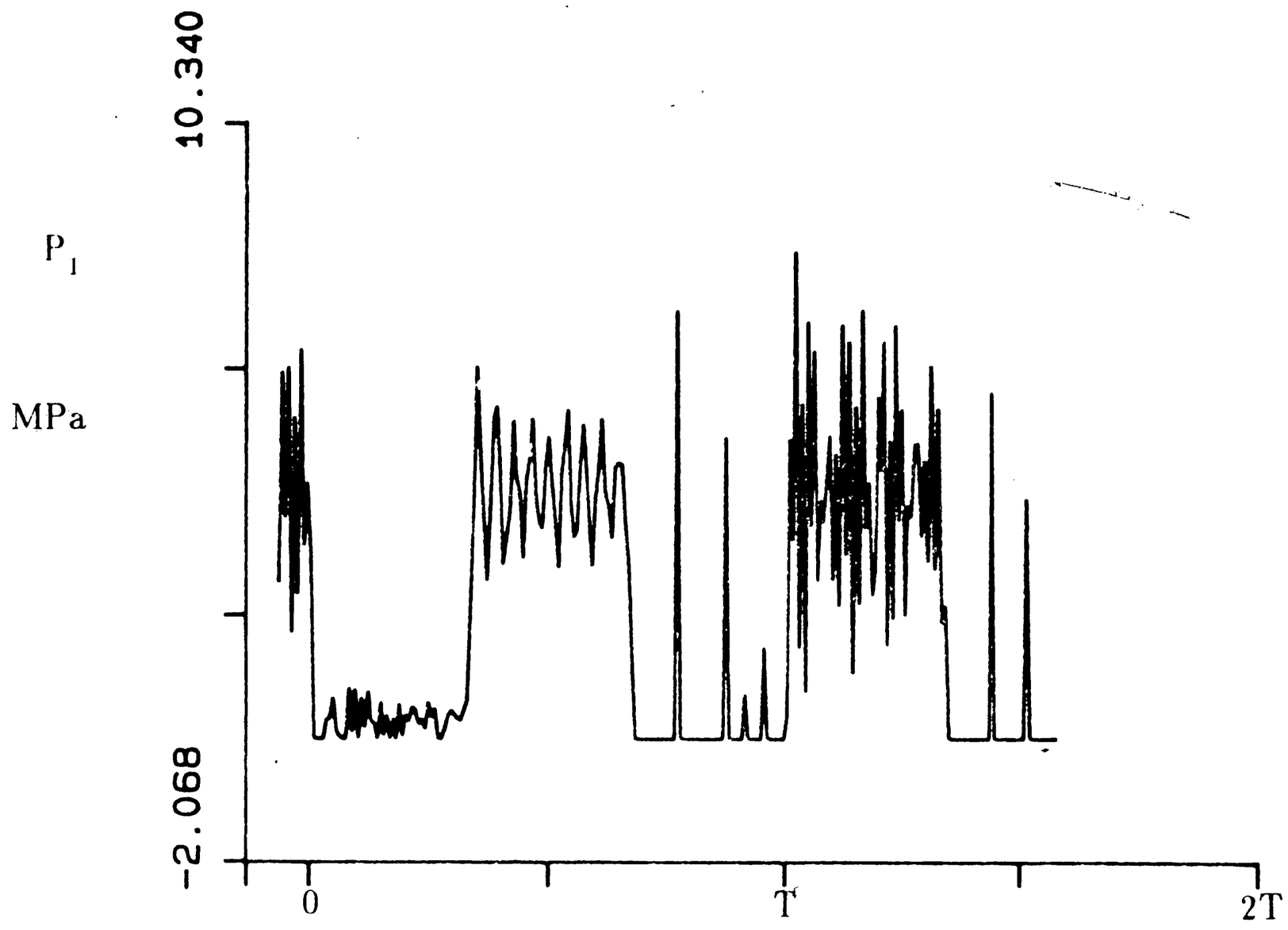

Figure 4-7: Case 1. Pressure P_1 at beginning of inertance tube (see Fig. 4.1)

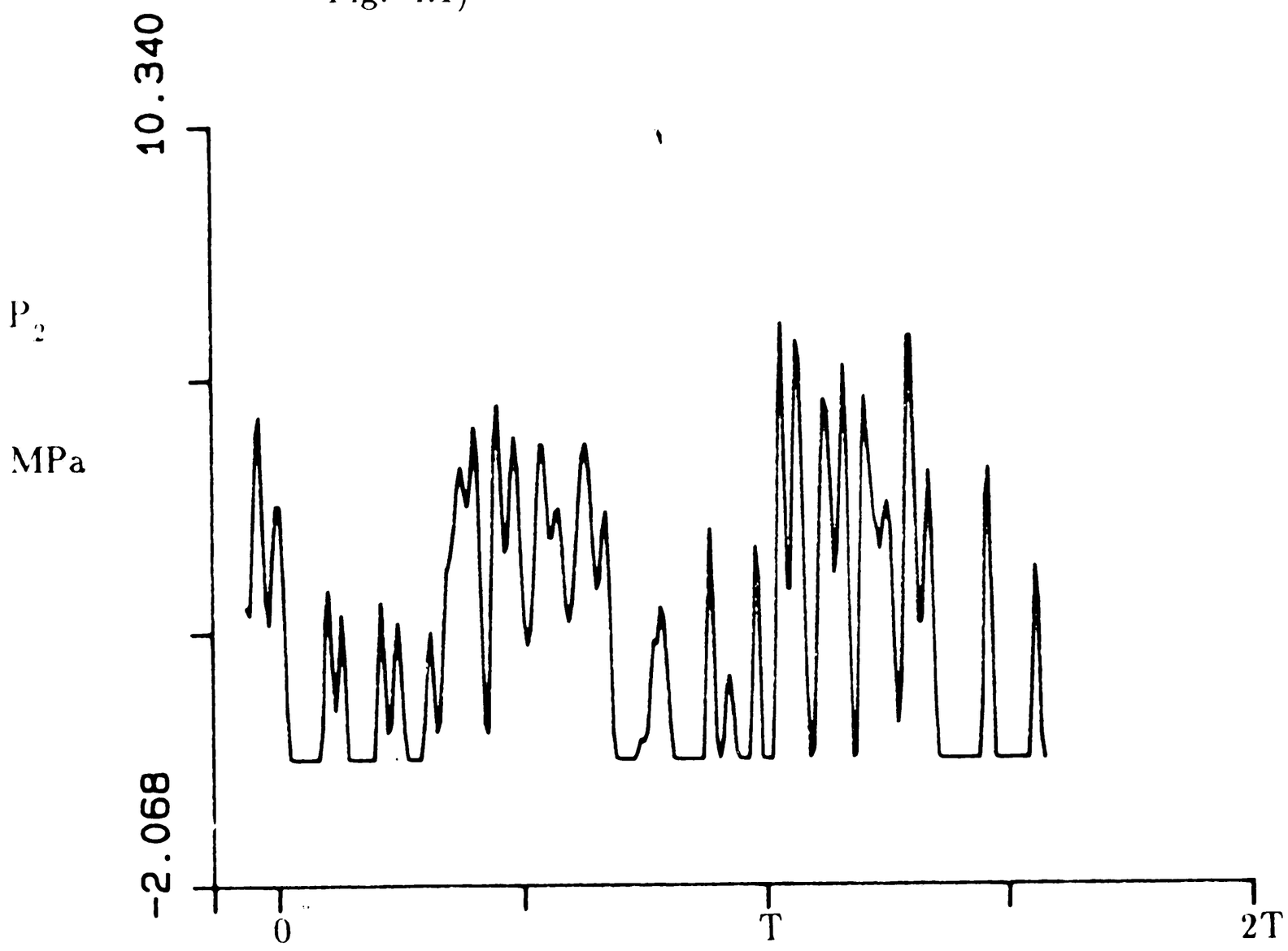

Figure 4-8: Case 1. Pressure P_2 in the inertance tube (see Fig. 4.1)

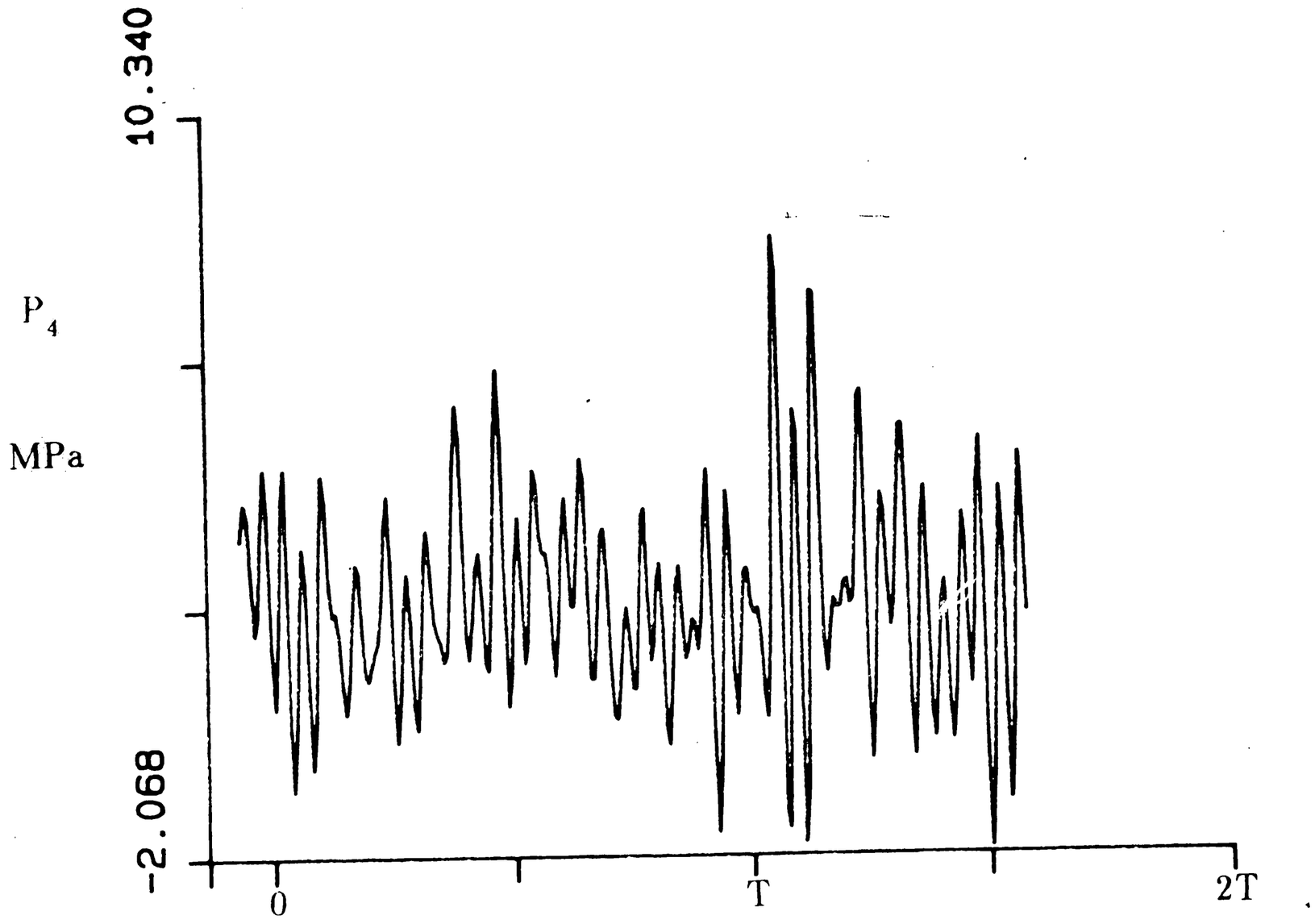

Figure 4-9: Case 1. Pressure P_4 in the inertance tube (see Fig. 4.1)

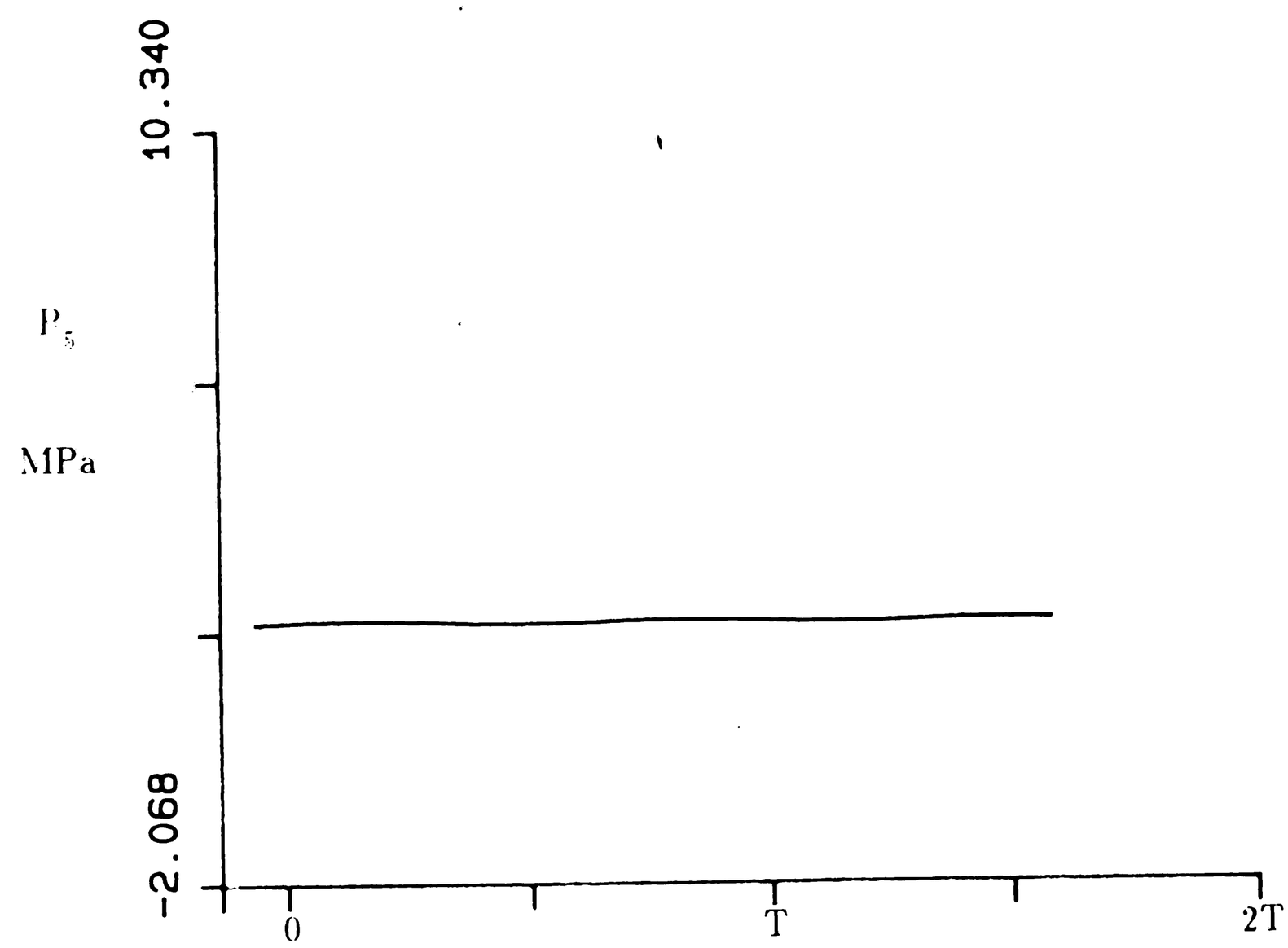

Figure 4-10: Case 1. Pressure P_5 at end of inertance tube (see Fig. 4.1)

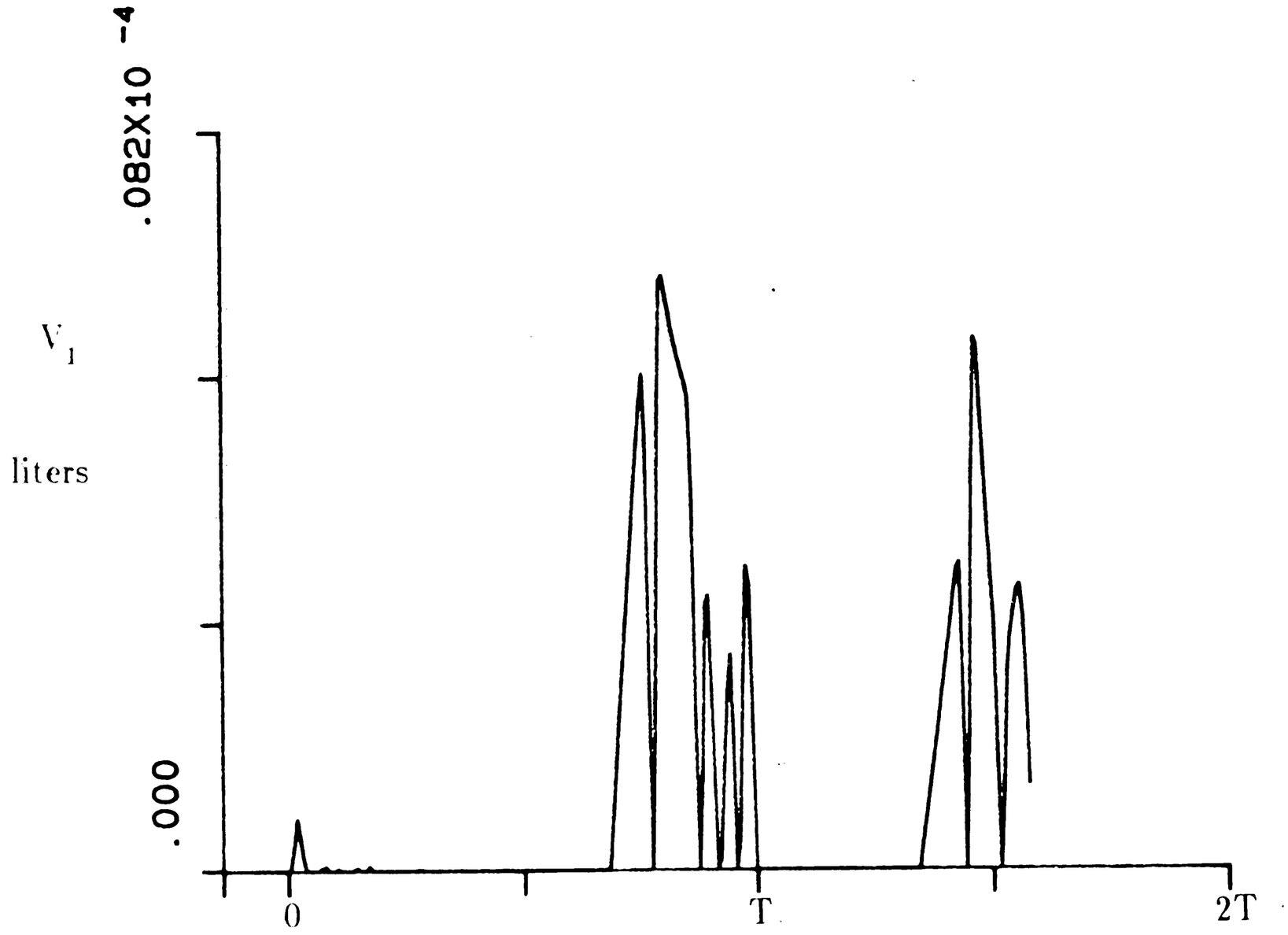

Figure 4-11: Case 1. Cavitation bubble at P_1, beginning of inertance tube (see Fig. 4.1)

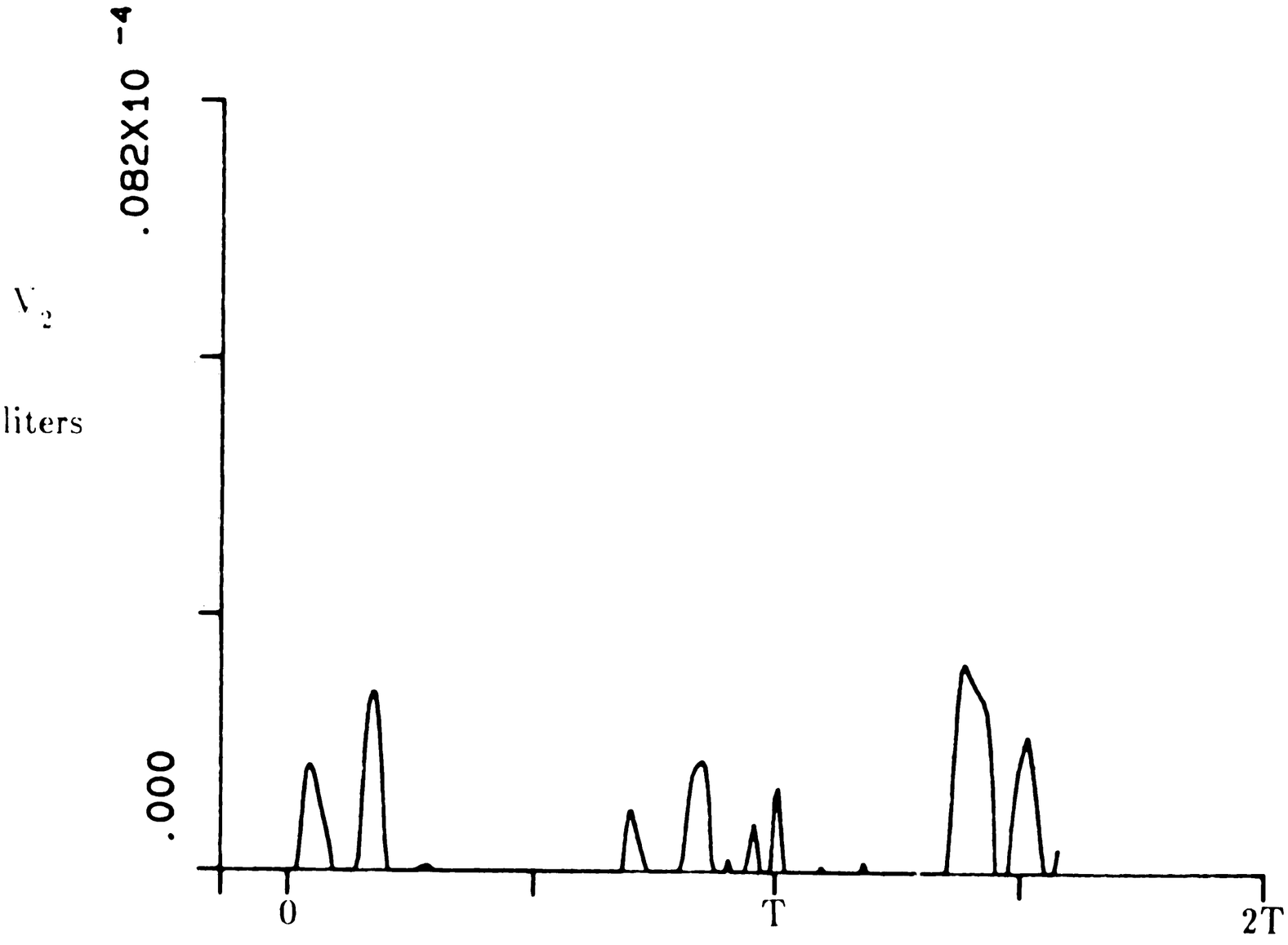

Figure 4-12: Case 1. Cavitation bubble at P_2, inside inertance tube (see Fig.4.1)

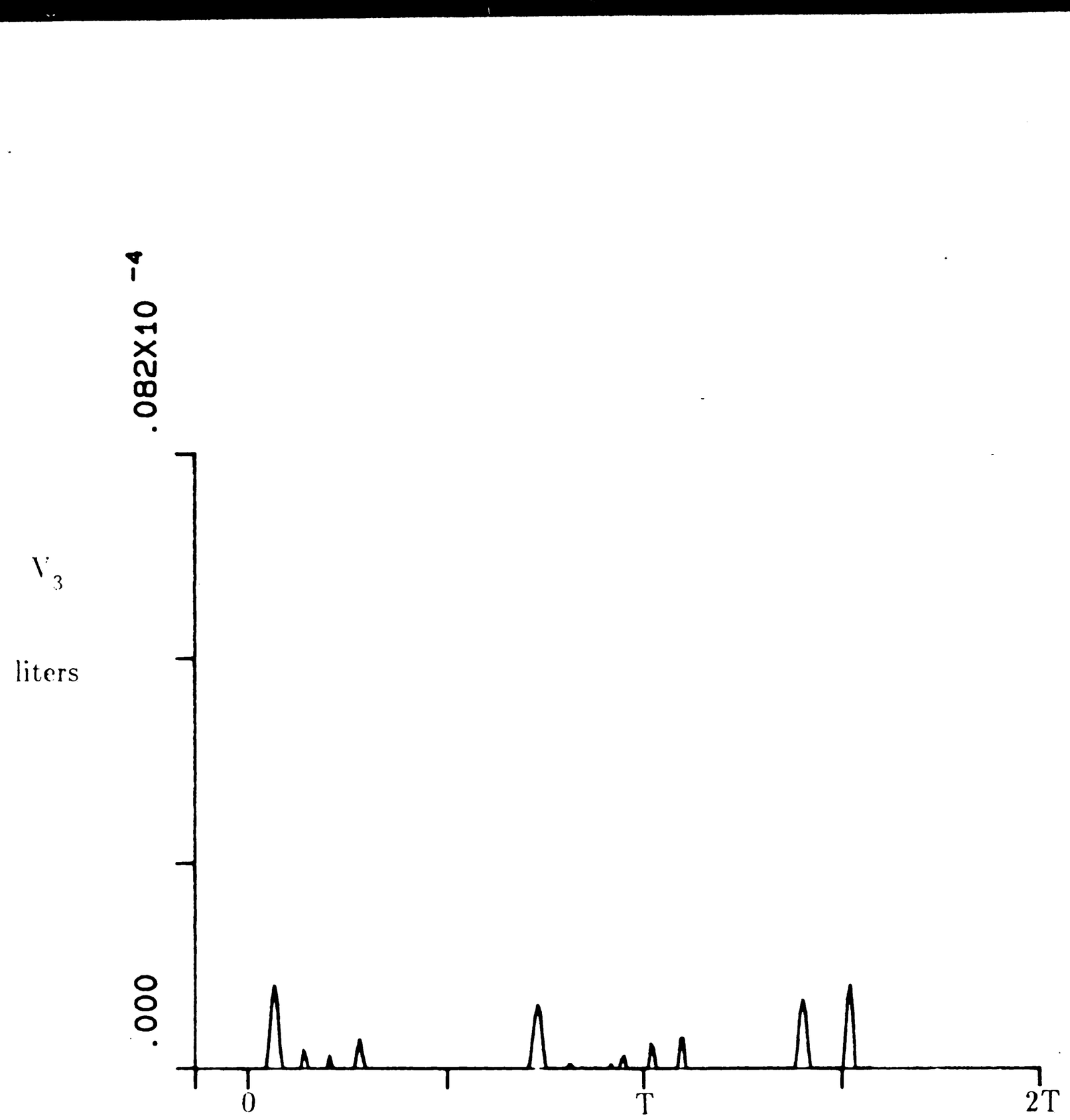

Figure 4-13: Case 1. Cavitation bubble at P_3, inside inertance tube (see Fig. 4.1)

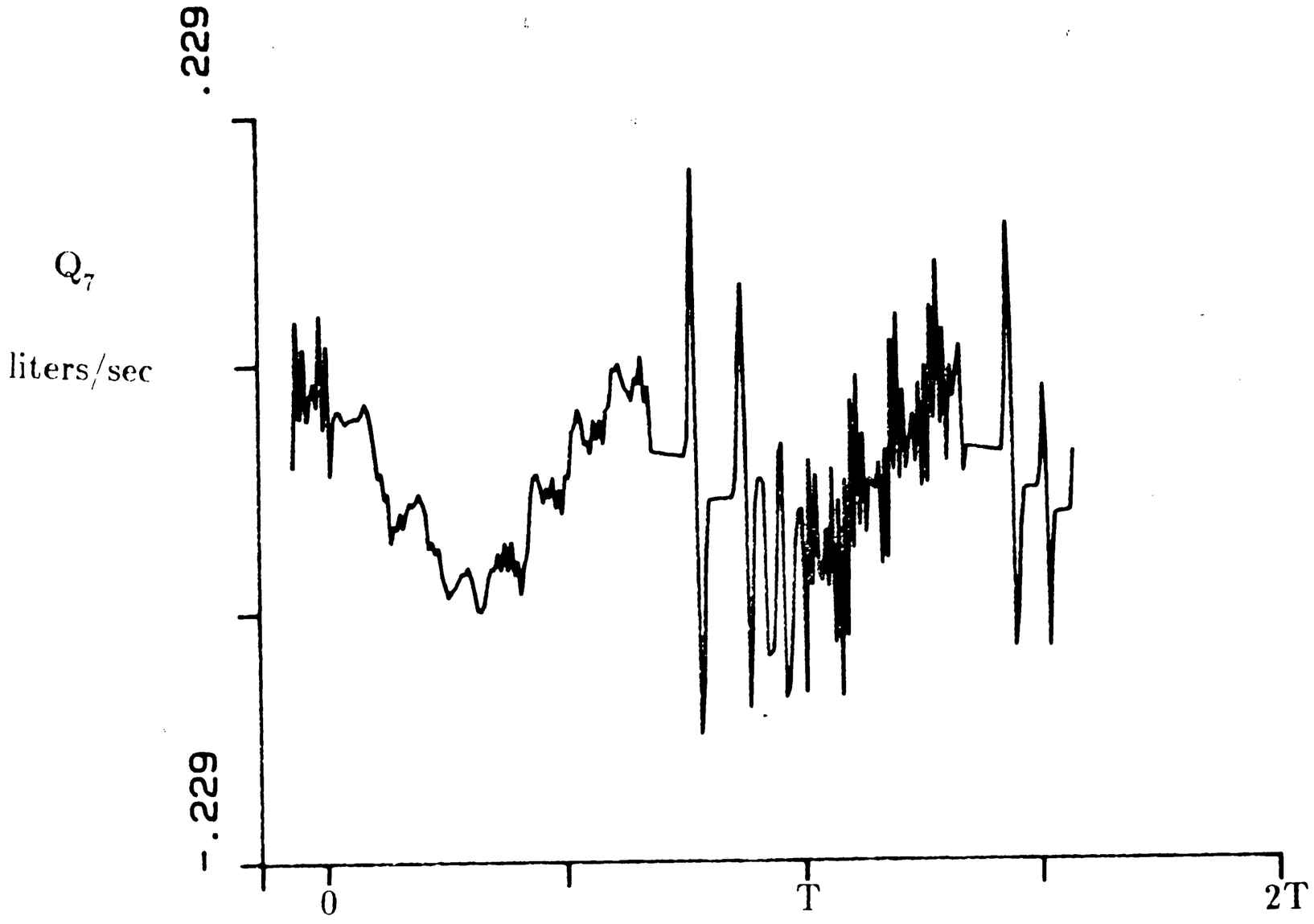

Figure 4-14: Case 1. Flow Q_7 inside valve (see Fig. 4.2)

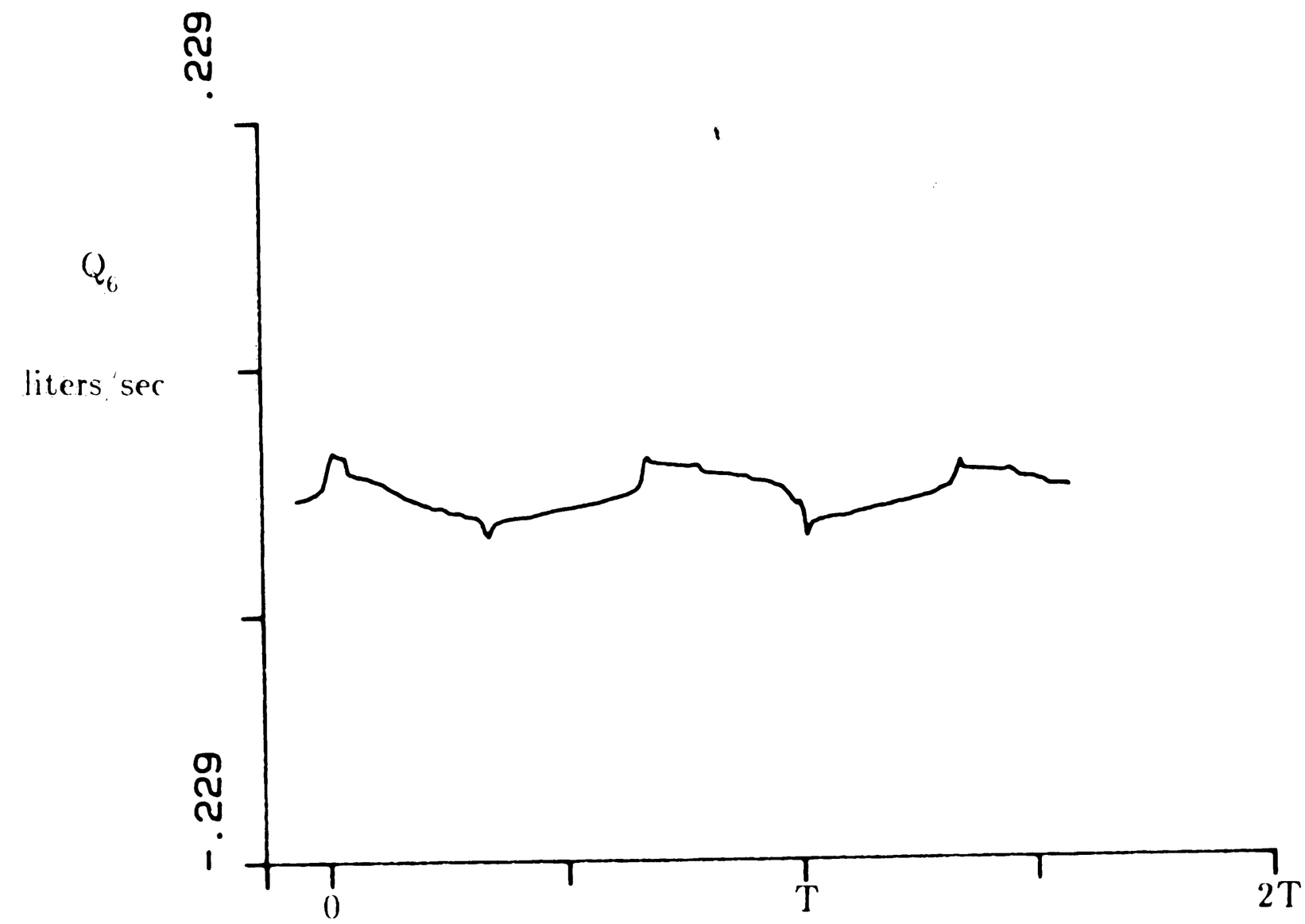

Figure 4-15: Case 1. Flow Q_6 inside valve (see Fig. 4.2)

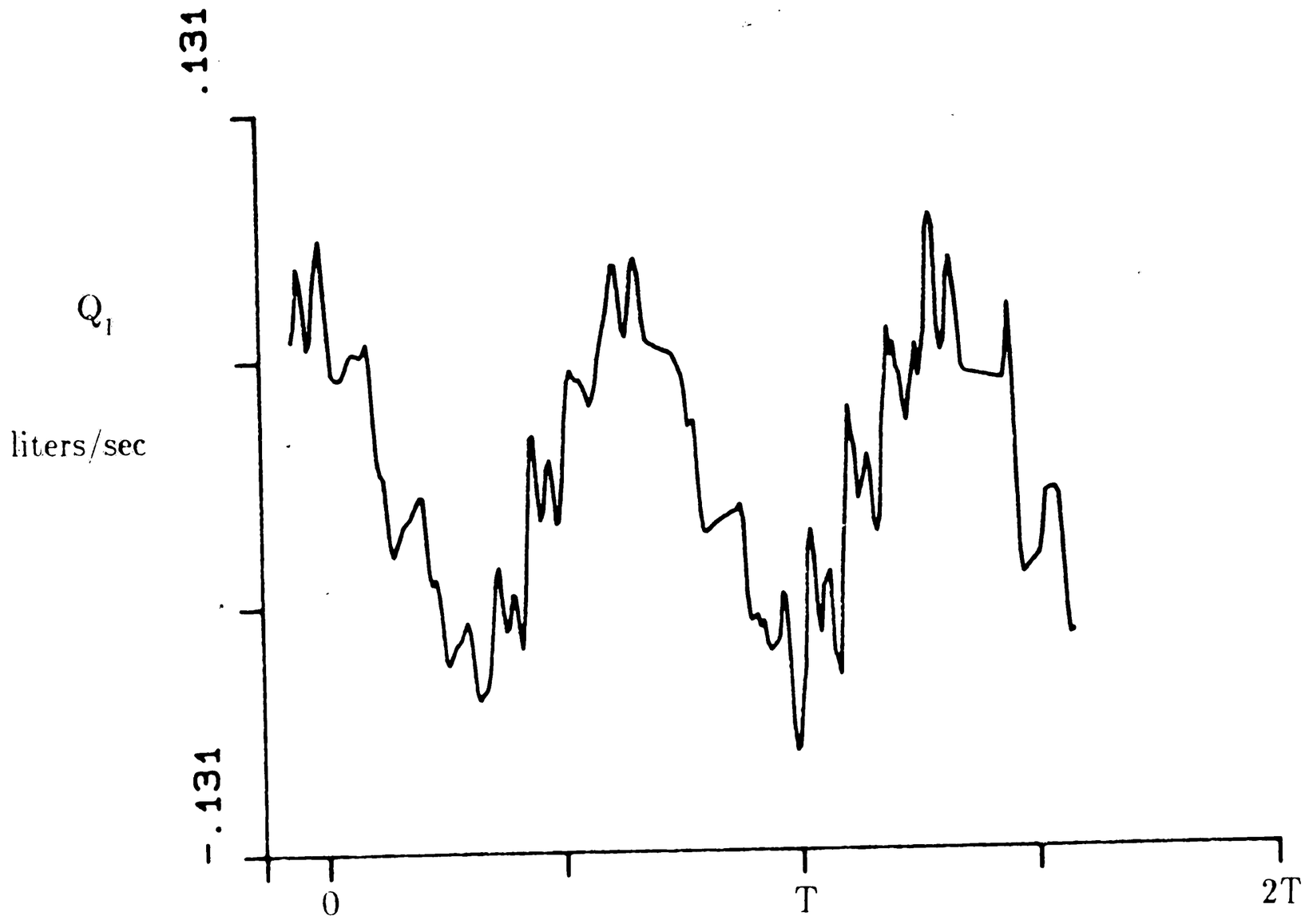

Figure 4-16: Case 1. Flow Q_1, beginning of inertance tube (see Fig. 4.1)

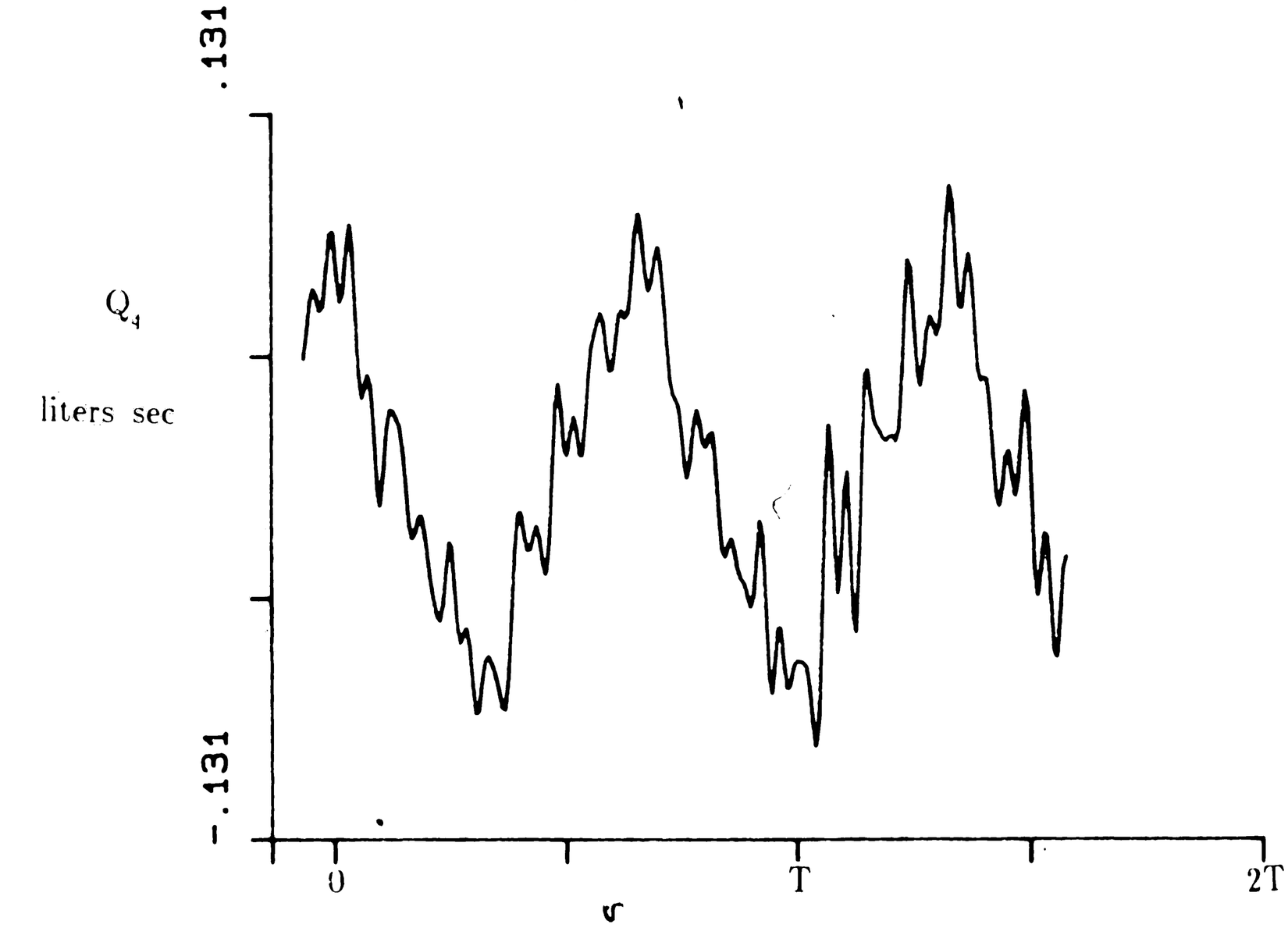

Figure 4-17: Case 1. Flow Q_4, end of inertance tube (see Fig. 4.1)

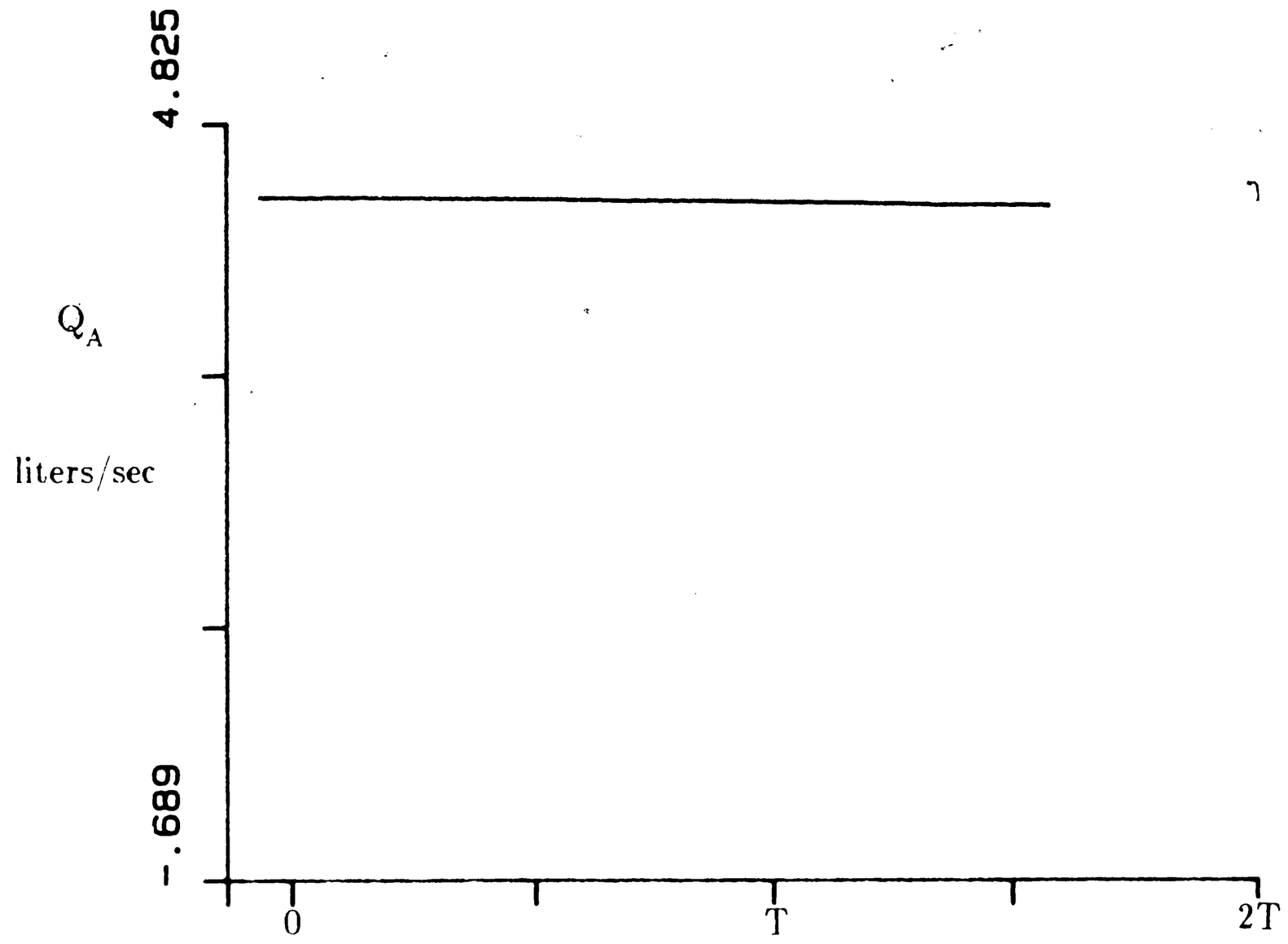

Figure 4-18: Case 1. Flow Q_A, into accumulator "A" where supply pressure connects into valve (see Fig 4.3)

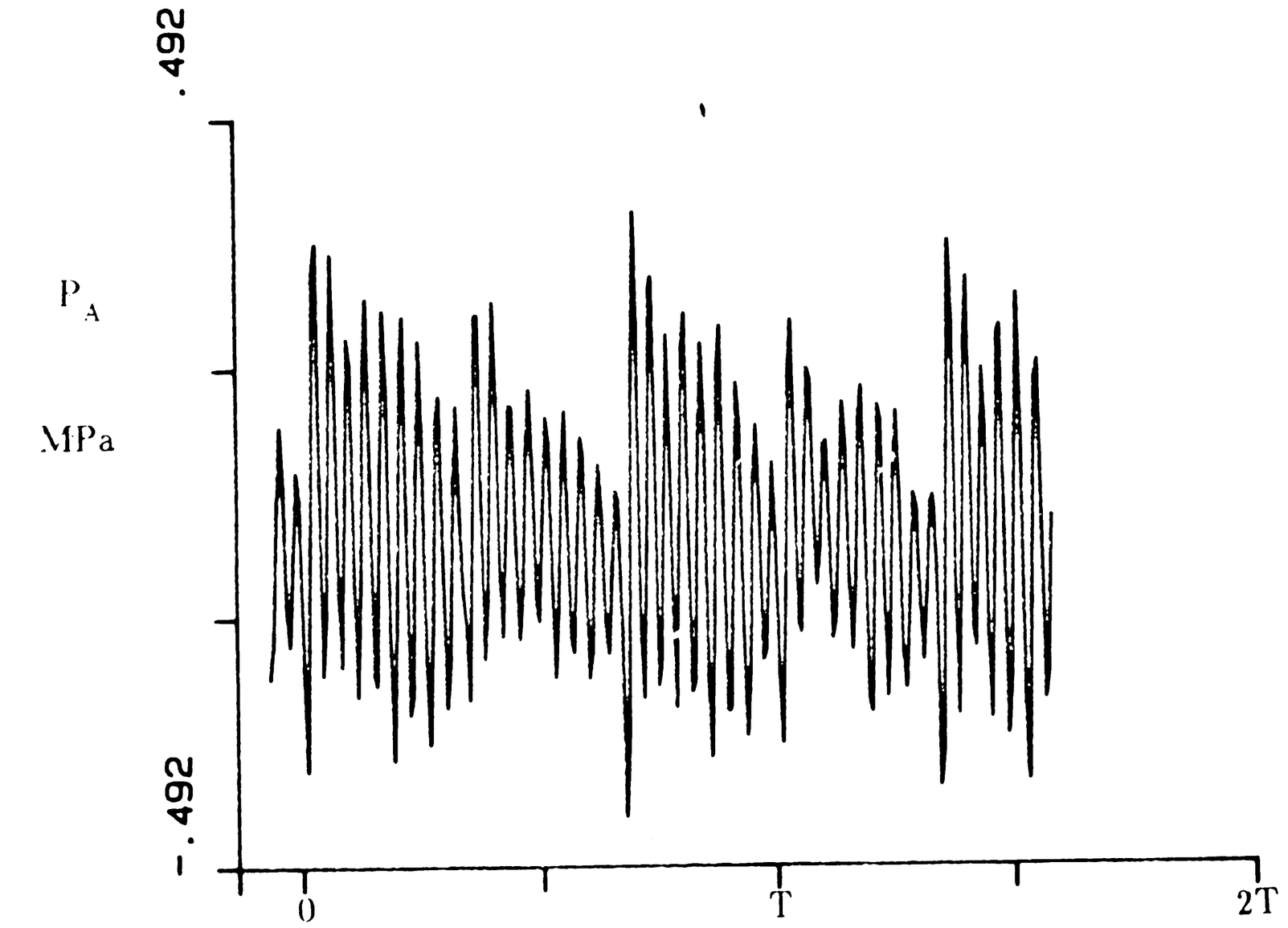

Figure 4-19: Case 1. Pressure P_A in accumulator "A" (see Fig. 4.3)

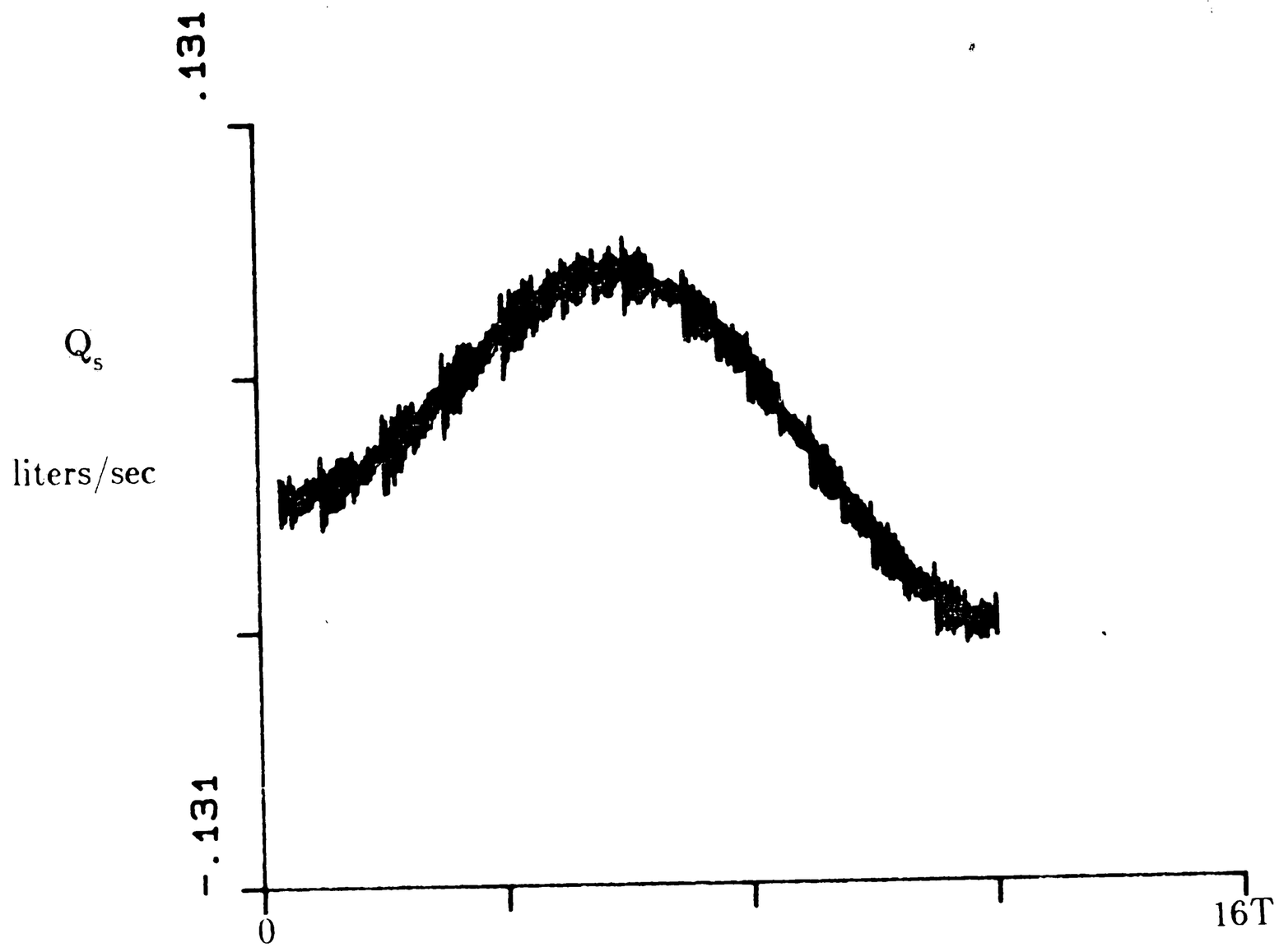

Figure 4-20: Case 1. Flow Q_s into valve on supply side (see Fig. 4.3)

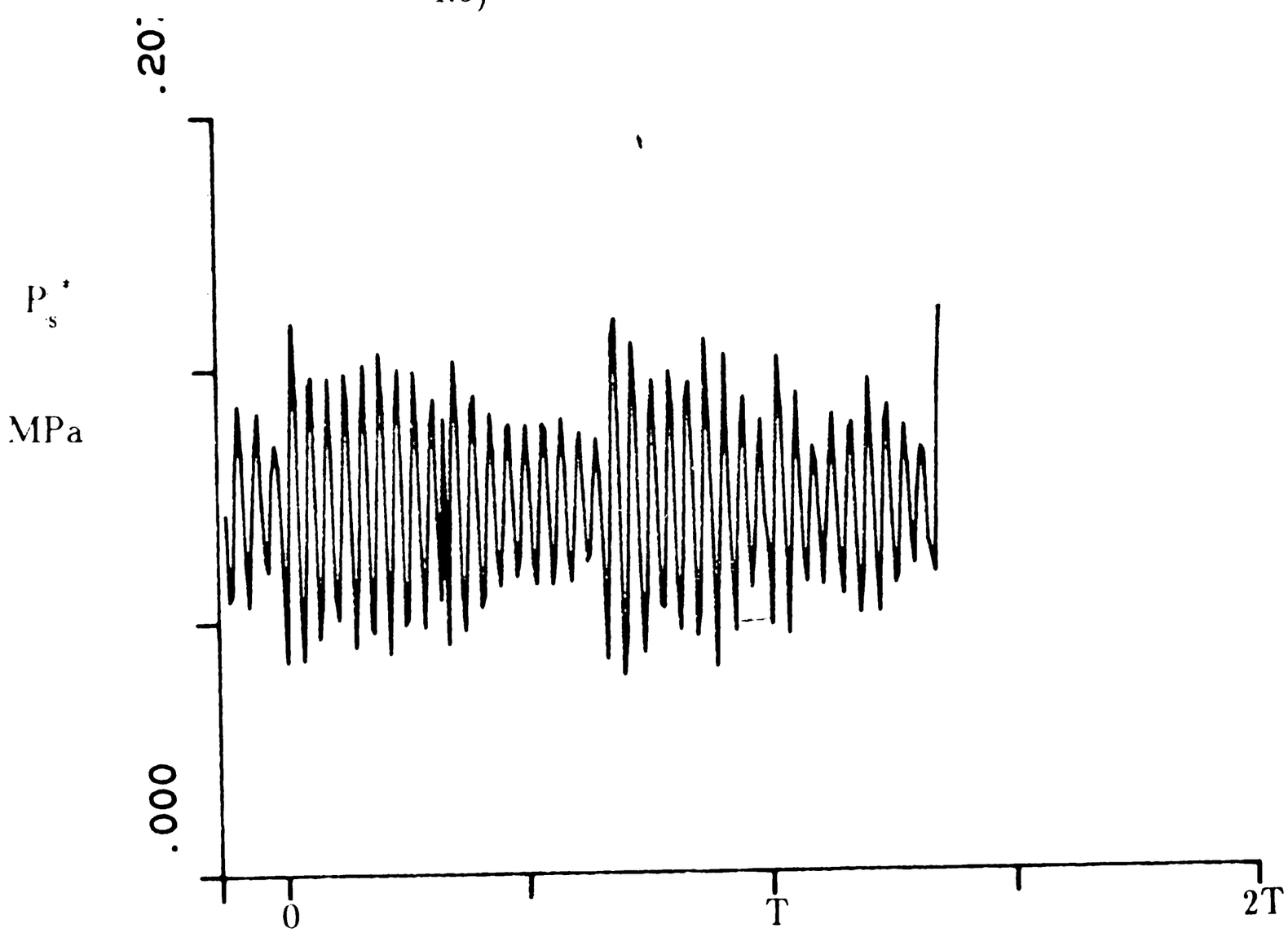

Figure 4-21: Case 1. Pressure P_s^* at supply-to-valve connection (see Fig. 4.3)

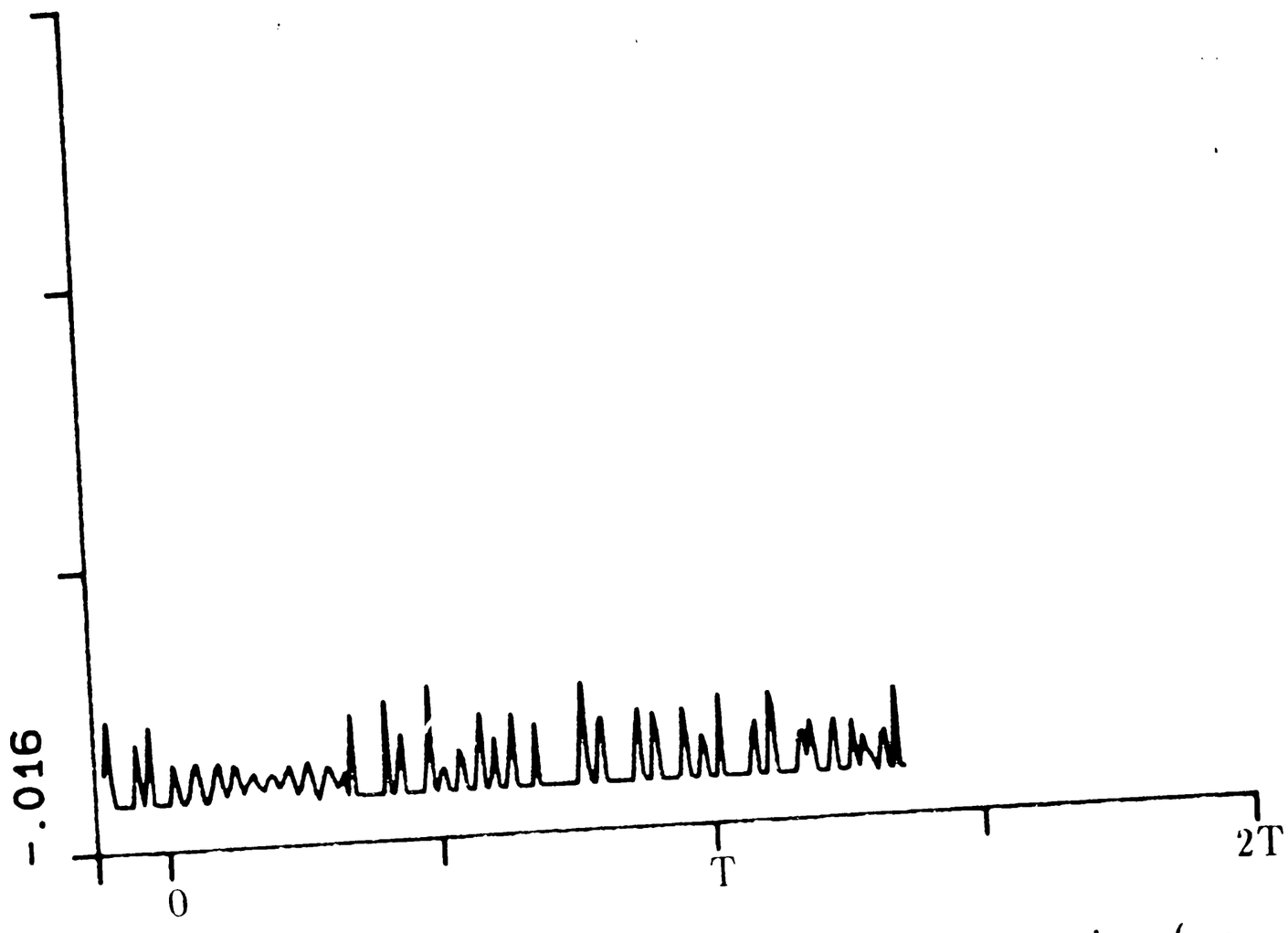

Figure 4-22: Case 1. Pressure P_T^* at tank-to-valve connection (see Fig. 4.3)

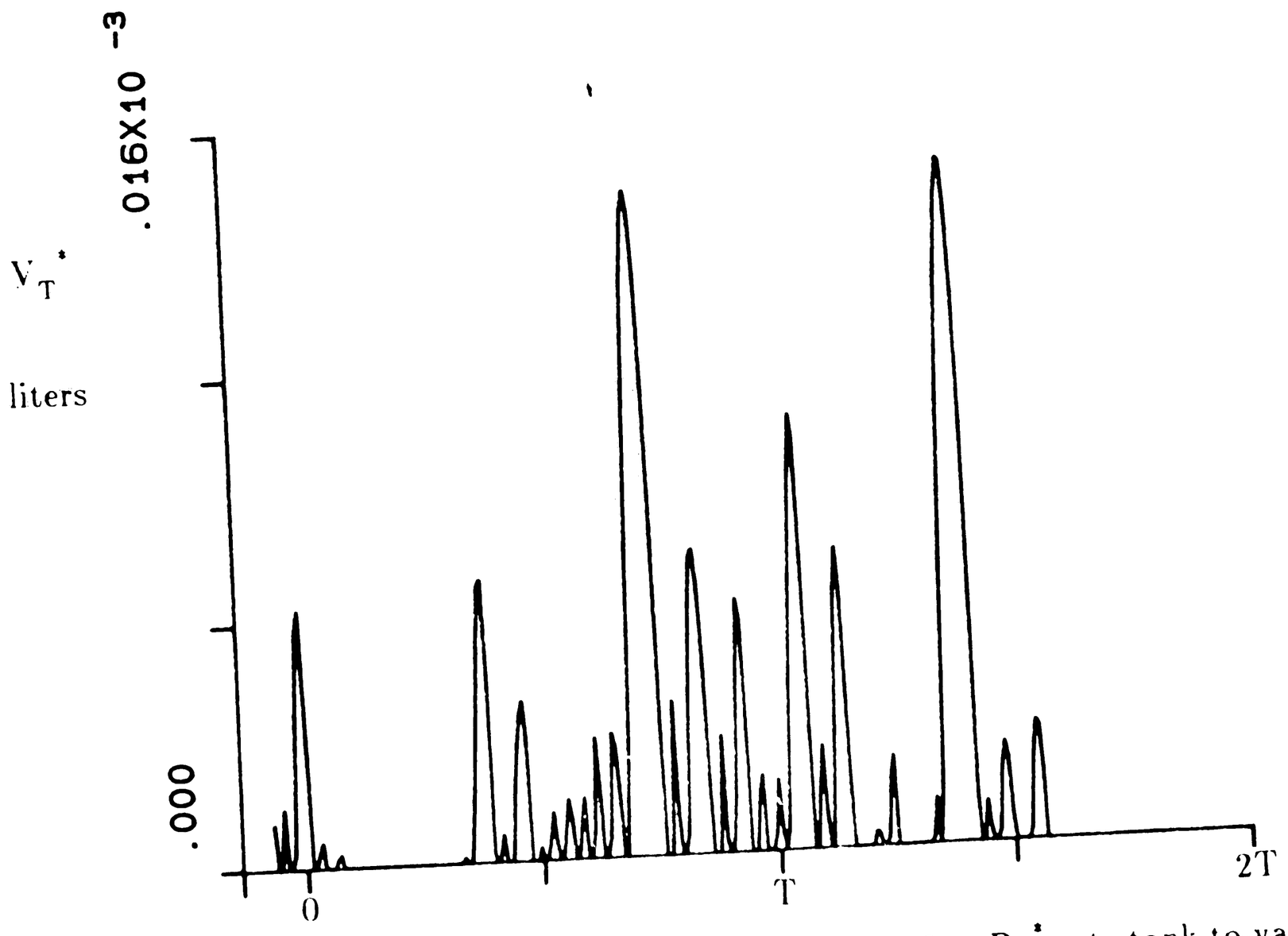

Figure 4-23: Case 1. Cavitation bubble for P_T^* at tank-to-valve connection (see Fig. 4.3)

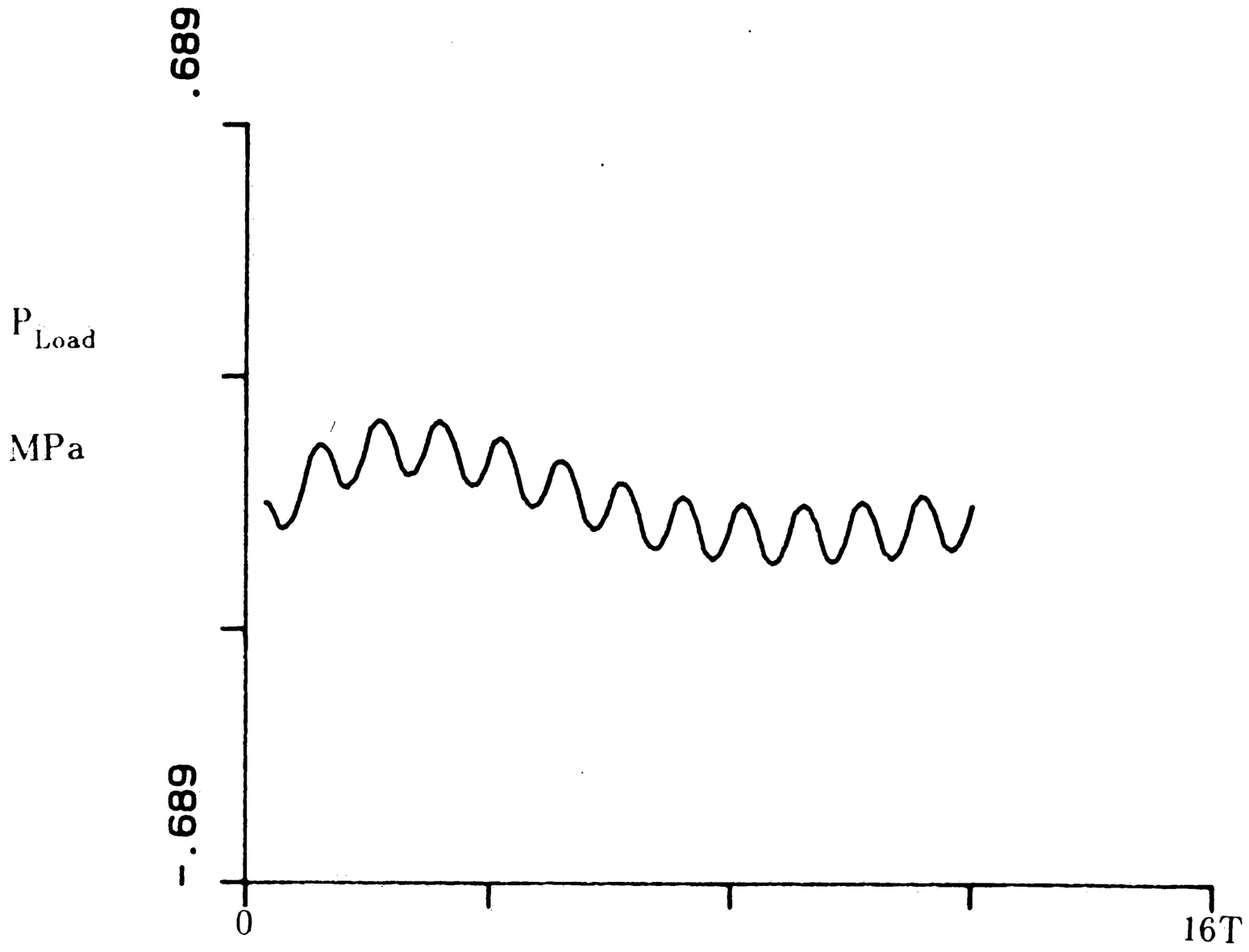

Figure 4-24: Case 1. Load pressure P_{load} (see Fig. 4.4)

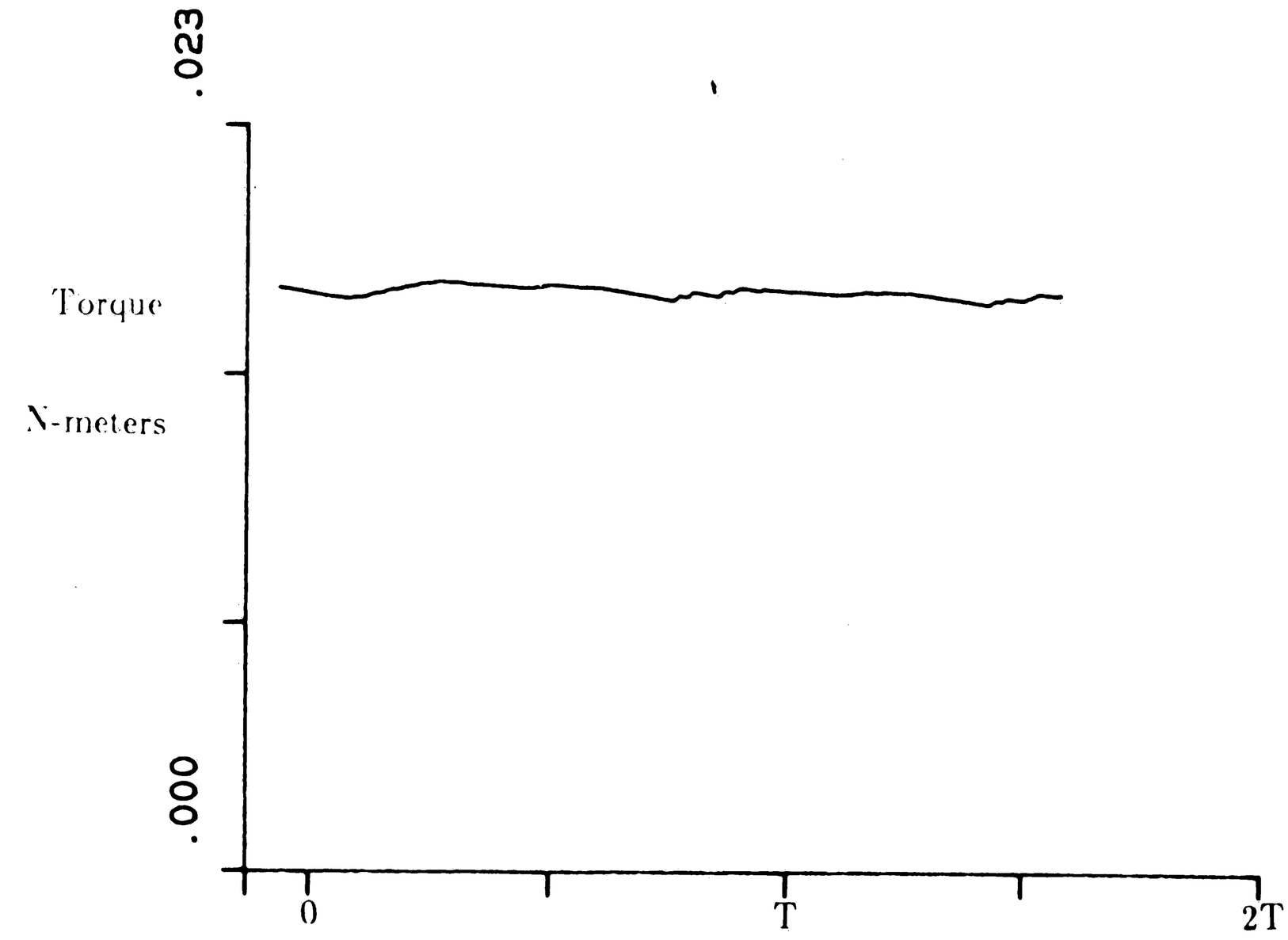

Figure 4-25: Case 1. Torque felt by control shaft

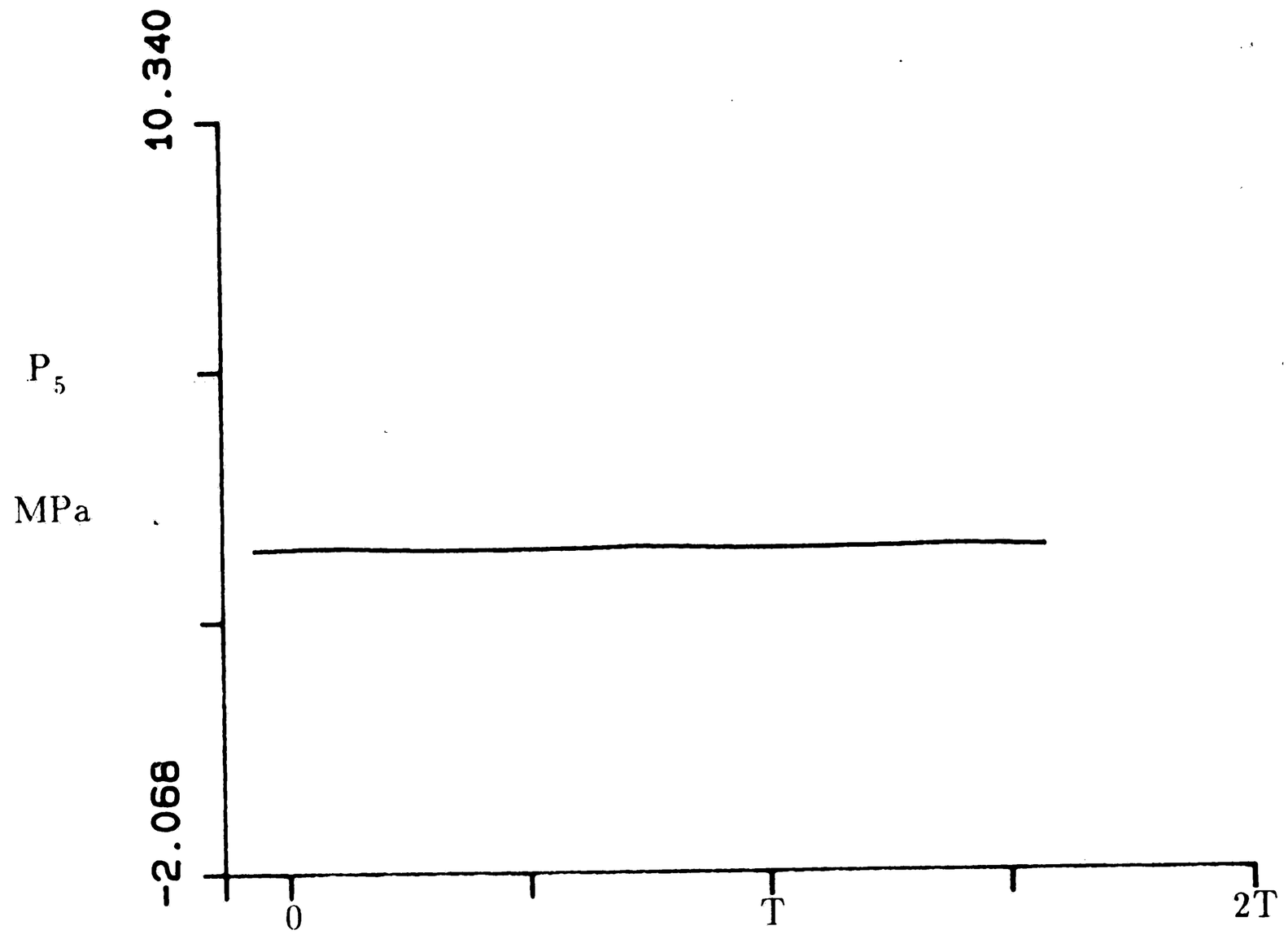

Figure 4-26: Case 2. Pressure P_5 at end of inertance tube on higher pressure side (see Fig. 4.1)

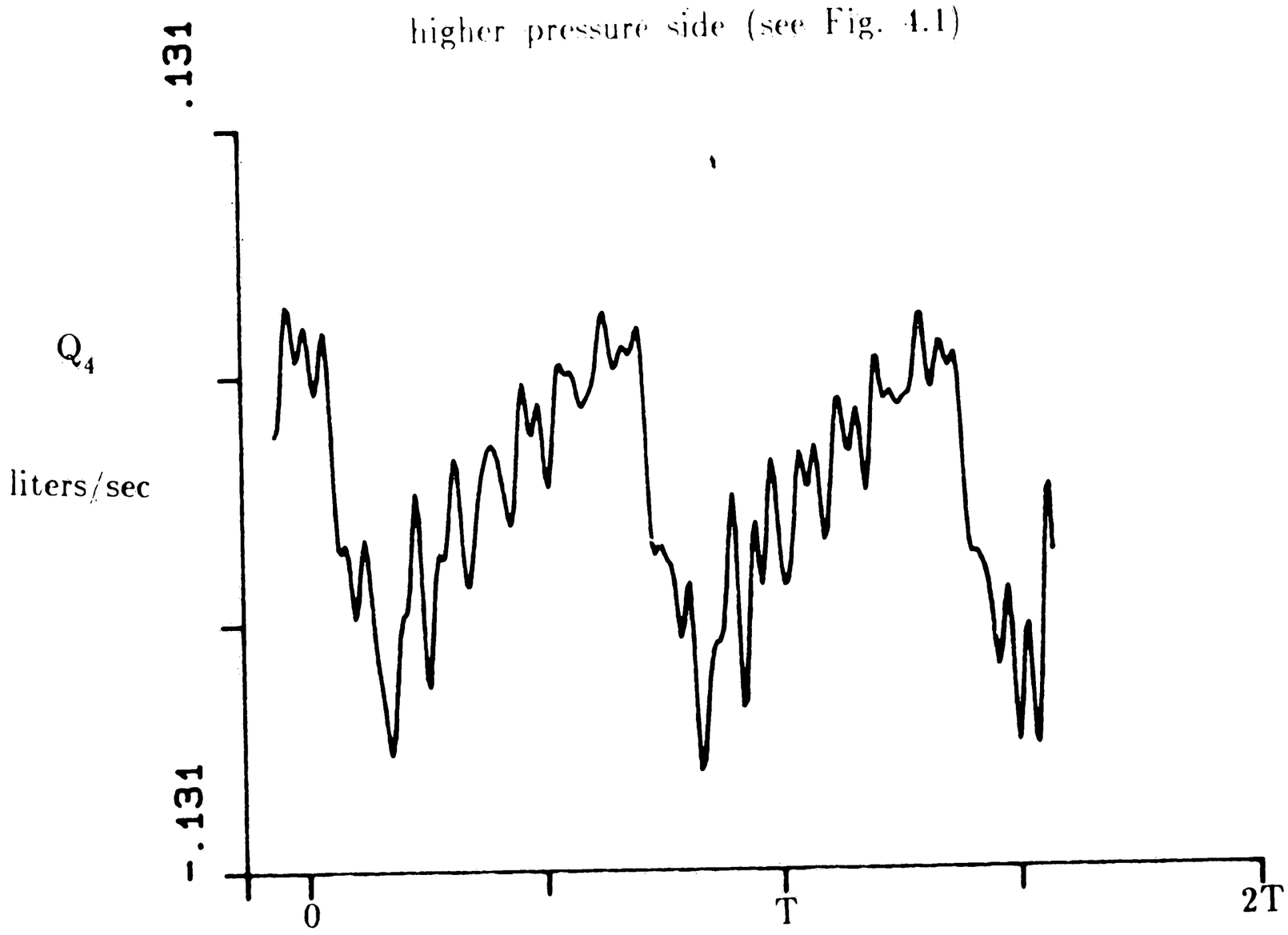

Figure 4-27: Case 2. Flow Q_4 from end of inertance tube on higher pressure side (see Fig. 4.1)

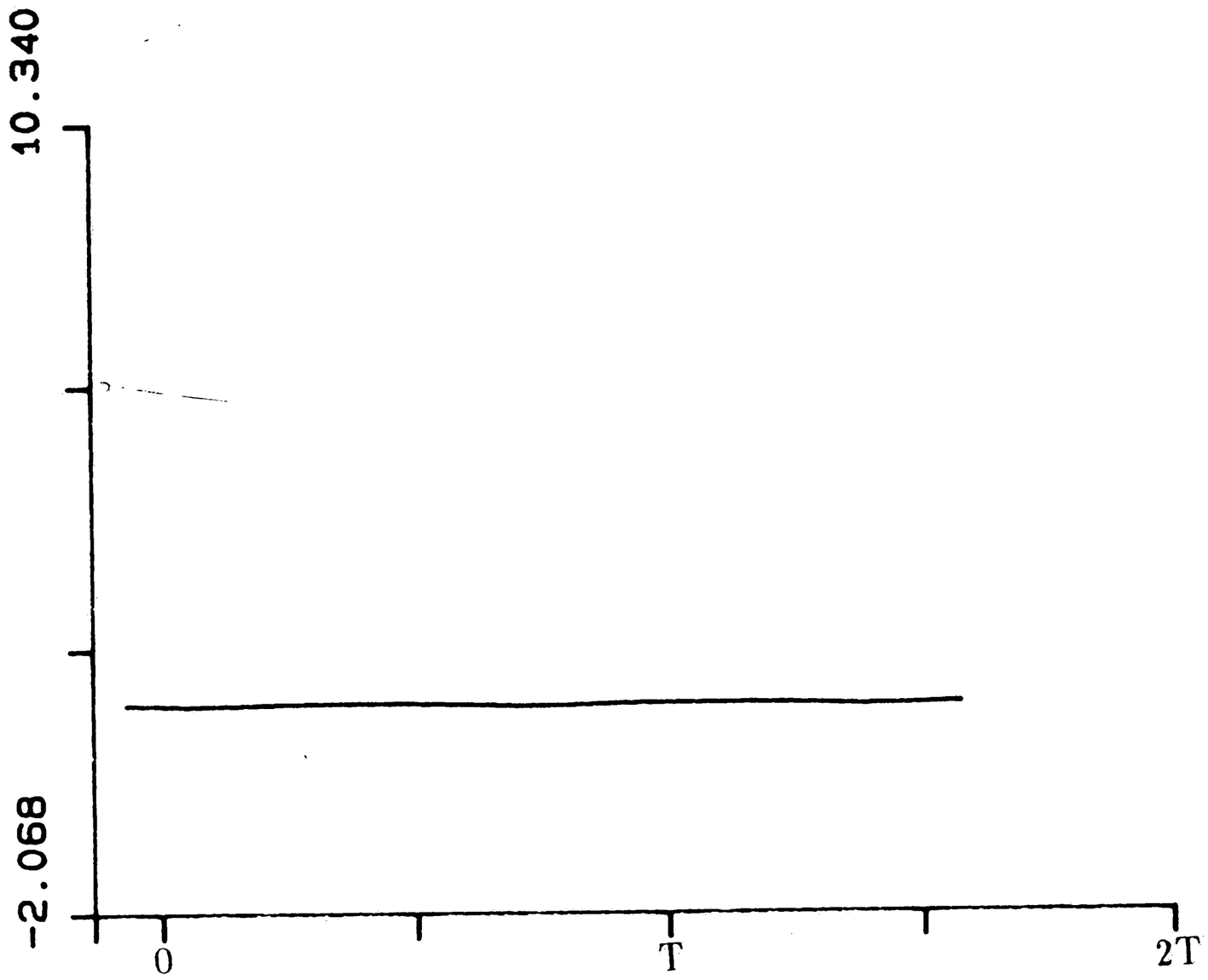

Figure 4-28: Case 2. Pressure P_5 at end of inertance tube in lower pressure side (see Fig. 4.1)

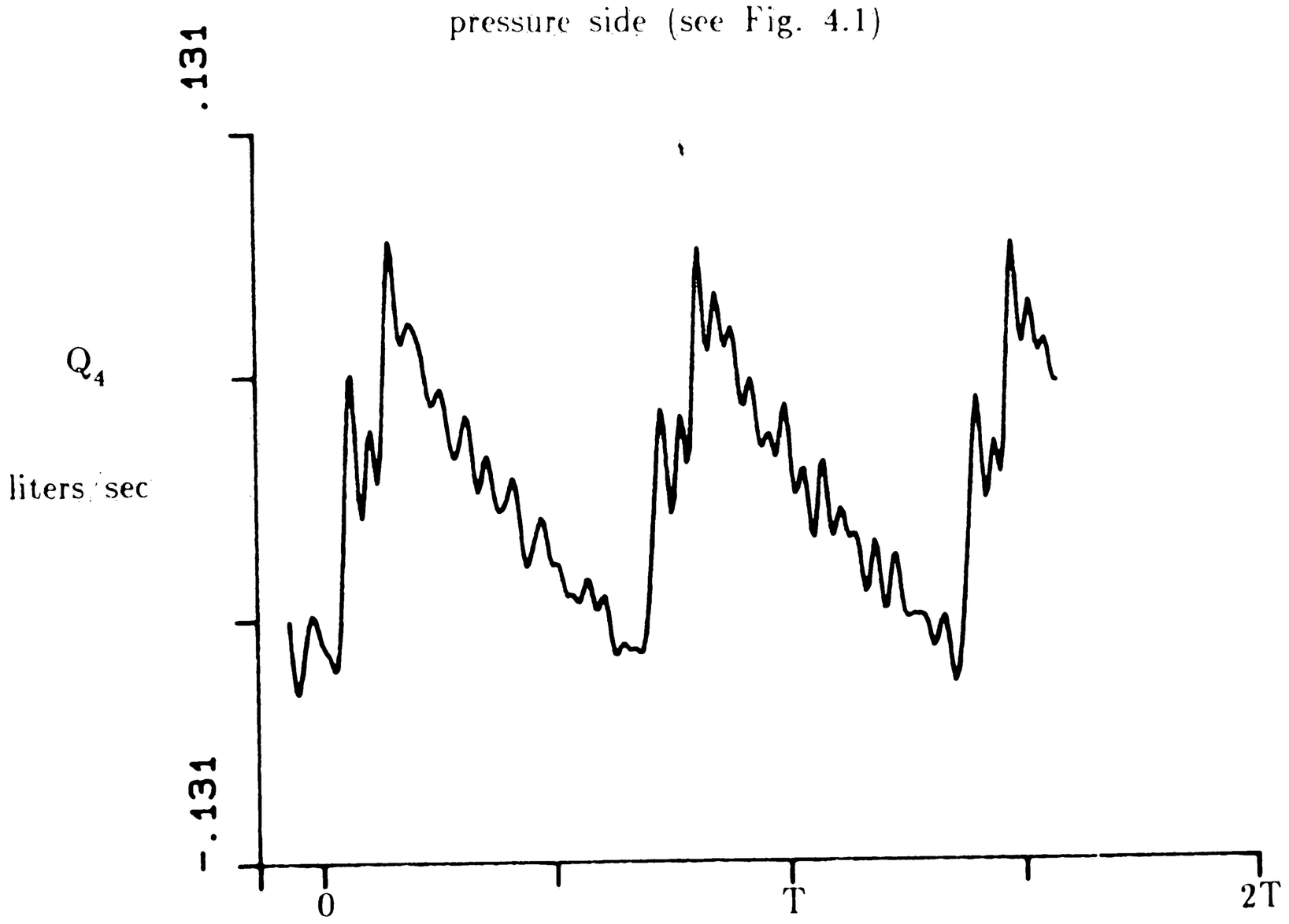

Figure 4-29: Case 2. Flow Q_4 from end of inertance tube on lower pressure side (see Fig. 4.1)

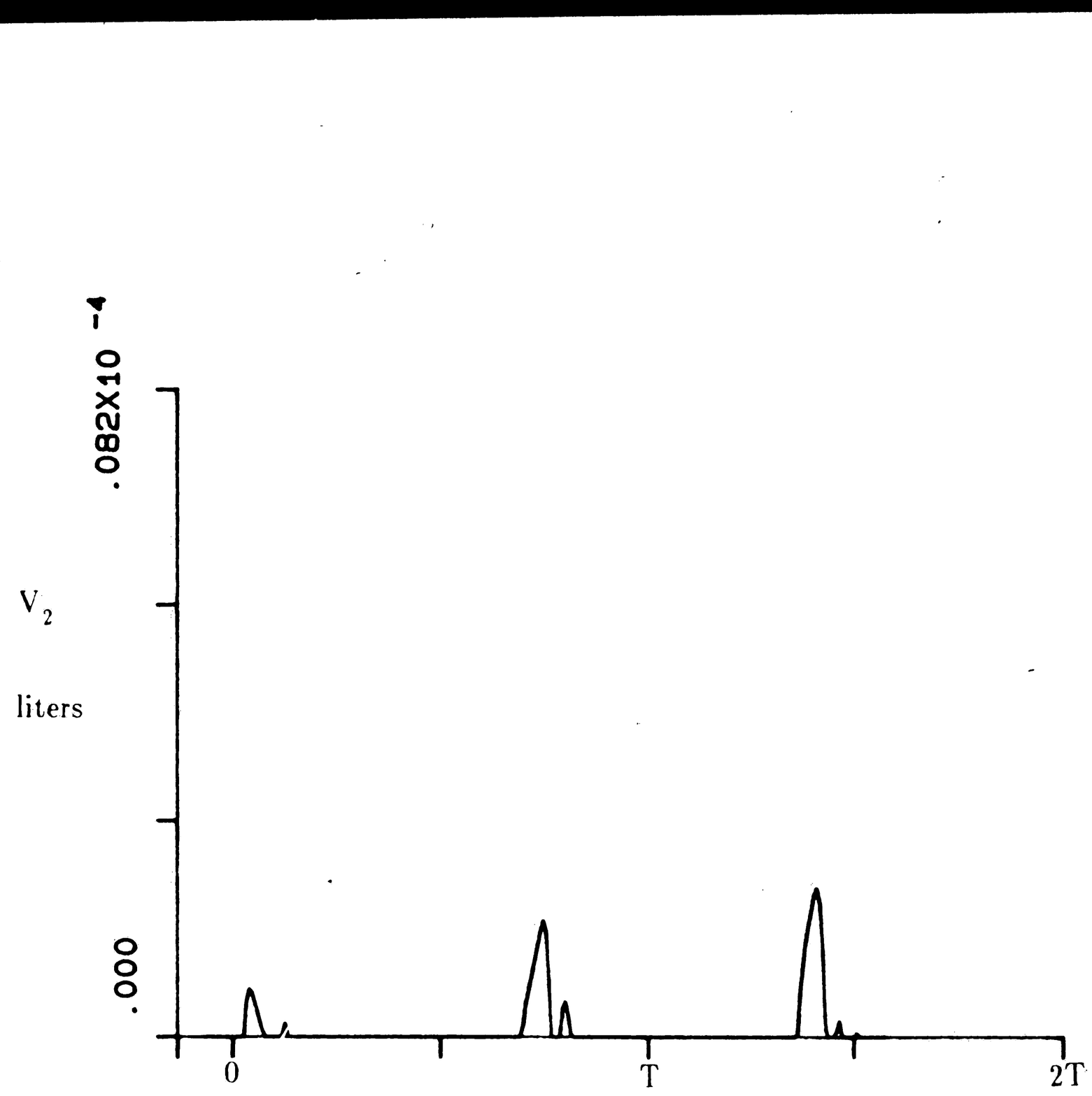

Figure 4-30: Case 2. Cavitation bubble at P_2 on higher pressure side (see Fig. 4.1)

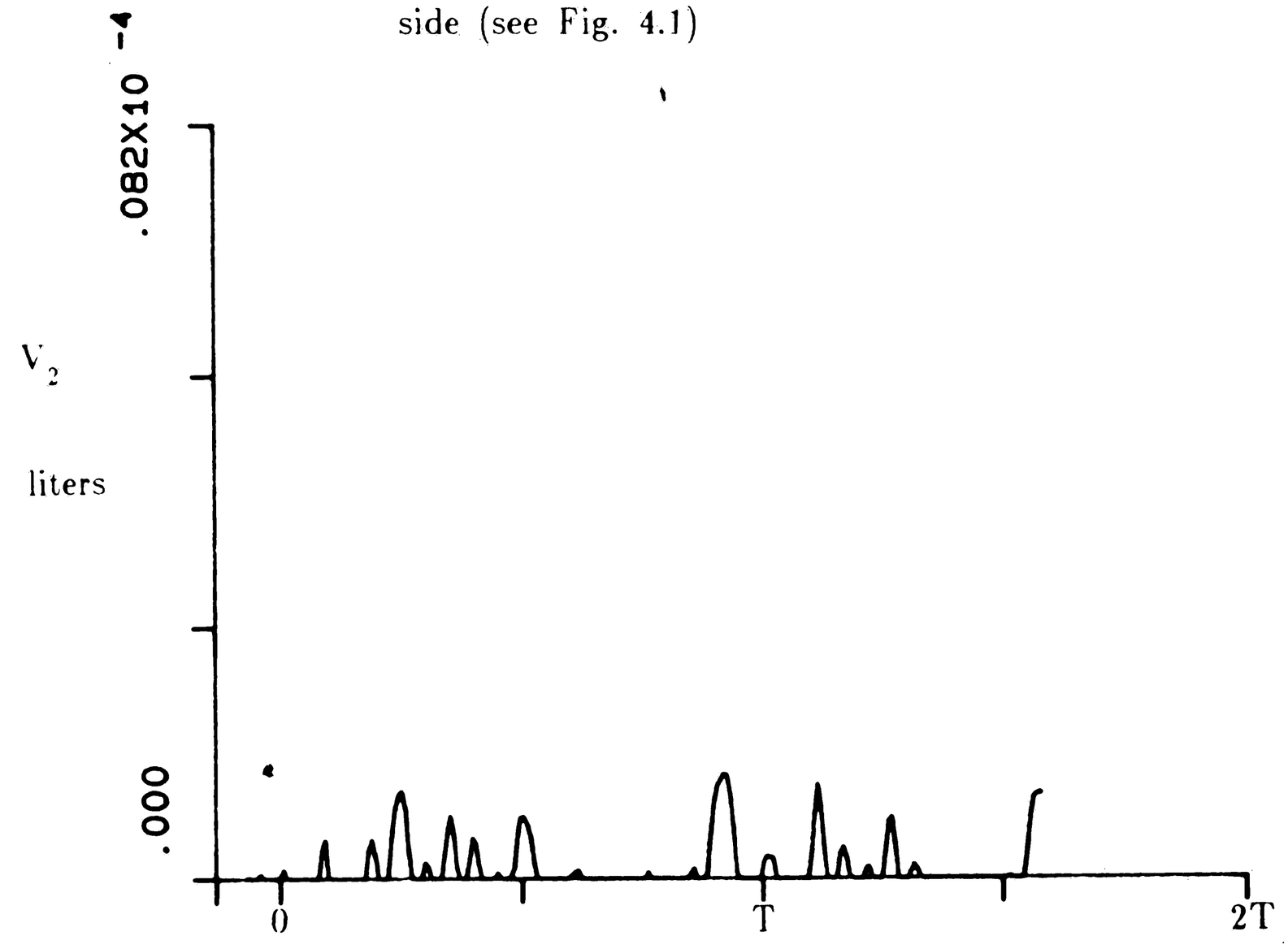

Figure 4-31: Case 2. Cavitation bubble at P_2 on lower pressure side (see Fig. 4.1)

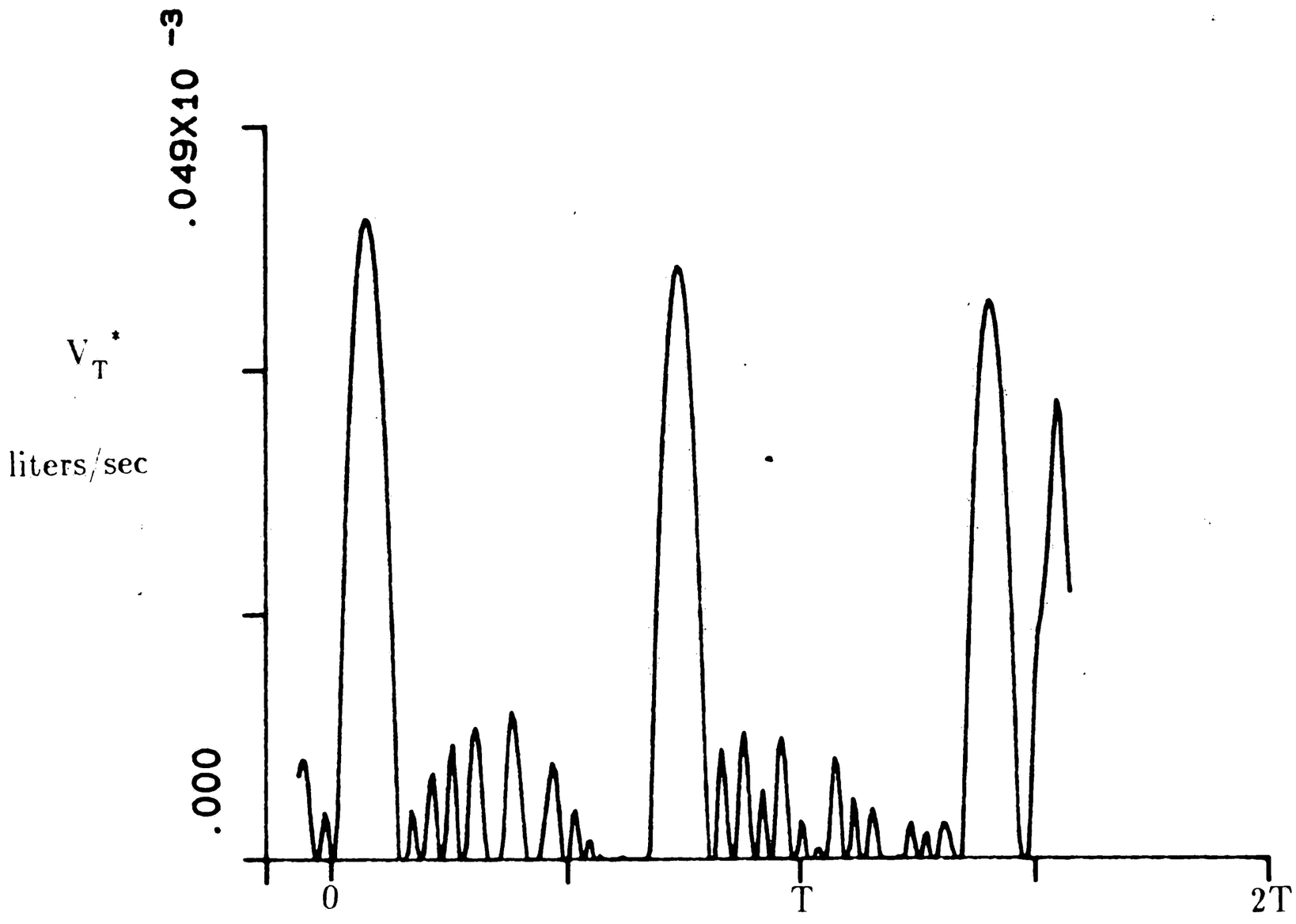

Figure 4-32: Case 2. Cavitation bubble at P_T^*, tank-to-valve connection (see Fig. 4.3)

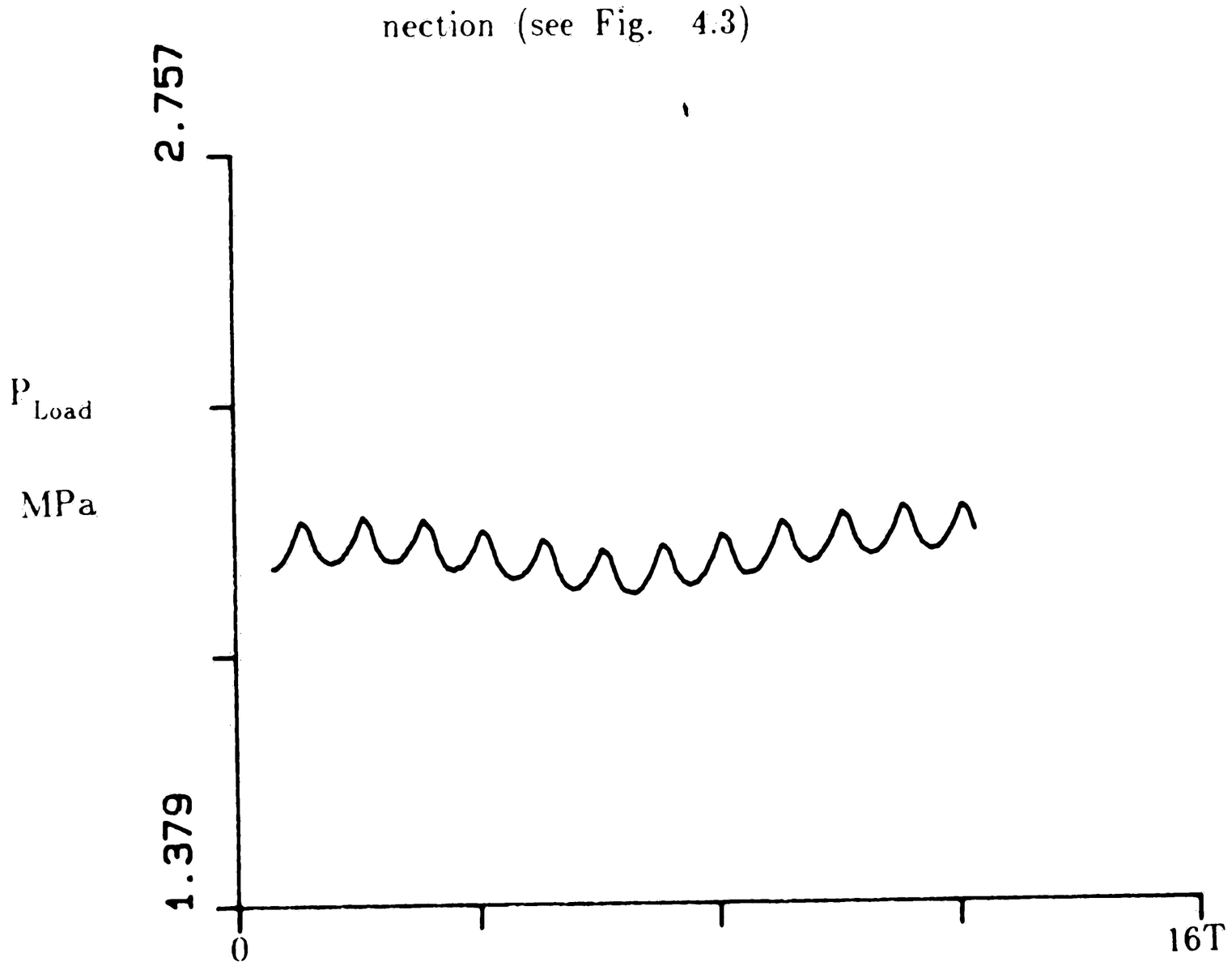

Figure 4-33: Case 2. Load pressure P_{load} (see Fig. 4.4)

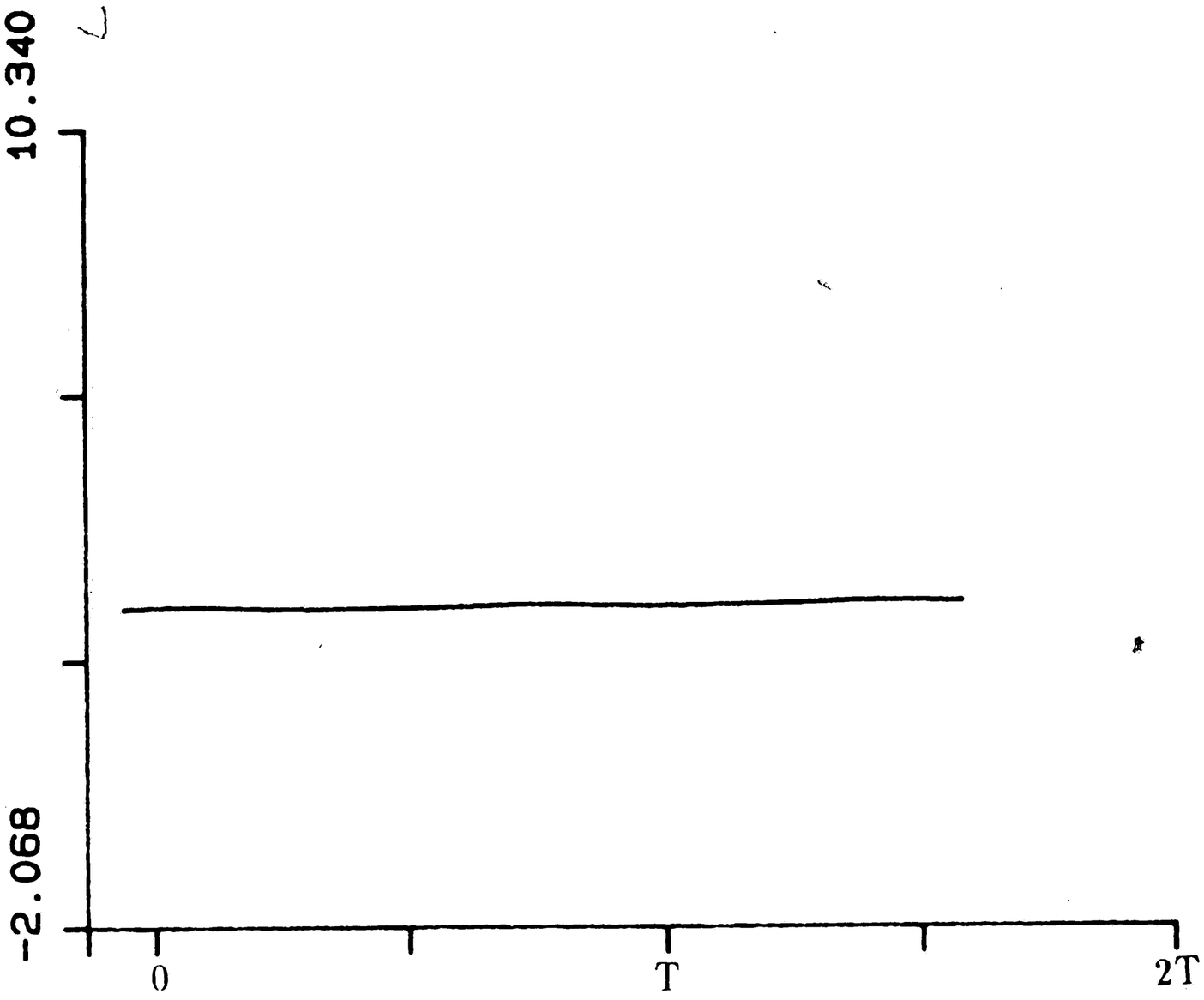

Figure 4-34: Case 3. Pressure P_5 at end of inertance tube on higher pressure side (see Fig. 4.1)

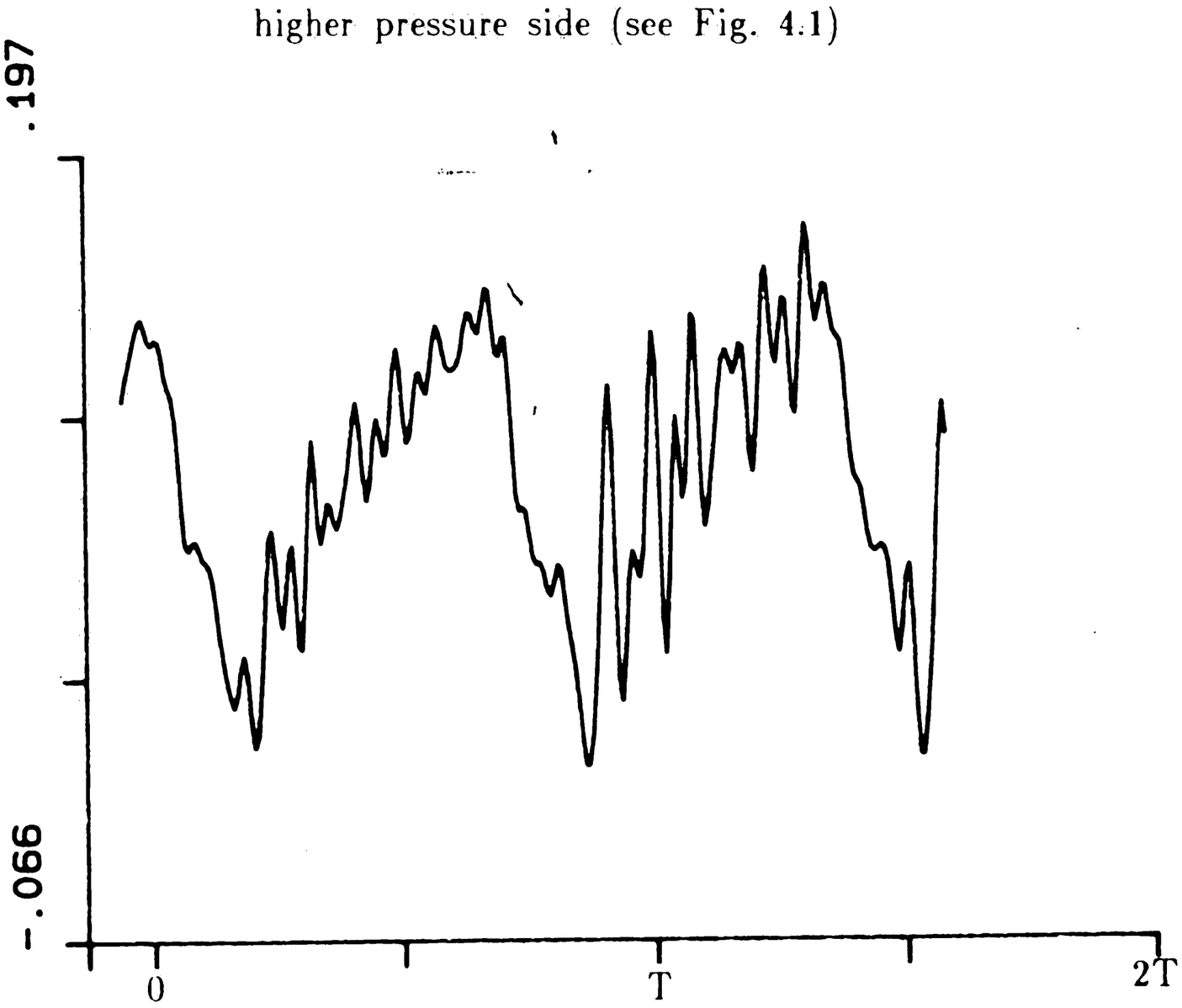

Figure 4-35: Case 3. Flow Q_4 from end of inertance tube on higher pressure side (see Fig. 4.1)

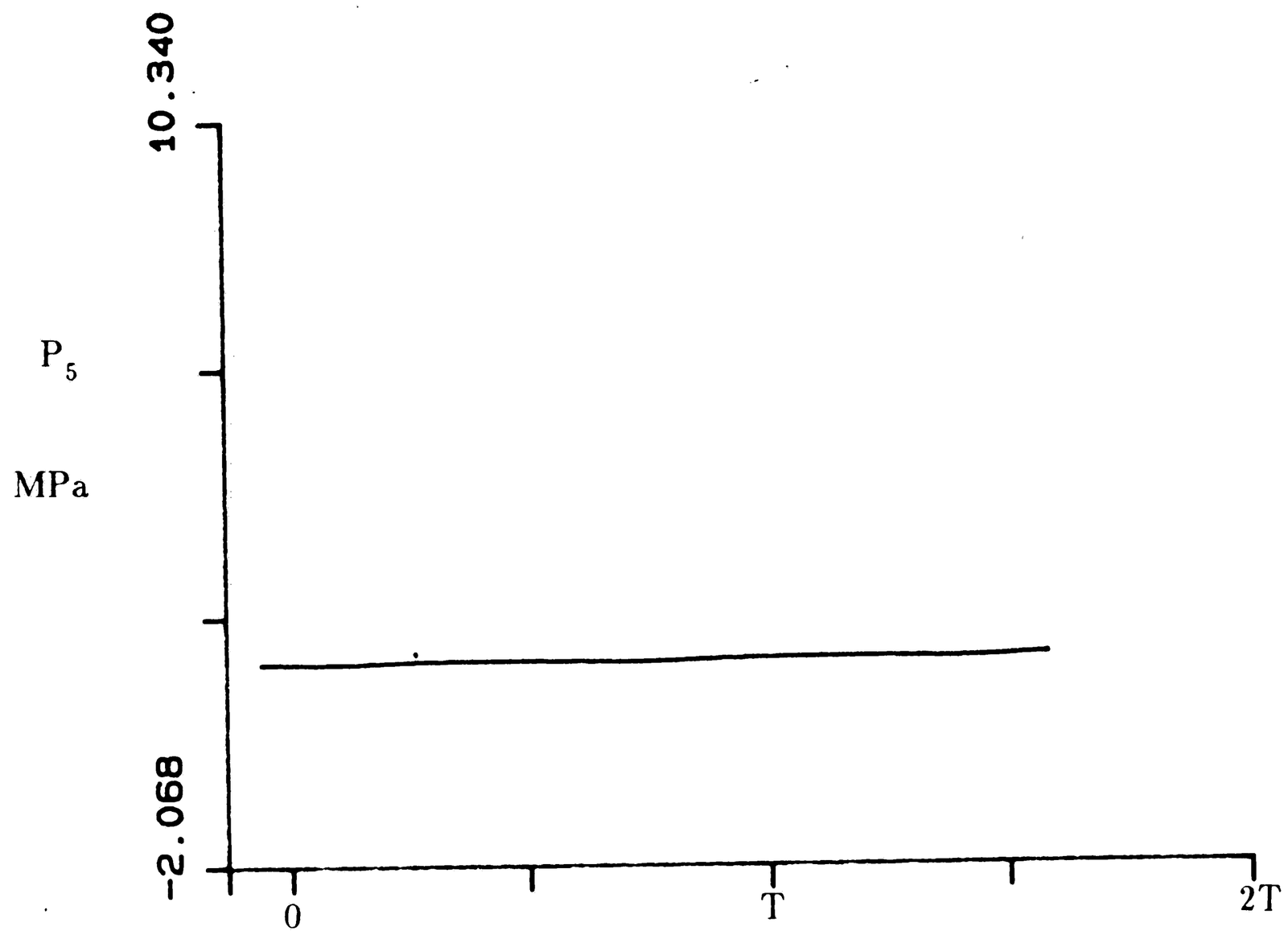

Figure 4-36: Case 3. Pressure P_5 at end of inertance tube on lower pressure side (see Fig. 4.1)

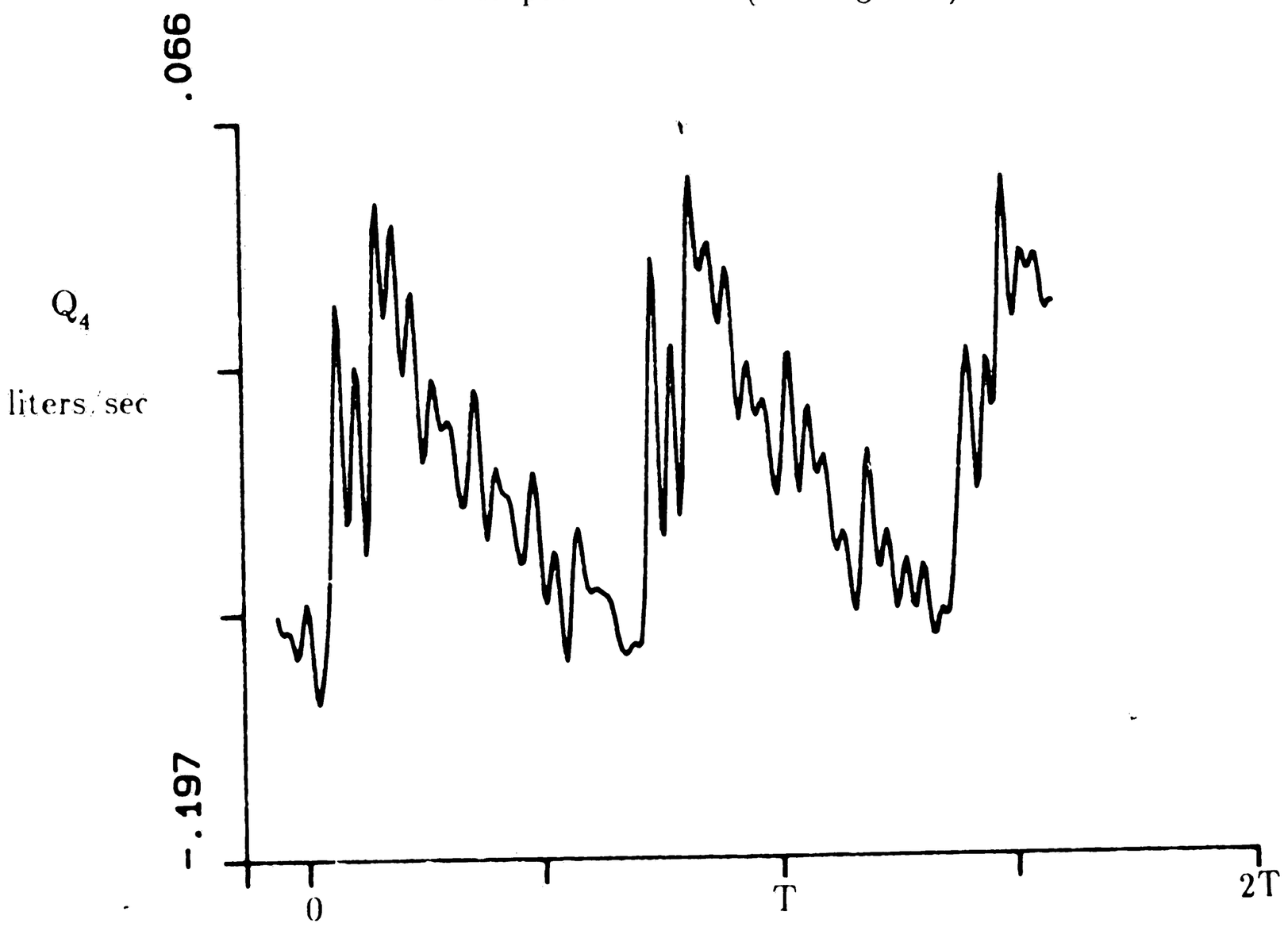

Figure 4-37: Case 3. Flow Q_4 from end of inertance tube on lower pressure side (see Fig. 4.1)

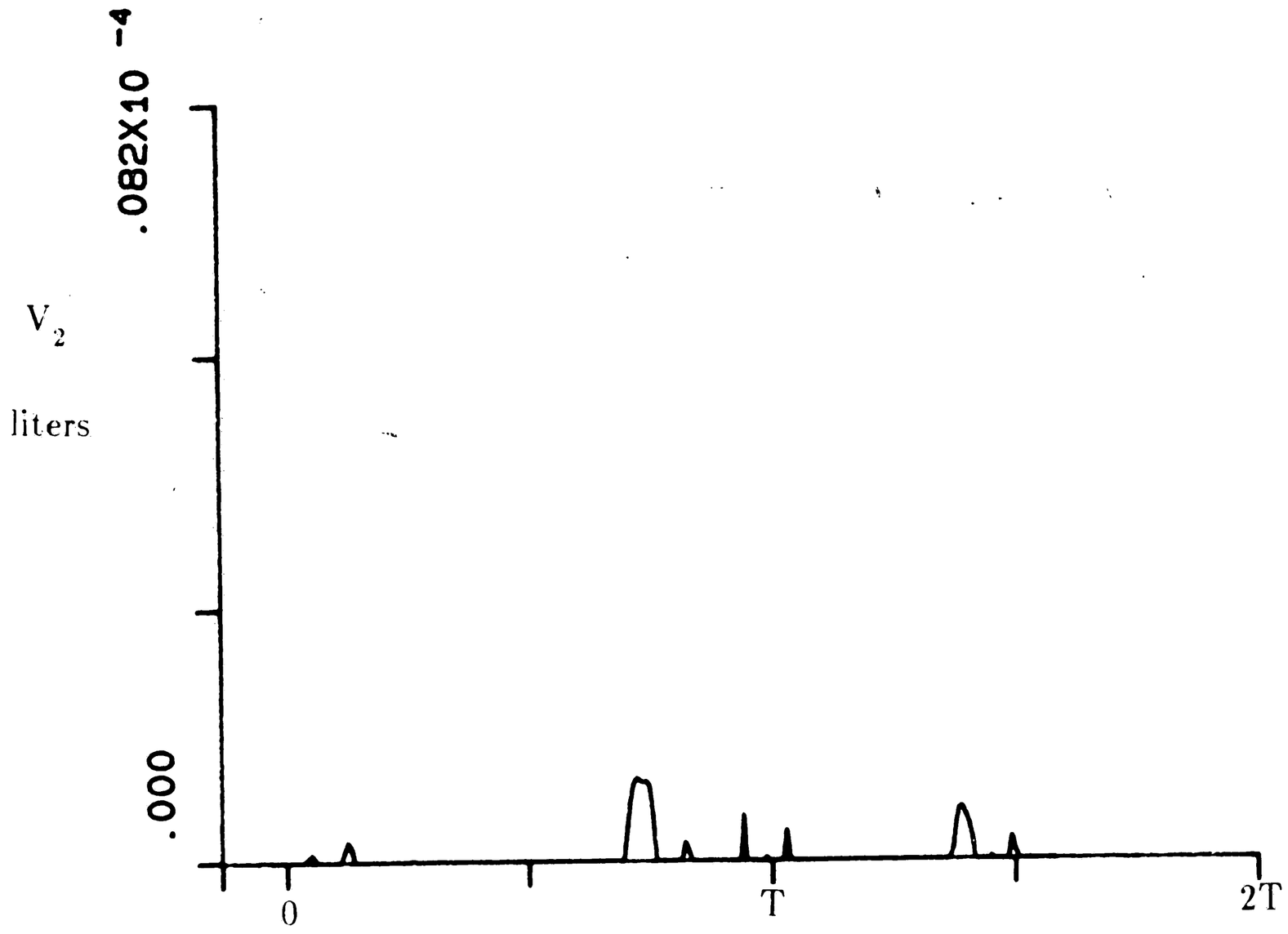

Figure 4-38: Case 3. Cavitation bubble at P_2 on higher pressure side (see Fig. 4.1)

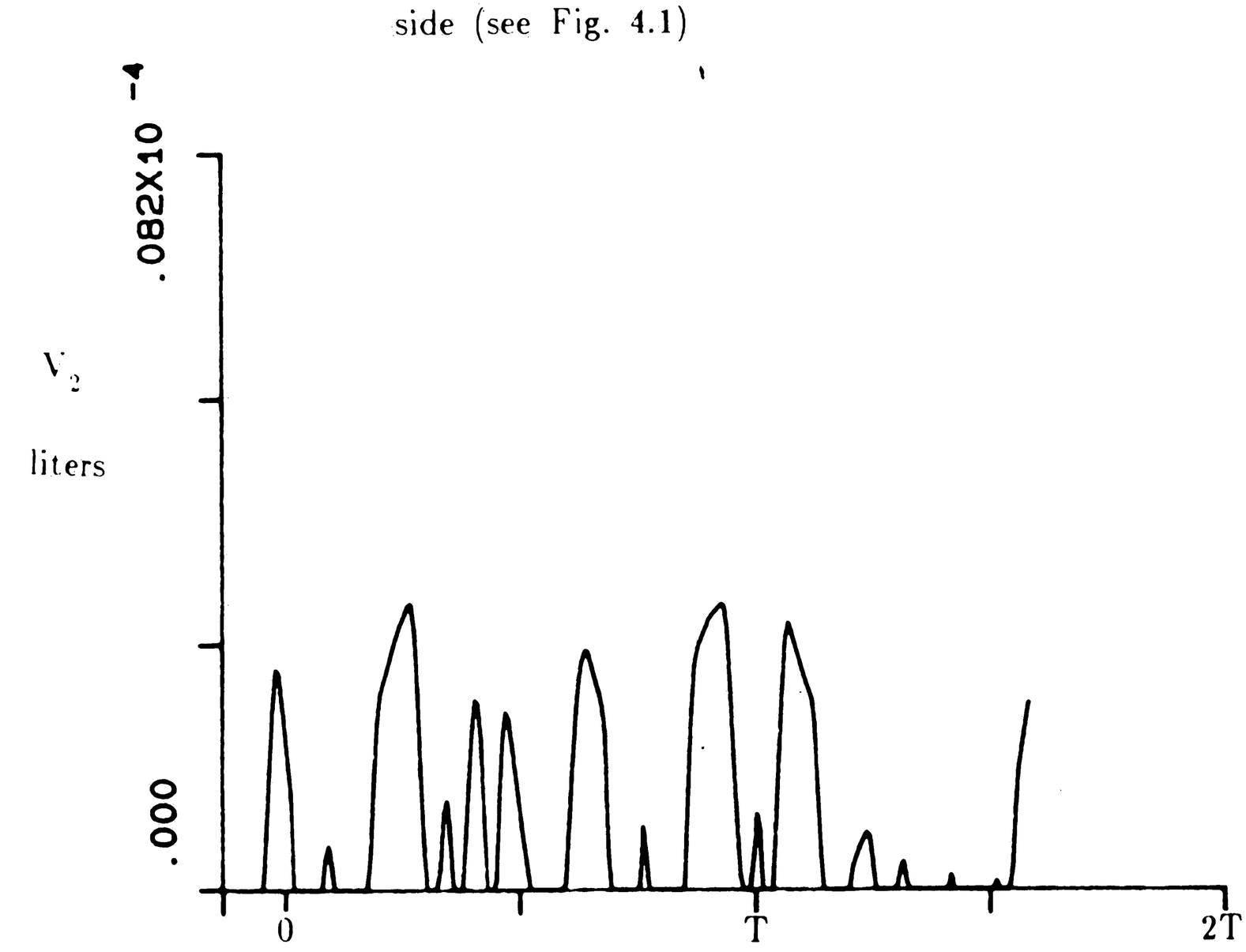

Figure 4-39: Case 3. Cavitation bubble at P_2 on lower pressure side (see Fig. 4.1)

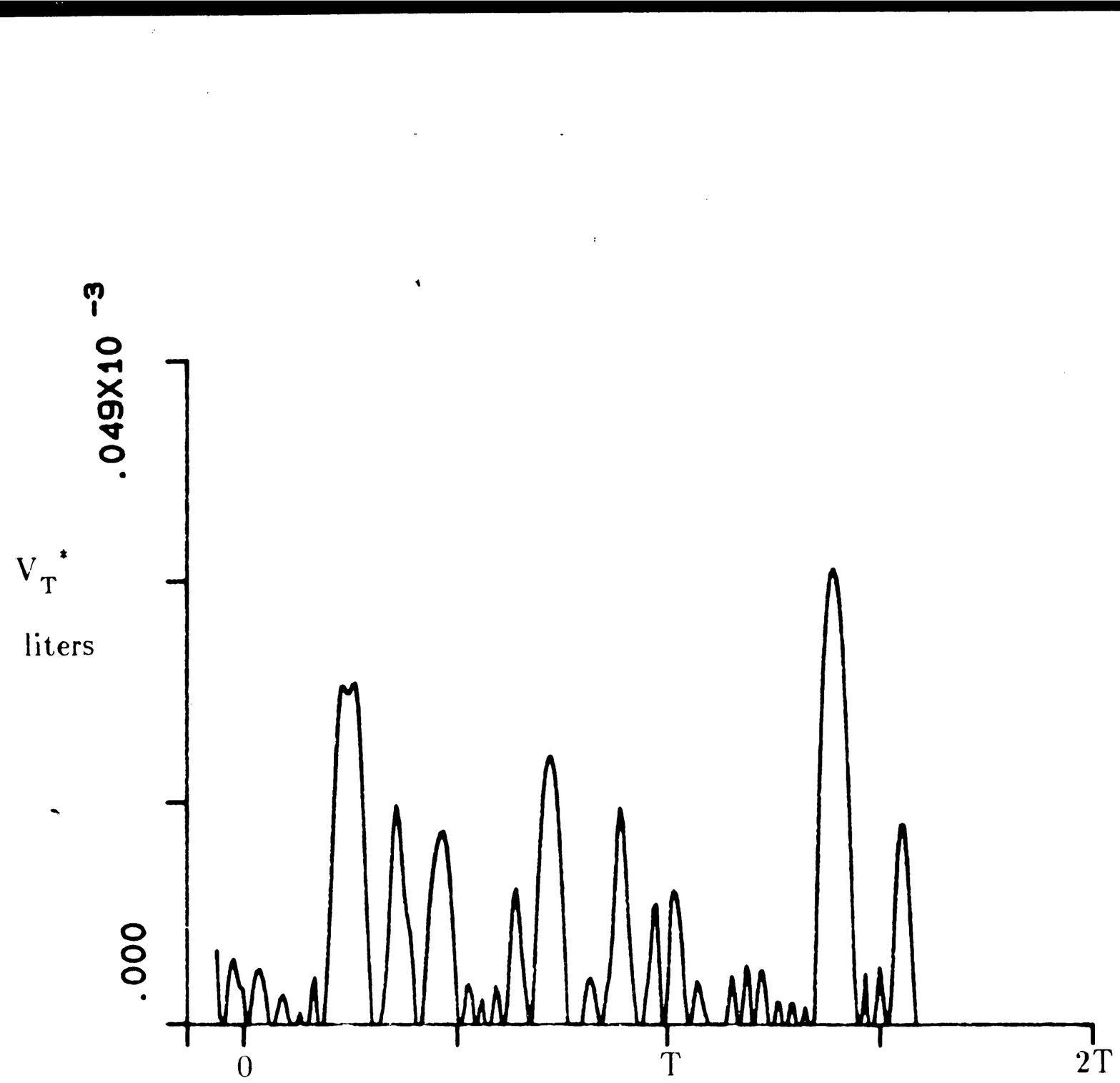

Figure 4-40: Case 3. Cavitation bubble at P_T^* (see Fig. 4.3)

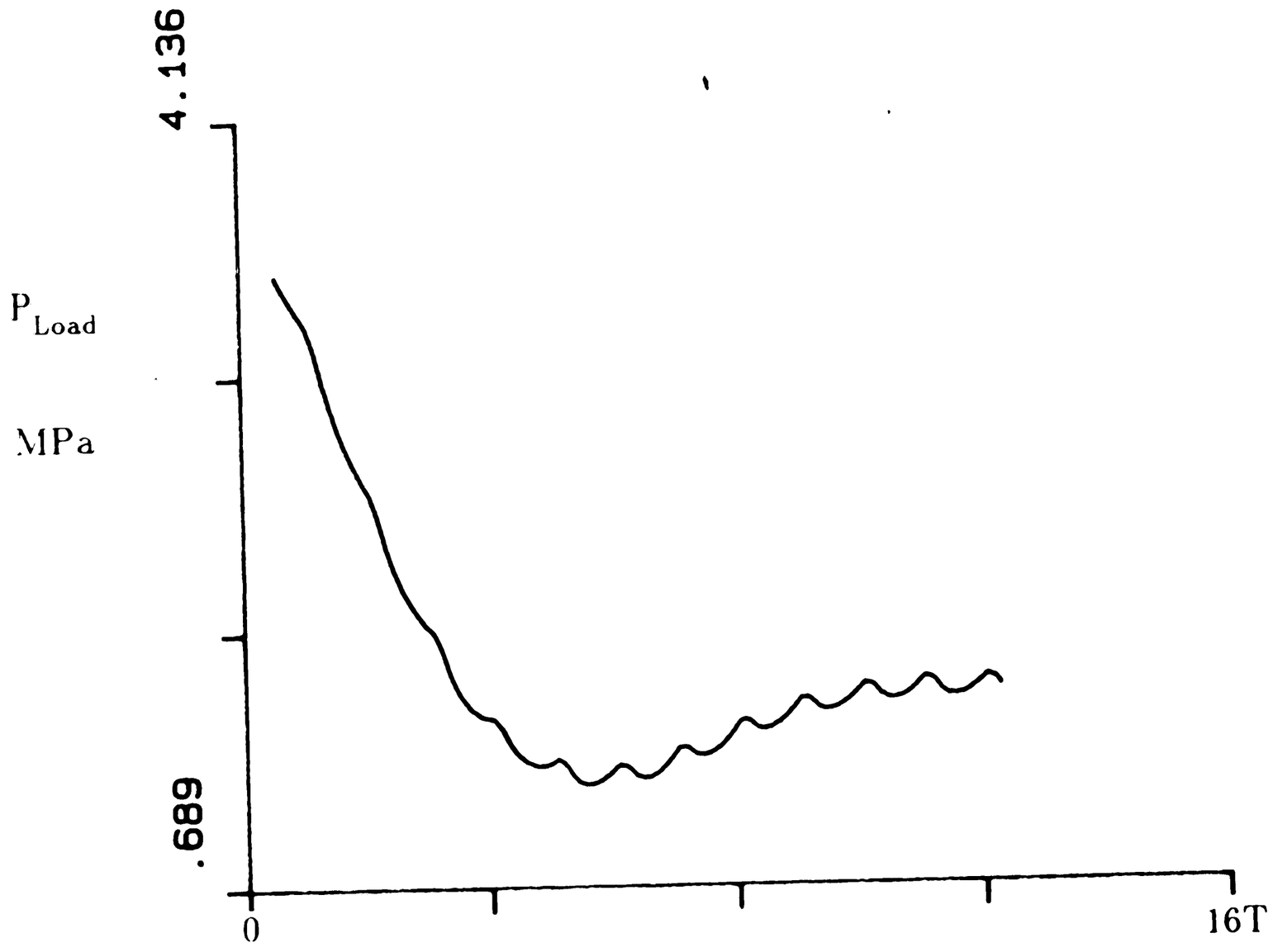

Figure 4-41: Case 3. Load pressure P_{load} (see Fig. 4.4)

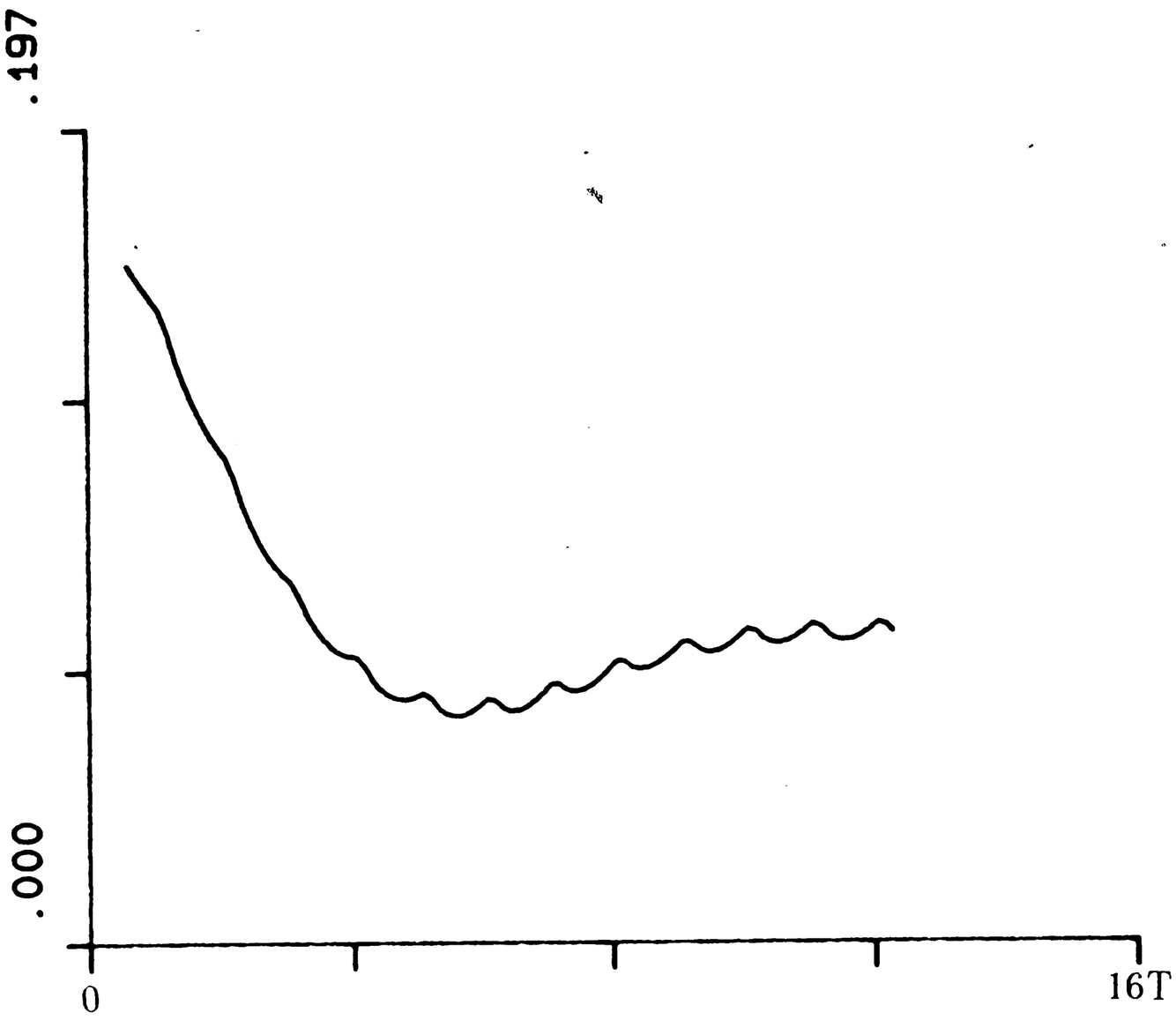

Figure 4-42: Case 3. Load flow Q_{load} (see Fig. 4.4)

Chapter 5
Experimental Set-up and Results

A prototype of the rotary switching valve was built and implemented into a hydraulic switched-inertance servo-transformer. This chapter will describe the experimental set-up used in testing the device. Next, it will give experimental results on static leakage or pressure characteristics to evaluate the manufacturing precision of the valve and to indicate to what extent ideal switching is achieved. In addition pressure-gain curves for blocked conditions, and flow vs pressure curves will be presented and then compared to the analytical results of Fig. 3.5 for a switching frequency of 500 Hz.

5.1 Experimental Set-up

Fig. 5.1 is a circuit diagram of the experimental test equipment. All components used are standard stock equipment except the switching valve and the inertance tubes. Flow is supplied by a Parker gear pump which has a maximum flow capacity of .22 liters/sec at 10 MPa. All fluid lines are either standard .402 in (10.21 mm) ID steel tubing or Parker hoses with quick disconnect ends. The two pressure guages are Bourden guages rated at 0-13.8 MPa and 0-1.1 MPa. All four accumulators are Greer bladder accumulators with a total volume of .0246 liters each. The pressure transducer is a variable reluctance differential pressure transducer made by Validyne, and is rated at 22 MPad with an accuracy of 0.6 kPad. The flow meter is a turbine flow meter made by Hoffler Flow Controls Inc., and it is rated at .0126 to .285 liters/sec with an accuracy of 0.1% of full scale. The potentiometer connected to the end of the control shaft is a rotary potentiometer. The load is a Parker needle valve.

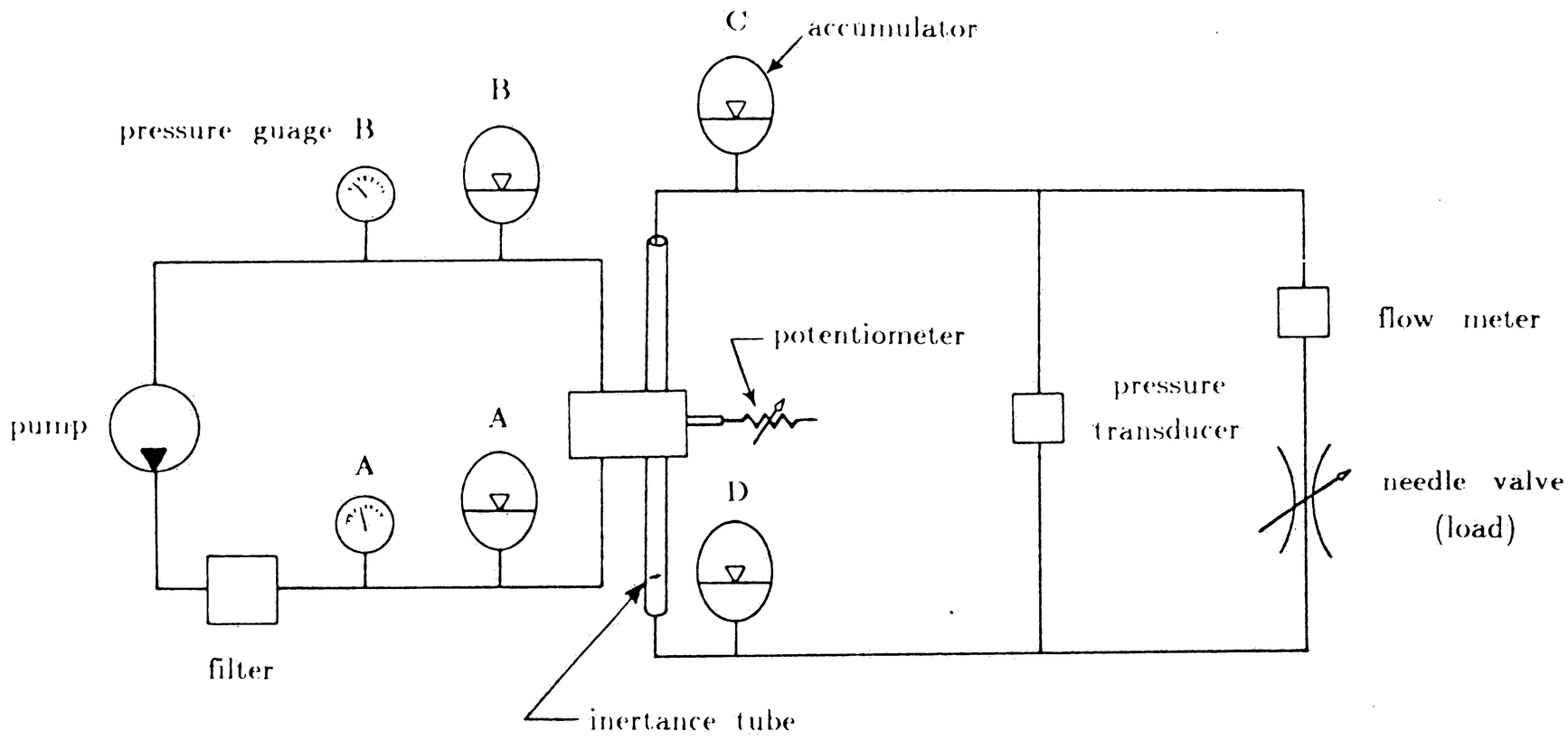

Figure 5-1: Circuit diagram of experimental set-up for four-way operation

And finally, the hydraulic fluid used is BEL RAY LT-56 oil.

The only custom parts are the switching valve and the two inertance tubes. The valve is a prototype of Figs. 2.6 and 2.7. The inertance tubes were made from a piece of 10.16 cm long, .32 cm ID tubing with slightly rounded inlets to reduce entrance losses. Special threaded sleeves were then welded to each end of the tubes to mate with either the valve housing or standard pipe fittings.

Typical system operation is as follows:

Flow supplied by the pump passes through the filter to clean the oil of dirt particles. Accumulator "A" is charged to about one-half of P_s and helps to stabilize pressure at the supply port in the valve to about the supply pressure P_s. Accumulator "B" is charged to atmospheric pressure and similarly helps to stabilize the pressure at the tank port in the valve to about P_T. The two dial pressure guages measure P_s and P_T so that the total pressure difference across the valve is known. With P_S and P_T connected to their appropriate valve ports, the electric motor spins the rotor at 5000 rpm to produce the desired 500 Hz PWM pressure signal seen by the inertance tubes. This signal alternately accelerates and decelerates flow in the inertance tubes. Accumulators C and D complete the IC filter which smooths the pressure at the output ends of the inertance tubes to a desired time average. The difference between these average output pressures is the load pressure P_l and is measures by the pressure transducer. Finally, the needle valve acts as the load with P_l applied across it and the load flow supplied to it, is measured by the flow meter.

5.2 Experimental Results

An initial test was performed to observe the sharpness of switching that is possible with the valve. The electric motor was disconnected from the rotor shaft and replaced with a rotary potentiometer. With the control shaft held fixed and the needle valve closed, the rotor was turned very slowly. This resulted in a PWM signal seen at the input ends of each inertance tube. Since the load was blocked, flow through the inertance tubes was zero giving no pressure drop through them. The pressure transducer then measured the pressure difference between the two inertance tube inputs.

Fig. 5.2 shows an experimental plot of rotor angle vs. ΔP measured by the pressure transducer for a supply pressure of about 1.5 MPa, tank pressure of zero, and α equal to about 0.5. Ideally this curve should have perfectly square corners and vertical lines as in Fig. 3.2. There is a little rounding of the corners in the experimental plot probably due to slight underlapping and clearances in the valve. This rounding effects only a small portion of the switching period and essentially has negligible effect except for extreme values of α. Overall, the switching is relatively sharp and this result is considered quite good.

With the motor connected to the rotor shaft pressure-gain curves were produced using the set-up in Fig. 5.1. Because of deflections inside the valve due to fluid pressure, the supply pressure used in testing was set at only 4.14 MPa. Fig. 5.3 is an experimental plot of the load pressure P_l measured by the pressure transducer vs. α for a 500 Hz switching frequency and a blocked load condition. This curve should be a straight line for pressure control. Notice that the experimental curve is rather straight over most of α. Slight variations

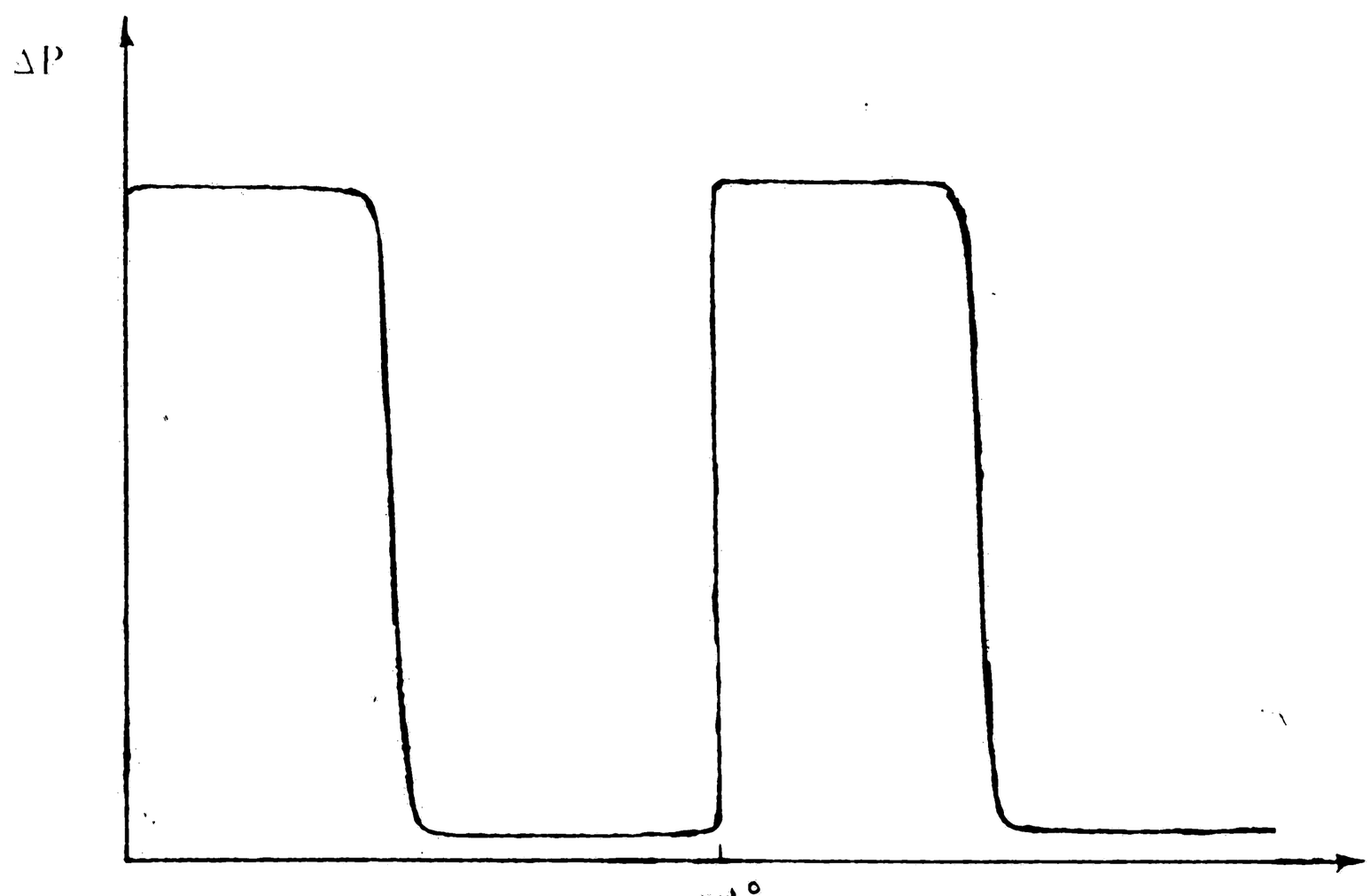

Figure 5-2: Experimental PWM switching signal

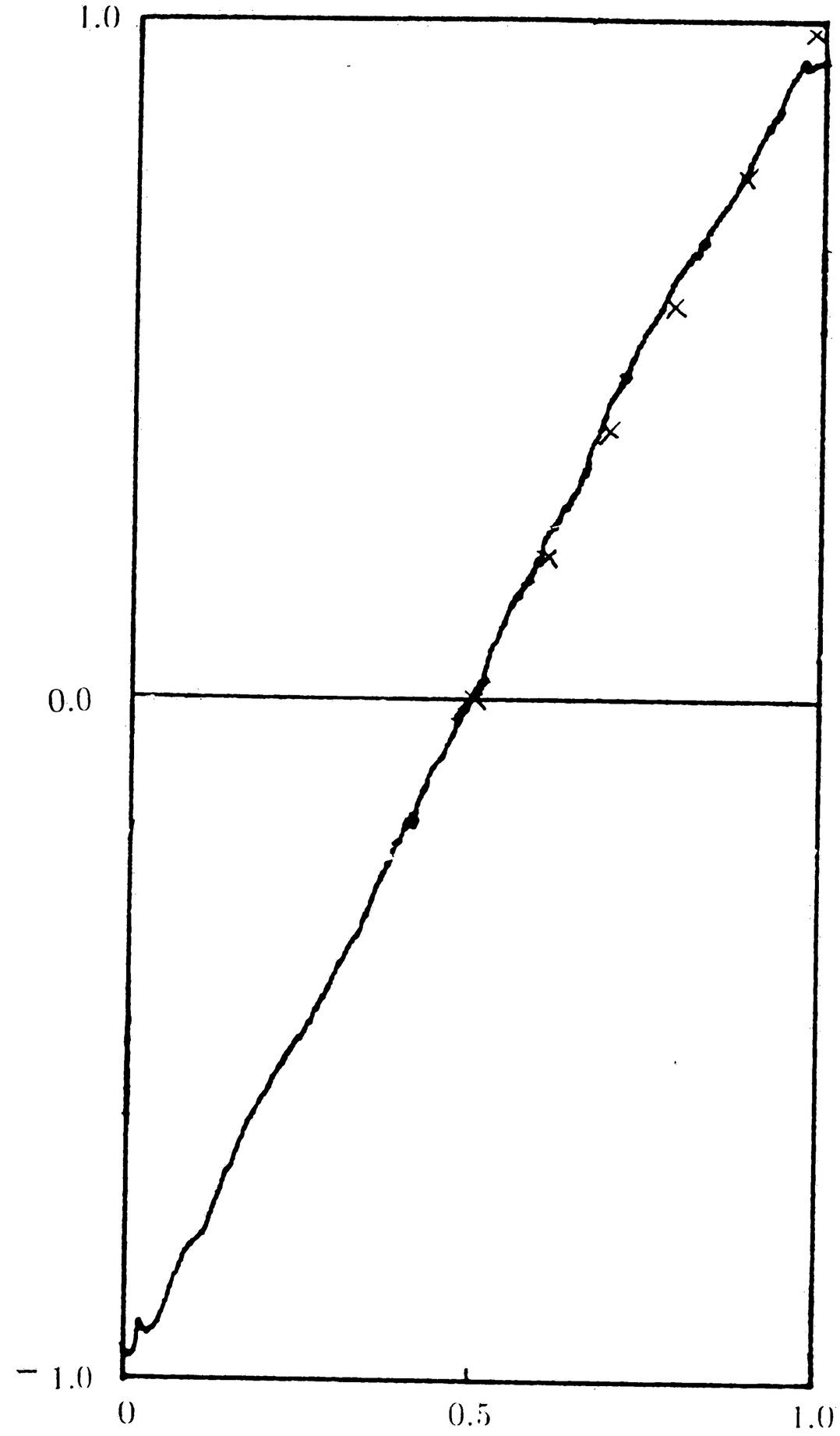

P_S-P_T = 4.14 MPa

f - 500 hz

Figure 5-3: Experimental blocked-load pressure gain

in the curve from a straight line partly result from jerkiness of the x-y recorder in response to manual changes in α, but may also result from the excitation of natural frequencies and/or wave propagation effects. At the ends of the curve, where α is less then 0.05 or greater than 0.95, the rounded corners of Fig. 5.2 become important and their non-linear effect bends the pressure-gain curve. Also included in Fig. 5.3 are points taken from Fig. 3.5 where the non-linear model predicts the characteristic curves cross through the P_l axis.

Another set of tests were performed to generate pressure-flow characteristics for the system. This time the input supply pressure P_s, measured by guage "A", was 4.24 MPa. The tank pressure P_T, measured by guage "B" for zero load flow was about .1 MPa due to leakage flow having to push open check valves in hose connectors. As the load flow increased, P_T also rose slightly to about .2 mPa at a load flow of .2 liters/sec. In this experiment the electric motor turned at 5000 rpm to give a 500 Hz switching frequency. Fig. 5.4 shows this set of pressure-flow characteristics for α set set equal to 0.57, 0.65, 0.75, 0.83, 0.92, and 1.0. Notice how the curves are bent over sharply when Q_l is above .17 liters/sec. This is due to pump saturation (ie: the pump could not supply enough flow). At lower flows however, the curves look, very similar to each other, just shifted side to side. The slopes near the P_l axis are all quite consistent at about Q_l/P_l = .183 liters/(MPa-sec). Obtaining this uniformity was one of the design tasks since it means linear characteristics.

For comparison, one characteristic curve from Fig. 3.5 is also plotted in Fig 5.4. At low flows the theoretical and experimental curves are quite similar. The pressures for zero flow are almost identical. Similarly, the slopes of the characteristic curves agree very well. As flows increase, the two results begin to

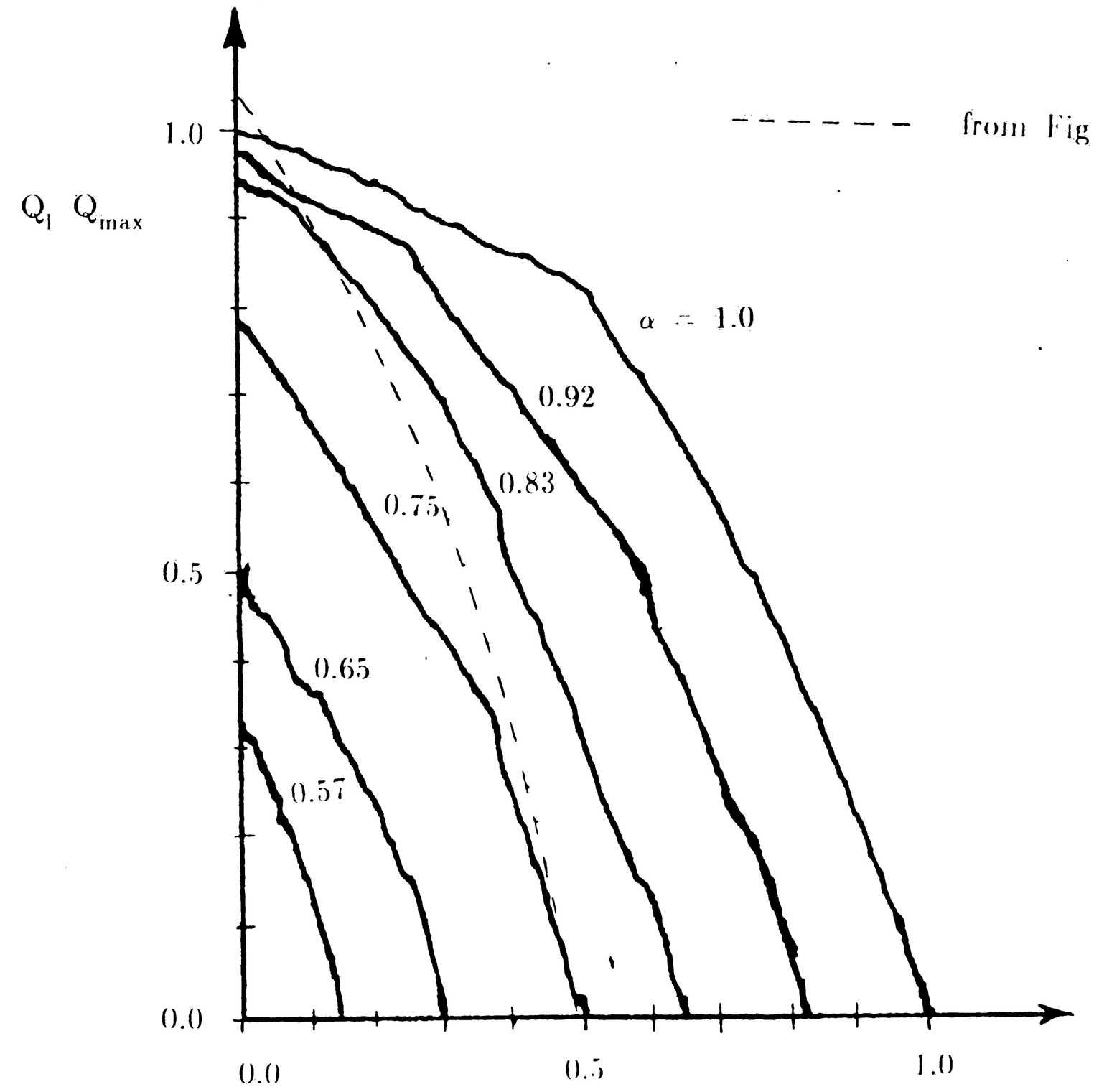

Q_{max} .205 liters sec.

$P_s - P_T$ 4.14 MPa

f 500 hz.

Figure 5-4: Experimental pressure vs flow characteristics

diverge and non-linear phenomena not included in the model bend the experimental curves. By using the elaborate model in chapter 4 it might be possible to better predict the experimental curves, but this was not done because of the extensive computing time required. It also seems likely that transition to turbulent flow is occuring, since the peak (but not the average) flows are well within the nominal turbulent range for steady flows. Unfortunately, since flow is violently accelerated, steady-flow transition results will not apply.

Chapter 6
Conclusions

The switched-inertance hydraulic servo-transformer using the rotary switching valve of Figs. 2.6 and 2.7 proved to be quite effective. The experimentally produced blocked-load pressure gain curve in Fig. 5.4 is very close to the desired and theoretically predicted results. Only at extreme values of α does the curve deviate significantly from the ideal straight line. The pressure-flow characteristics in Fig 5.5 are also encouraging. All the characteristic curves are fairly uniform with each other and are very linear for small flows. Therefore the system displays pressure-control behavior and is fundamentally different from conventional flow control.

Improved energy efficiency over conventional systems is another inherent advantage of the switched-inertance system. The two models presented in chapter 3 support this claim. Figs. 3.3 and 3.5 both indicate a much improved efficiency over most of the mapping. Only at small flows (below .015 liters/sec), where there is relatively little dissipated energy, is efficiency worse than conventional systems.

These same models imply two more results regarding effects of the fluid inertance and the supply Pressure P_s, on the system's energy efficiency. Since dissipated energy is a function of the instantaneous flow through the tube, and not the average flow through the tube, keeping the amplitude of flow oscillations at a minimum is essential to higher energy efficiency. Fig. 3.3 gives results for $\Omega = 5$ and $\Omega = 9$ from the linear model. The larger Ω means a larger inertance I, which in turn means smaller flow oscillations since the same pressure forces now have to accelerate and decelerate this larger inertance. As

a result efficiency is higher for larger Ω. We might also expect efficiency to increase if the input pressure drop across the valve, (P_s-P_T), decreases, since this too can cause decreased flow oscillations. Generally this concept is true but cannot be predicted with this linear model. However, the non-linear model in chapter 3 can show the effect on energy efficiency which results from changing the input pressure drop. A few points were generated with P_s-P_T less than 4.14 MPa to qualitatively show that efficiency increases as P_s-P_T decreases. Consequently, operating at very high input pressure drops may cause efficiency that is worse than conventional flow control valves.

The general purpose for developing the elaborate model in chapter 4 was to verify that sufficient smoothing of the PWM input signal occurred for the various compliances and inertances designed into the system. Also, it intended to quantitatively predict the size of cavitation bubbles which may develop. Results from the three conditions simulated showed that sufficient smoothing of the PWM signal did occur at the output end of the inertance tubes, to the extent where load pressure oscillations were limited to about 2% of P_s-P_T (see P_{Load} Fig. 4.10 and 4.24). Wave propogation effects causing the higher frequencies present in the flows also were sufficiently smoothed. Cavitation bubbles were calculated at several locations along the inertance tubes and also at the tank-to-valve connection (P_T^*). The largest bubble developed at P_T^* for the case with α=0.75 and load flow about equal to 0.1 liters/sec. According fo Fig. 4.40, the cavitaion bubble reached .16 ml, which converts to about 0.1% of the inertance tube length. All other cavitation was significantly less.

There are several possibilities for future work using this elaborate model. By developing a more efficient simulation code and/or by omitting some non-

essential variables to reduce the order of the system, it may become practical to simulate much longer periods of valve operation. This would allow us to attempt dynamic response predictions. It would also permit calculating pressure-flow curves, which might correlate more closely to experimental results.

Experimentally, testing dynamic response of the system may be a next step. The geometry of the valve matches very well to stepper-motor control and consequently microprocessor control. Since control motions are considerably larger than in conventional valves, some of the smaller stepping increments available (less than one degree) may be practical to allow direct drive of the control shaft. Then, with a stepper-motor implemented dynamic tests could be performed to analyze system response.

The generation of noise is a practical problem with this valve. During testing, valve generated noise was very loud, even painful, and required that ear-plugs be used. Reducing noise is therefore a practical necessity. A major cause for the radiated noise is the total unbalance of the forces on the body caused by the fluid accelerations in the two tubes. These forces would largely cancel, rather than add, if the two tubes were oriented in the same, rather than the opposite, direction. Other possibilities for noise reduction include the simultaneous use of several out-of-phase parallel tubes which open at higher frequencies, and the development of an acoustic muffler.

Future designs should address the need for higher flows and higher pressures. The flows can be increased by using larger diameter tubes, or more of them; ways to considerably increase the flow through the valve itself include the use of axial porting and higher rotational speeds. Since larger tubes do not become longer, for a given frequency, frictional losses should decrease, giving

higher efficiency. Higher pressure poses a basic problem, however, since it entails higher fluid velocities and consequently increases the dynamic heads and the dynamic head losses. The practical limitation involves the ratio P_s/β which must remain as small as possible. For conventional hydraulic oils it may not be practical to operate over about 15 MPa (and for a compressed gas the concept fails totally).

The limitation based on the ratio P_s/β would vanish if the kinetic energy were stored in a solid rather than a liquid. The design problems are considerable, particularly if the solid inertia substitutes fairly directly for the fluid inertia. An alternate approach in which the mean velocity of the inertia is zero has been shown to give flow control rather than pressure control [1]; the device becomes a modulated gyrator which is indeed rare amongst engineering concepts.

References

1. Brown, F.T., "Switched Reactance Hydraulics", to be published in Proceedings of National Fluid Power Conference, March 1987.

2. Pressman, A.I., Switching and Linear Power Supply, Power Converter Design, Hahden Book Co. Inc., Rochelle Park, N.J., 1978.

3. Liaw, C.J., "Optimal Design of Hydraulic Switching Valves for Use in High Performance Servosystems", unpublished Ph.D. dissertation, Lehigh University, 1986.

4. Brown, F.T., "The Use of Fluid Inertia for D/A Conversion in Hydraulic PWM Circuits with Seating Valves, Part I: Concepts", ASME paper 84-WA/DCS-4, presented at ASME Winter Annual Meeting, 1984.

5. Brown, F.T., and Koseoglu A.S., "The Use of Fluid Inertia for D/A Conversion in Hydraulic PWM Circuits with Seating Valves, Part II: Results", ASME paper 84-WA/DCS-5, presented at ASME Winter Annual Meeting, 1984.

6. Trikha, A.K., "An Efficient Method for Simulating Frequency-Dependent Friction in Transient Liquid Flow", Journal of Fluids Engineering, March 1975, pp. 97-205.

7. McCollum, P.A. . and Brown, B.F., Laplace Transform Tables and Theorems, Holt, Rhinehart, and Winston Inc., N.Y., 1965.

8. Merritt, H.E., Hydraulic Control Systems, J. Wiley and Sons, N.Y., 1967.

Appendix A

Solving the system of linear differential equations given by Eqs. 3.3, 3.4, and 3.5 using inverse Laplace transforms required extensive algebra. The following adds some of the missing detail to the precedure outlined in section 3.1.

The differential equations were rewritten using the differential operator s, giving

$$sy_i = -n_i \frac{\nu}{A^2} y_i + n_i sQ$$

$$IsQ = (P_{in} - P_{out}) - R_s Q - R_s(y_1+y_2+y_3)/2$$

$$Cs = Q - Q_l$$

Combining these equations to eliminate y_1, y_2, y_3, and P_{out} gives the transfer function between Q(s) and P_{in}(s) in Eq. 3.6. If we let

$$k_i = -n_i \frac{\nu}{A^2}$$

then

$$b_2 = k_1+k_2+k_3$$

$$b_1 = k_1k_2 + k_2k_3 + k_1k_3$$

$$b_o = k_1k_2k_3$$

$$a_4 = 2I$$

$$a_3 = 2R_s + 2IB_2 + R_s(m_1+m_2+m_3)$$

$$a_2 = a_4b_1 + 2R_sb_2 + R_sb_2(m_1+m_2+m_3) - m_1k_1 - m_2k_2 - m_3k_3$$

$$a_1 = a_4b_o + 2R_sb_1 + R_s(m_1k_2k_3+m_2k_2k_3+m_3k_1k_2)$$

$$a_o = 2R_sb_o.$$

Eq. 3.6 is then converted back to the differential form in Eq. 3.7 by letting s denote d/dt. Taking the Laplace transform of this and noting that P_{in}

is a step input, we get the Laplace transform Eq. 3.9. with the new constants:

$$A_3 = (a_4 Q'_o + a_3 Q_o \quad 2P_o + 2P_{in})/a_4$$

$$A_2 = (a_4 Q_o'' + a_3 Q_o' + a_2 Q_o - 2b_2 P_o + 2a_2 P_{in})/a_4$$

$$A_1 = (a_4 Q_o''' + a_3 Q_o'' + a_2 Q_o' + a_1 Q_o - 2b_1 P_o + 2b_2 P_{in})/a_4$$

$$A_o = 2a_o P/a_4$$

The initial conditions for the derivatives of P_{in} are zero because it is a step input. The subscript $_o$ here means, evaluated at 0^+.

With the roots of the denominator in Eq. 3.9 known we can write Eq. 3.10 where

$$C_1 = -\frac{\lambda_1^4 - A_3\lambda_1^3 + A_2\lambda_1^2 - A_1\lambda_1 + A_o}{\lambda_1(\lambda_2 - \lambda_1)(\lambda_3 - \lambda_1)(\lambda_4 - \lambda_1)}$$

$$C_2 = -\frac{\lambda_2^4 - A_3\lambda_2^3 + A_2\lambda_2^2 - A_1\lambda_2 + A_o}{\lambda_2(\lambda_1 - \lambda_2)(\lambda_3 - \lambda_2(\lambda_4 - \lambda_2)}$$

$$C_3 = -.....$$

$$C_4 = -.....$$

Eq. 3.10 is now written twice, once for each portion of the switching period with the appopriate initial conditions and appropriate input pressures, to give $Q_1(t)$ and $Q_2(t)$. Then, since the flow must be continuous, and the system is fourth order the relations in Eq. 3.11 must hold. These can then be substituted back into A_3, A_2, A_1, and A_o as the initial conditions for $Q_1(t)$ and $Q_2(t)$. Next these can be substituted into C_1, C_2, C_3, and C_4 for both $Q_1(t)$ and $Q_2(t)$ to give a system of eight linear algebraic equations. Solving the system produces C_1, C_2, C_3, and C_4 for both $Q_1(t)$ and $Q_2(t)$. $Q(t)$ is simply $Q_1(t)$ for $0<t<\alpha T$ and $Q_2(t)$ for $\alpha T<t<T$.

Vita

Stephen Clyde Tentarelli was born in Abington, Pennsylvania on Feb. 26, 1963 to Patrick Tentarelli and Mary Faye Tentarelli. He graduated suma cum laude from Lehigh University in June of 1985 receiving a B.S. in Mechanical Engineering. In August of 1985 he enrolled in the graduate school at Lehigh University.